UNIVERSITAT ROVIRA I VIRGIL

MODELING OF SELF-ORGANIZATION OF MICROTUBULES IN PLANT CELLS

Alexander Muratov

Dipòsit Legal: T 966-2014

DOCTORAL THESIS

Modeling of Self-Organization of Microtubules in Plant Cells

Alexander Muratov

Universitat Rovira i Virgili
Departament d'Enginyería Química

2

Alexander Muratov

MODELING OF SELF-ORGANIZATION OF MICROTUBULES IN PLANT CELLS

DOCTORAL THESIS

Supervised by Dr. Vladimir Baulin

UNIVERSITAT
ROVIRA I VIRGILI

Departament d'Enginyería Química

Tarragona

2014

Acknowledgments

First, I would like to thank my PhD supervisor Dr. Vladimir Baulin for the opportunity to do this PhD project, for many provided opportunities during doing this project, for support during the work and for helpful advices. I am very grateful to him for his kindness and guidance. Second, I would like to thank Dr. Josep Bonet i Avalos and Dr. Allan D. Mackie for their support and helpfulness.

I would also like to specially thank Teresa Marmol for her priceless aid in solving administrative issues. Another special thanks goes to my PhD coordinator Nuria Juanpere for the patience and quickness in solving urgent questions. I would also like to thank my former and present group colleagues for quiet and working atmosphere. I specially appreciate the help of my ex-colleague Dr. Sergey Pogodin, who helped me a lot during my first months in Spain.

Many thanks to all my Russian-speaking friends here in Spain and back in Russia for sharing their spare time and priceless support. Apart from that I would also like to thank my precious fiancée Gabriela - without her priceless help this work might have never seen a light.

Last, but not least, I would like to express my deep gratefulness to my family and especially to my mother Tatiana, my father Dmitry and my sister Arina.

Tarragona, February 2014.

5

UNIVERSITAT ROVIRA I VIRGILI
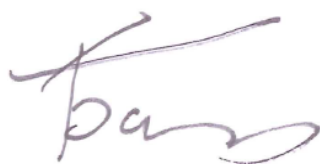
Departament d'Enginyeria Química

Av Països Catalans, 26
43007 Tarragona
Tel. 977 558675
Fax. 977 559621

I STATE that the present study, entitled "Modeling of Self-Organization of Microtubules in Plant Cells", presented by Alexander Muratov for the award of the degree of Doctor, has been carried out under my supervision at the Department of Chemical Engineering of this university, and that it fulfils all the requirements for the Doctoral Degree.

Tarragona, 18 February 2014
Doctoral Thesis Supervisor

Dr. Vladimir Baulin

Acknowledgments

Abstract

Microtubules are ubiquitous elements of any eucaryotic cell, serving many functions at different stages of its life. In plant cells they form so-called plant cell cortex, where they are organized into parallel arrays. These arrays serve as a matrix of synthesis of a plant cell wall, defining the direction of growth. Microtubule arrays are sensible to tropic stimuli. However, the nature of such sensibility is still not well established, although it has been investigated since 19th century. Here we provide a computational analysis of this phenomenon. Using both kinetic Monte-Carlo simulations and theoretical investigation, we show that compression due to mechanical stress may cause orientation of microtubules along major stress lines. We also show that anisotropic distribution of chemical agents interacting with microtubule-associated proteins also causes orientation of microtubules in the direction defined by such stimulus. Such mechanisms are primarily connected with gravitropism but similar reorientations of microtubules in response to light may suggest that these mechanisms can also be relevant for other tropisms.

Contents

Contents

1

1. Introduction

1.1. Microtubules' properties and dynamics

Microtubules are important elements of the eucaryotic cell carrying out many functions. In the interfase state microtubules are essential components on the cell's cytoskeleton, thus executing the locomotory function. In the cell division state the most of microtubules are included into the mitotic spindle.

Microtubule is a hollow tube-like object with external diameter of twenty five nanometers and internal diameter of fifteen nanometers. In eucaryotic cells microtubule walls are consisted of thirteen longitudinal protofilaments, each of which is formed by tubulin dimers [1]. Tubulin dimer has the measures of ten nanometers in width and eight nanometers in height. In microtubule protofilaments are slightly shifted respectively to each other, so they form a three-start helix (Consult Fig. 1.1) [2].
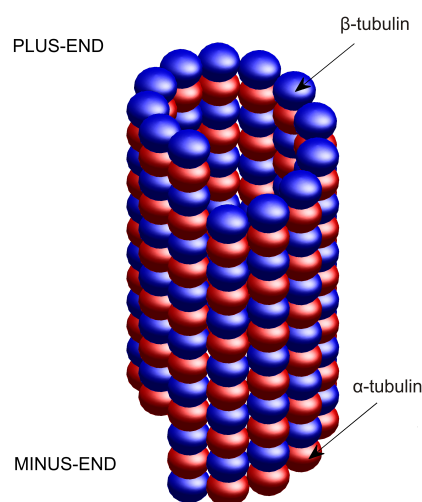
Figure 1.1.: Schematic view of a microtubule.

Tubulin's dimer is a polar molecule, consisting of two different, but nonetheless very similar subunits: α-tubulin and β-tubulin [2]. Both subunits can bind with GTP. In the microtubule polymerization process participate only those dimers, both subunits of which are bounded with GTP (they are called T-dimers). Soon after polymerization GTP in β-subunit is hydrolyzed, thus in microtubule wall in general are found the dimers, whose α-subunit is bounded with GTP, and β-subunit – with GDP (they are called D-dimers). The significant difference between T-dimers and D-dimers consists in the fact that T-dimer has uncurved equilibrium conformation, and D-dimer has distorted conformation with the equilibrium angle 0,2 [3, 4].
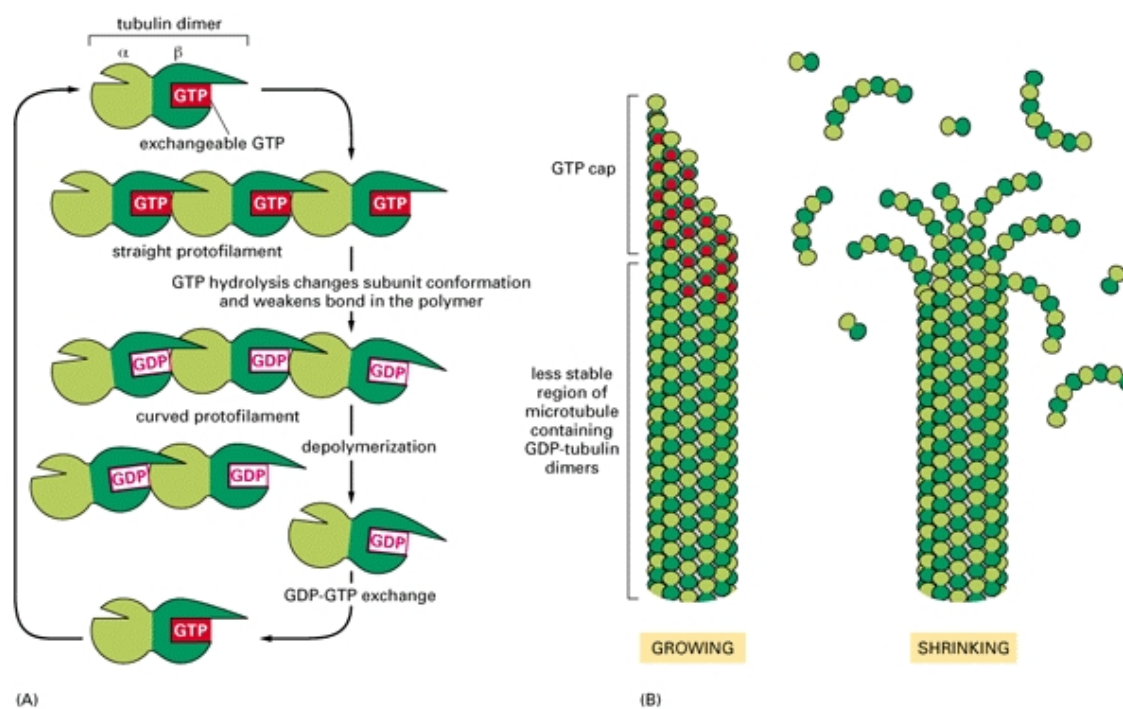
Figure 1.2.: Structure of microtubule plus-end in growth and shortening phases. Picture taken from [1], http://www.ncbi.nlm.nih.gov/books/NBK28419/

Tubulin dimers polymerize not in an arbitrary way, but only by accession to β-tubulin of a dimer α-tubulin of another dimer. Thereby all the microtubule is a polar object, on one end of which α-monomers are localized ("minus-end"), and on another end β-monomers are localized ("plus-end"). Dimers of a protofilament interact not only with each other, but also with the dimers of the neighbor protofilaments [1]. These interactions are called lateral.

Protofilaments in a microtubule contact each other in such way, that generally

4

1.1 Microtubules' properties and dynamics

α-monomers of a protofilament contacts with α-monomers of another (Refer to Fig. 1.1). But since microtubule is a three-start helix, a contact between protofilaments exists, where α-tubulin of a protufilament contacts with β-tubulin of another, and vice versa. This contact is called "the seam", and its existence allows the protofilaments to be numbered [1]. If the microtubule is placed in a way when its plus-end is on the top, then left protofilament in respect to the seam is usually numbered the first, and the right protofilament is numbered evidential thirteenth. Such kind of organization of microtubule is called B-lattice.

Microtubules are not always consisted of thirteen protofilaments. Microtubules, that were assembled in vitro in the tubulin solution, may have the number of protofilaments ranging from twelve to seventeen. The number of starts in a microtubule helix also may vary. The fact that in a living cell microtubule always has B-lattice of a three-start helix and the number of protofilaments always equals thirteen, is explained by the presence of the ring-like fuse-patterns of γ-tubulin in the microtubule organizing center [5].

The observations of the microtubules show that they are dynamic objects. On the microtubule ends the processes of attachment and dis-attachment of dimers may happen, in other words, the processes of polymerization and de-polymerization of a microtubule. In the dynamics point of view microtubule may presence in two states: polymerization (also assembling, also elongation or growing) and de-polymerization (also disassembling, also contraction or shrinkage). Also so-called "pause" is distinguished, that is stable state, characterized by the absence of both assembling and disassembling. The transition from the growing state to shrinkage state is called "catastrophe", the reverse process is "rescue". The behavior of microtubules is called dynamic instability, when the switchings between polymerization and de-polymerization are very often (Consult Fig. 1.3) [6]. Plus-end of microtubules is more dynamic than minus-end [3, 7]. In animal cells minus-end is usually attached to γ-tubulin ring-like complex, while in plant cells minus-end is free [8]. The plus-end is always free in all living cells.

The catastrophe of a microtubule may be connected with the change in conformation of a tubulin dimer during the GTP hydrolysis in β-subunit. GTP hydrolysis happens after the attachment of a dimer to microtubule, thus leading to the dimer's intention to distortion. Nevertheless, in microtubule dimers remain straight, not so much due to their retaining by lateral interactions (which are much more weaker than

5
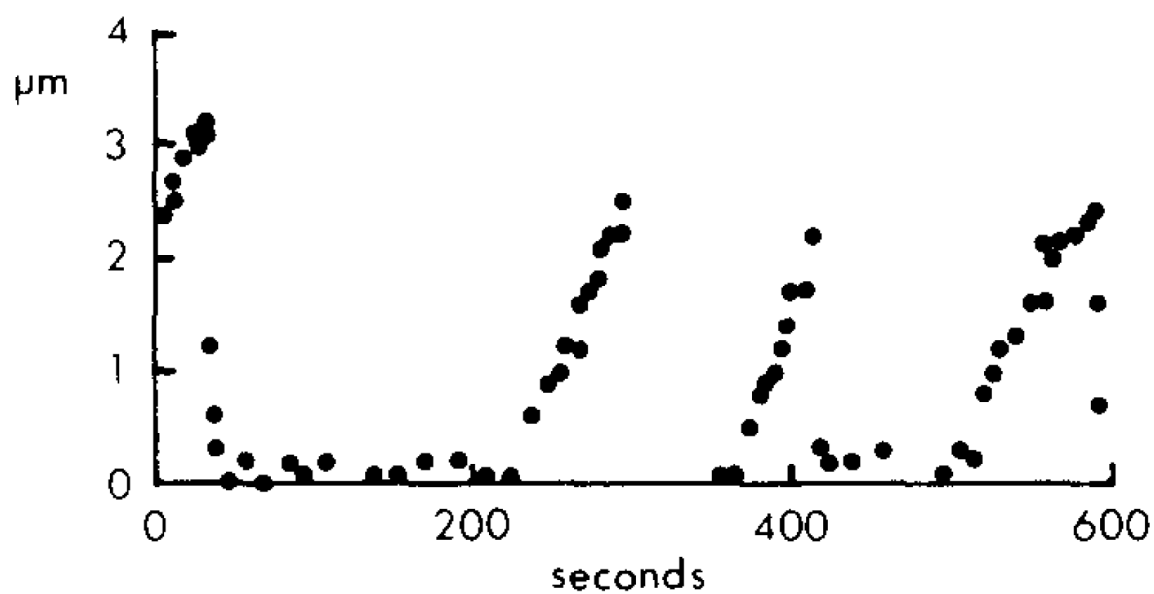
Figure 1.3.: Example of the dynamics of a "plus-end" of a single microtubule. Sample taken from [6].
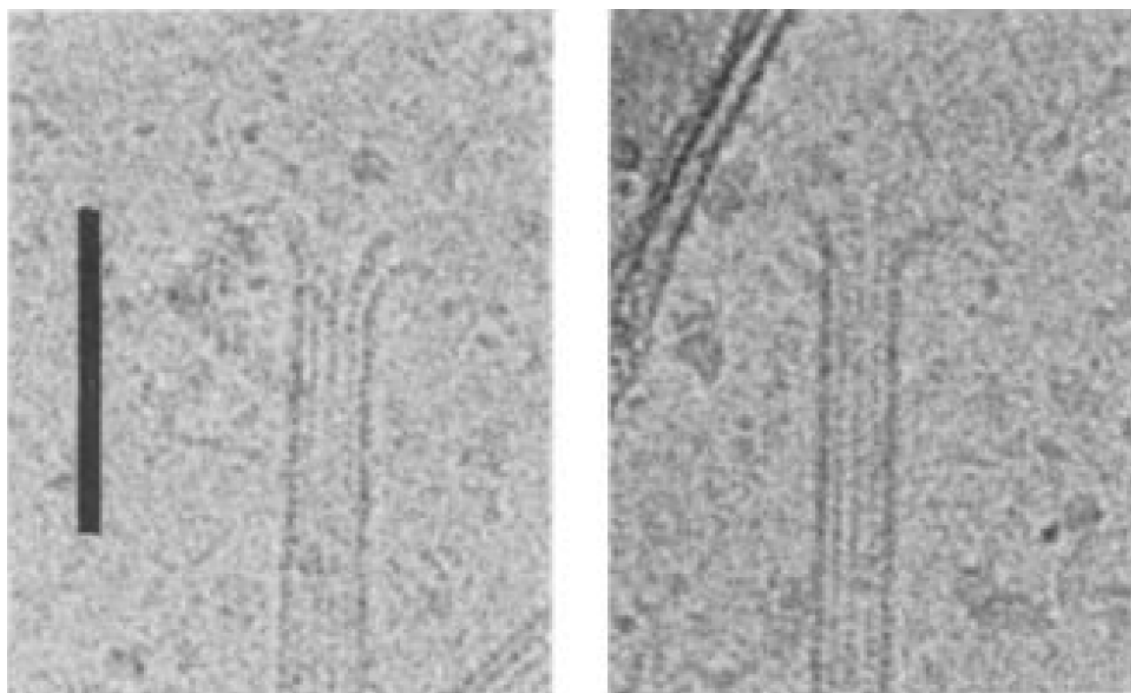
Figure 1.4.: Examples of "ram horns" of a disassembling microtubules. Bar indicates 100 nm. Picture taken from [9].

the longitudinal), but apparently more because of the presence on the plus-end of the microtubule of several layers of tubulins, which are still not hydrolyzed – so-called GTP-cap, which was proposed in 1987 by Mitchison and Kirschner [3, 7, 10]. Although this kind of structure was never observed in the experiments, its existence is generally recognized. Indirectly its presence can be justified in the experiments with tubulin bound with non-hydrolyzible analogue of GTP – GMPCPP. Therefore, the GTP hydrolysis energy in conserved in microtubule wall as the energy on the distortion of the dimers. Later, it is excelled with microtubule de-polymerization [3].

The loss of the GTP-cap destabilizes the plus-end of microtubule and it starts to disassemble. The different from the straight form of the D-tubulin molecules gives the protofilaments on the plus-end of microtubule the form of the "ram horns", which is clearly seen on micro-photographs (Consult Fig. 1.4) [7, 9].

1.2. Microtubule cortical arrays in plant cells

Plant cells lack centrosome, a microtubule organizing center, which is found in
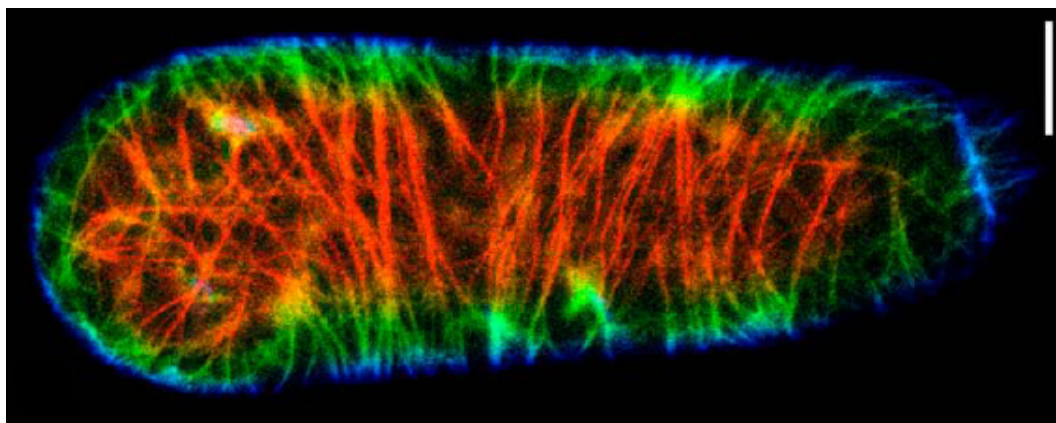
Figure 1.5.: Confocal laser scanning microscopy image of microtubules in plant cell (tobacco BY-2 suspension culture cell). Green fluorescent protein linked to α-tubulin. Bar indicate $10\mu m$. Picture taken from [11].

animal cells, anchoring minus-ends of the microtubules and promoting the nucleation of new microtubules. Microtubules in plant cells have their minus-end free and it usually demonstrates slow shrinkage. Thus, the organization of microtubules

Figure 1.6.: Schematic view of microtubule cortex in plant cell. Picture taken from [12].

1.2 Microtubule cortical arrays in plant cells

normally happens after the nucleation. In plant cells microtubules are organized in parallel arrays which are adjacent to the cell's membrane (See Fig. 1.5, Fig. 1.6) [1, 13]. These arrays are called cell cortex and are sensitive to gravitropism or other tropisms through the mechanism that is still unknown and they reorganize in response to the change in environment [14, 15].

Cell cortex serves as a template for directed growth of cellulose microfibrils [16]. Cellulose microfibrils are the main ingredients of external plant cell skeleton - cell wall [1]. These microfibrils help to maintain the shape of plant cells and prevent cells from exploding due to high internal turgor pressure [15]. As cellulose microfibrils have high tensile strength, they provide the cell wall mechanical stiffness and strength [15]. Thus since cellulose microfibrils in the cell wall are organized anisotropically, the orientation of cellulose microfibrils arrays controls the anisotropy of the cell wall [17].

Cellulose in plant cells is produced by cellulose synthase complexes (CSCs or rosettes), which are multi-subunit enzymes [1]. These complexes are located at the plasma membrane, where they add glucose molecules to the existing cellulose fibrils. It was suggested that the movement of the rosette is guided by cortical microtubules, which explains the collinearity between microtubules and cellulose fibrils in growing cells [18, 19, 20]. Transmission electron micrographs show that cellulose microfibrils are oriented in the same direction with cortical microtubules (Refer to Fig. 1.7) [21, 20]. Clearly microtubules regulate mechanical properties of cellulose microfibrils and other aspects of cellulose biosynthesis. A direct evidence exists [21, 22] that microfibrils of cellulose in cell wall during plant growth are deposited in the same direction as microtubules in the cell cortex. Various agents, such as microtubule depolymerizing drugs, ethylene or other agents, affect the orientation of microtubules [23, 24, 25] and also cause consequent reorientation of cellulose microfibrils leading to the spherical form of a plant cell [26]. When microtubules are disrupted by pharmacological or herbicide treatments or by mutation, cells stop elongating and swell by expanding radially[24]. That is, anisotropy of the cell wall is provided by cellulose microfibrils, and the cell wall becomes more rigid in the directional parallel to arrays of cellulose microfibrils than in perpendicular direction. This way an isotropic turgor pressure is transduced into directional cell growth [27, 28, 29, 23].

The direction of growth of a plant is defined by gravity, light, chemical or other external stimuli. Such growth is called tropic growth, and the movements are called

9

UNIVERSITAT ROVIRA I VIRGILI
MODELING OF SELF-ORGANIZATION OF MICROTUBULES IN PLANT CELLS
Alexander Muratov
Dipòsit Legal: T 966-2014

Chapter 1   Introduction
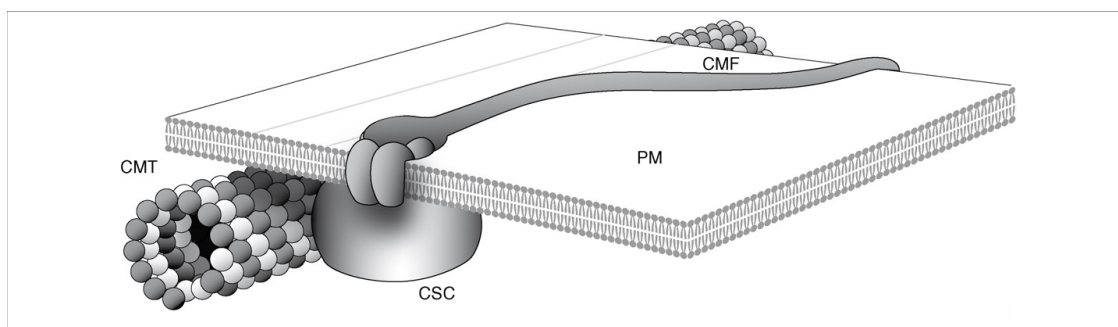
Figure 1.7.: A schematic view how cortical microtubules (CMT) guide the rosette, cellulose synthesis complex (CSC) sitting in plasmatic membrane (PM) which produces cellulose microfibril in the cell wall (CMF) parallel to CMT. Taken from [20].

gravitropism, phototropism or chemitropism respectively. Despite different nature of stimuli causing these tropisms, they have much in common, as they alter the orientation of cortical microtubules, thus leading to the consequent reorientation of cellulose microfibrils and the changing of the growth direction. In the further description we will concentrate more on gravitropism, as it is quite well investigated and is present in all plants from algae to higher plants [14].

Cells and their constituents, such as molecules, their aggregates and organelles, are too small to sense the gravitational field directly, however tissues of roots or shoots of many plants are able to sense the direction of gravity with the help of statocytes, specific cells located in the growing tip of roots or shoots [14]. Statocytes can efficiently perceive the direction of the gravity and direct plant growth along the gravity vector. Directed growth is observed only in the presence of gravitational or centrifugal force and disappear in the absence of gravity or when the direction of gravity is altered [30, 15]. The perception of gravity in statocytes is usually attributed to amyloplasts, macroscopic, heavy organelles that sediment in a lower part of the cell [14, 30, 31] in root gravitropism and can exhibit saltatory upward movements in shoot gravitropism [17, 31].

Sedimenting amyloplasts inside statocytes are probably the main driving force for root gravitropism. Since the radius of amyloplasts, , is about few microns [32, 33], their concentration corrected for buoyancy is $\Delta\rho = 0.5$ g/ml [34] and $g \approx 9.8$ m/s, the resulting sedimentation force of one amyloplast at the bottom of the cell is $\Delta\rho g (4/3\pi)r^3 \sim 1$ pN [35]. Thus, the gravitational force of sedimenting amyloplasts may not be sufficient for global changes or significant deformations of the

cell wall, which can sustain pressures of MPa [36], but it may be enough to trigger local changes, for example, local deformations of cell constituents *e.g.* cortex endoplasmatic reticulum [37]. Several hypothesis aim to explain the mechanism of transduction of the gravity signal to the elongation of the root in the direction of the gravity vector, ranging from activation of ion channels in the endoplasmatic reticulum [38, 37], to release of Ca^{2+} ions [39, 38, 15, 31]. The most common concept is that amyloplast sedimentation causes alternation of auxin flux, which causes reorientation of microtubules [40, 41, 42, 43]. Most probably, gradients in hormonal fluxes change the stability of MTs depending on their direction [44, 45, 43]. It is necessary to mention that the elongation takes place in the epidermis, which is distant of the coot cap by several mm, or ~ 20 cell layers [39, 38, 31] (See Fig. 1.8). Similar reorientations of microtubules in response to light [46] and mechanical deformation [47] may suggest that such mechanism can also be relevant for other tropisms.

In turn, there is an evidence that microtubuless respond directly to mechanical stress of the cell [48, 47, 15]. It can be directly observed during phyllotaxis in shoot apical meristem [28, 49, 50]. This suggests that microtubuless might feel mechanical stress and reorient themselves inducing anisotropic cellulose deposition. Such mechanism is also observed in the experiments with shoot apical meristem compression, laser ablations of its cells or weakening of the cell wall [28, 51, 52].

For directional growth the orientation of microtubules is essential. They are reported to be aligned along main stress lines even in cells of root apical meristem, where gravitropism does not play any role [28, 15]. They were also reported to reorient to transverse arrays in hypocotyl cells [53]. The main question is how do they actually perceive pressure and remain aligned in a growing cell - that is necessary for synthesis of cellulose microfibrils for further direction of the growth - is still open [23, 41, 15].

1.3. Models for investigation of microtubule orientation

Different models describing the behavior of a microtubule array have been previously described in the literature [54, 55, 56, 57, 58, 59, 60, 61, 62, 63, 64, 65, 66, 67, 68, 69, 70].
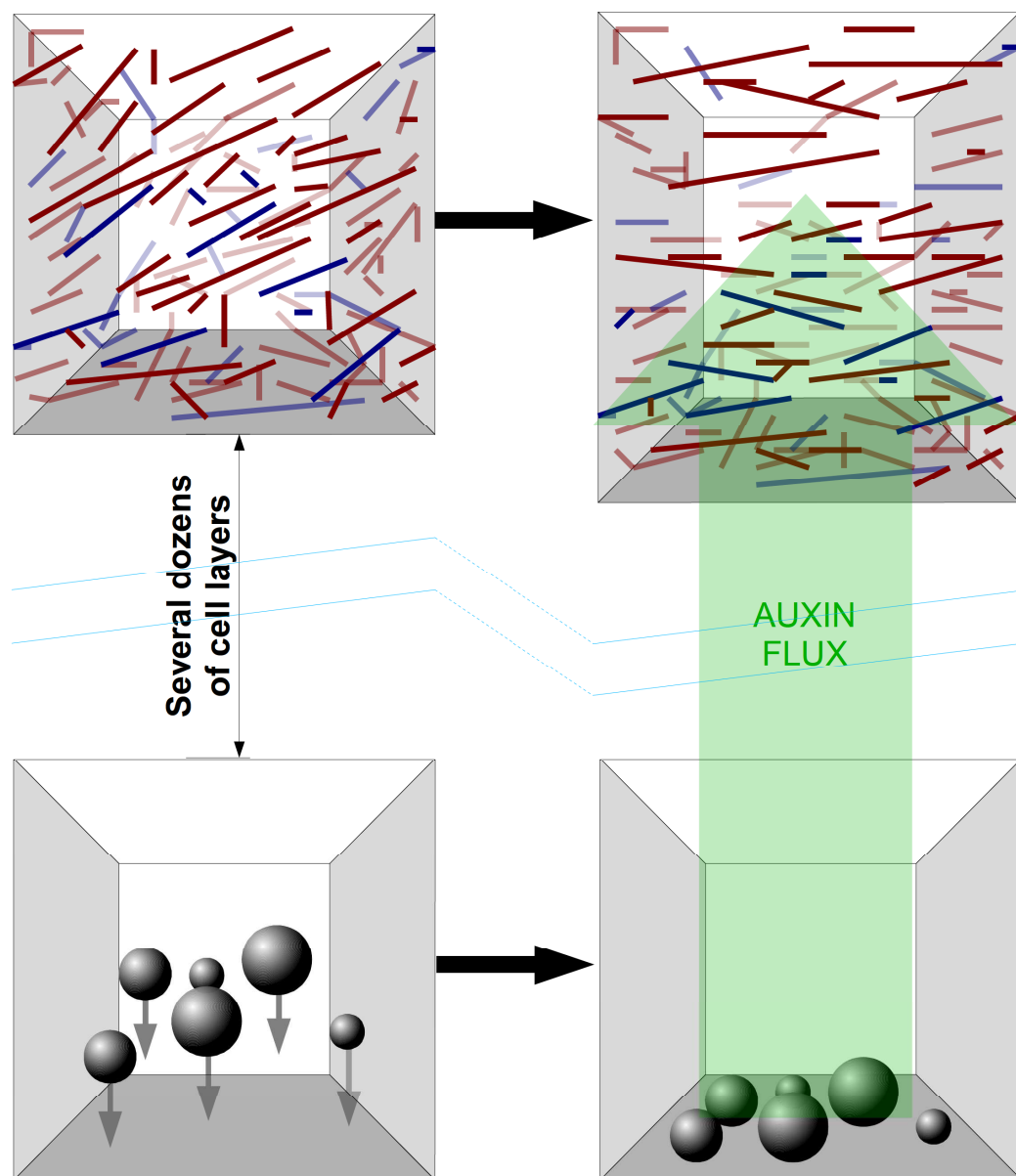
Figure 1.8.: A model for plant cell elongation and microtubules reorientation due to amyloplasts sedimentation in statocytes.

1.3 Models for investigation of microtubule orientation

In the model by Tabony and Job and its later variations microtubule cell cortex was considered as a chemically dissipative structure. Such structures may actually be responsible for self-organization and pattern formation - nonlinearities during formation of solutions lead to bifurcations and instabilities, what, in turn, causes formation of self-organized states of different morphology. In the described model gravity was considered as the reason for symmetry breaking, thus leading to the formation of an array oriented perpendicular to gravitational field. However, it is highly doubtful that microtubule array may be treated as chemically dissipative structure [54, 55, 56, 57, 58]. Although a single microtubule stores a significant amount of energy inside its structure [3, 4, 71], the presence of differences in tubulin concentration during cortex formation or any kind of chemical waves has been never observed experimentally. Moreover, a microtubule is too small to sense gravity.

In the model by Dogterom and Liebler microtubules have been nucleated by a flat surface for an analysis of their growth through dynamic instability. They remained attached to that surface by their minus-end growing in the direction perpendicular to the surface (See Inset of Fig. 1.9). The model predicts the existence of two states of growth of an isolated microtubule: bounded (b), when the average length of microtubule remains stable through time, and unbounded (u), when the length increases infinitely (Consult Fig. 1.9). It also shows that dense structures comprised of microtubules can exist depending on the parameters defining the dynamic instability of microtubules [59].

A group of models was proposed where filaments in cytoskeleton were considered motile, i.e. able to change their orientation [60, 62, 63, 64, 66]. Although it may be consistent for actin cell cortex present in animal cells, for instance in fibroblasts [60], this hypothesis is hardly appropriate for microtubules in plant cells. In some works microtubule movements are connected with the action of molecular motors [64, 66]. However, it is valid mostly for centrosomal microtubules in animal cells, while in plant cells microtubules are attached to plasmatic membrane.

In 2004 Dixit and Cyr introduced a Monte-Carlo model for investigation of interactions between microtubules corresponding to the experiments they had carried on. In their model they have simulated 20 microtubules and have shown that angle-dependent rules for intermicrotubule interactions are necessary and sufficient to facilitate the self-organization of microtubules. They considered only the plus-end's growing and shrinkage, thus the minus-end has been fixed in their model [61].

13
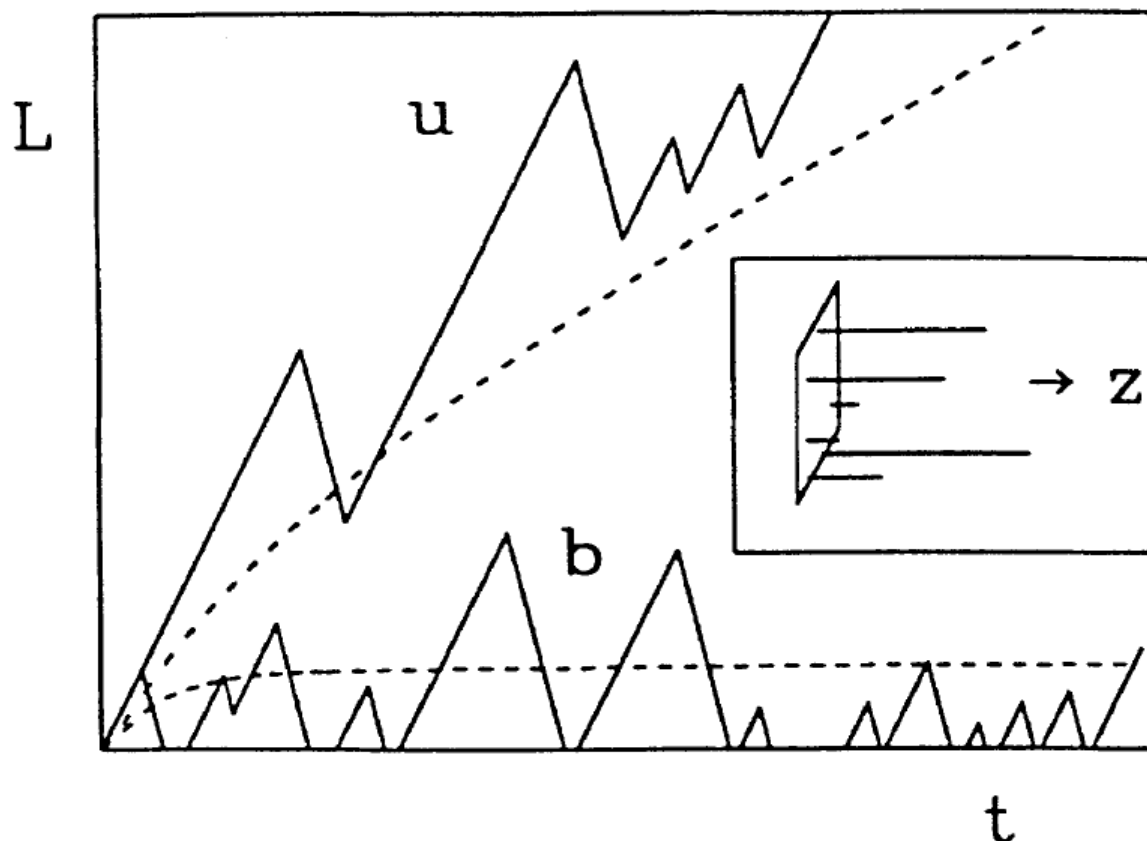
Figure 1.9.: Examples of dynamic instability of a single microtubule in the model
of Dogterom and Liebler: bounded (b) and unbounded (u) growth. Dotted lines
show average length over many microtubules. Inset: a schematic view of a surface
generating microtubules. Picture taken from [59].

In the next model by Baulin *et al.* dynamic instability has been ignored, while
the collisions between microtubules have been paid more attention. In this model
microtubules are lying on a two-dimensional surface, their plus-ends are constantly
growing while their minus-ends are constantly shrinking. In case of the collision be-
tween microtubules the growth of a colliding microtubule is stopped by a blocking
one. The model shows that ordered structures and patterns can be induced from an
initially isotropic and homogenous suspension. Microtubules can form highly but
randomly oriented domains that grow and compete with each other. The stability
of the domains is defined by long an old microtubules. Authors have also identified
two control parameters and shown that even a weak orientational bias is enough to
cause the global orientation of microtubules [65]. It may be noted, however, that
not all essential properties of microtubules have been introduced in this model; in

14

1.3 Models for investigation of microtubule orientation

particular, dynamic instability of microtubules hasn't been included. The orientation of microtubules has been caused only by their collisions. Nevertheless, their dynamic properties are also very important, as it was shown in Ref. [59].

Shi and Ma in their work have proposed a minimal model for an investigation of a phase behavior of microtubule model. The model unites microtubule dynamics with intermicrotubule interactions. Using Monte-Carlo simulations along with theoretical calculations they have shown that single microtubule dynamics can control self-organized patterns of cortical microtubules. They have built a phase diagram determining the parameters under which ordered arrays are formed. From biological point of view their results can be interpreted as the possible evidence of a essential regulation of microtubules dynamic instability parameters by microtubule-associated proteins, so-called MAPs. This fact can be indirectly proven by *in vivo* experiments [67].

Tindemans, Hawkins and Mulder examined a possible mechanisms that can drive alignment of microtubules. They presented both coarse-grained theoretical model and stochastic Monte-Carlo simulations. In their model they considered three possible outcomes of inter-microtubule collisions: crossover, induced catastrophe and so-called "zippering", or the entrainment of the plus-end of the colliding microtubule by the blocking microtubule (Consult Fig. 1.10). It is necessary to note that minus-ends of microtubues are fixed in this model. Authors have introduced a control parameter defined by intrinsic parameters of microtubiles and by nucleation rate. They have analyzed thoroughly stationary isotropic phase, defining its limits of stability, and have solved the simplified model for ordered state. They have also shown that catastrophe-inducing collisions are sufficient to cause the ordering [68, 72].

Completely different conclusion has been made in the article by Allard *et al.* They have constructed almost the same model as Tindemans *et al.* with the only difference: minus-ends of microtubules remained unstable, thus microtubules were "threadmilling". They managed to show that in this case catastrophe-inducing collisions do not lead to self-organization of microtubules into parallel arrays, while zippering does. They have also indicated that changes in dynamic-instability parameters modify self-organization, which, in turn, is in good correspondence with the results by Shi and Ma and by Tindemans *et al.* Authors also managed to show that microtubule-independent nucleation must dominate [69].

Apart from that, in the article by Eren *et al.* the authors have introduced a three-

15
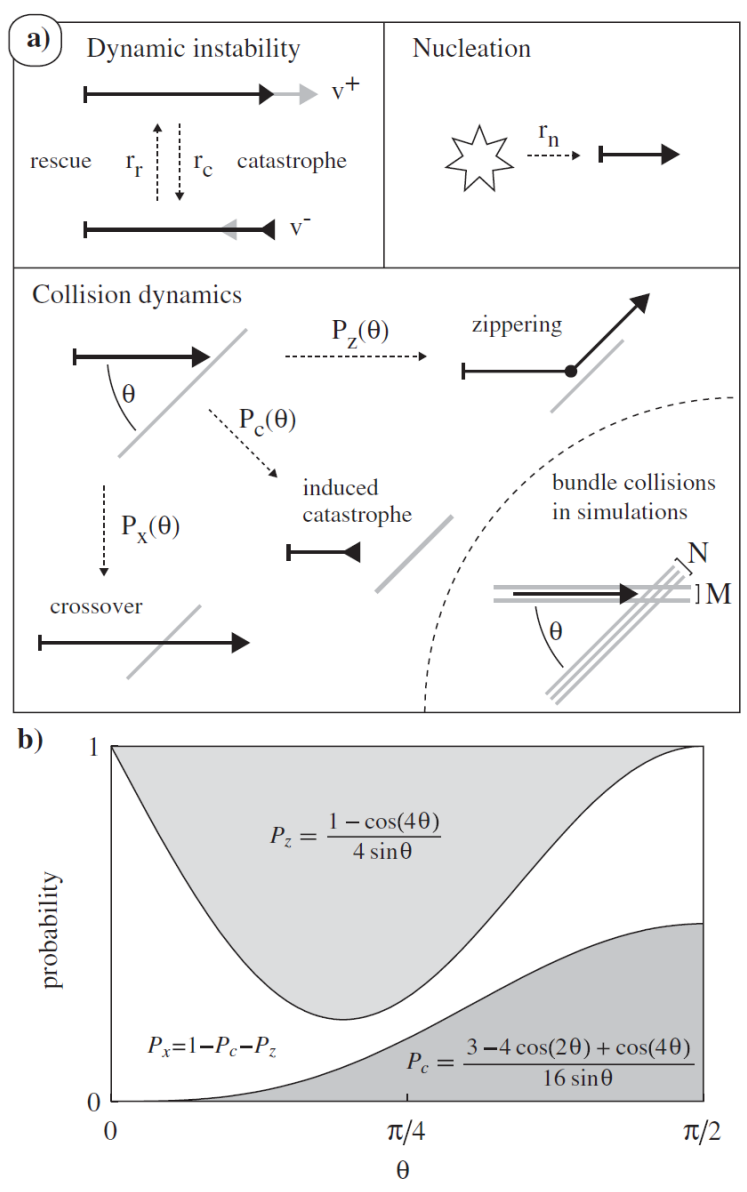
Figure 1.10.: a) Schematic overview of the effects and parameters included in the model by Tindemans, Hawkins and Mulder; b) Angle dependence of possible outcomes of collisions in their model. Picture taken from[68]

1.3 Models for investigation of microtubule orientation

dimensional model with the account for microtubules' dynamic instability and intermicrotubule interactions for the investigation of forming oblique arrays. They have shown that boundary conditions conditions at the end walls are important for stabilizing the system, but not as much as intermicrotubule interactions. However, dynamic instability parameters in their model were not able to generate oblique micrutubule arrays [70].

2. Ordering of microtubules: problem statement, methods and the model

2.1. Problem statement

As we have shown in sec. 1.3, the models presented so far have clarified our understanding of how microtubules form parallel arrays. However, most of them explain only the *existence* of the orientation of microtubules. The question why microtubules orient along major stress lines or how they reorient in response to changes in the environment remains open. Models by Tindemans *et al.* and by Allard *et al.* concentrate mostly on the investigation of collision rules, they predict the existence of the stable oriented state under certain conditions [68, 72, 69]. The existence of the same state is also predicted in the model by Shi and Ma [67]. However, these models do not explain the orientation of microtubules in the direction perpendicular to the growth axis. Neither they explain the action of the external stimuli, such as mechanic deformation or action of the hormones. In the model by Baulin *et al.* it has been shown that external stimuli can affect the microtubules, but the nature of the action of those stimuli remained undefined in their model. Moreover, this model lacked dynamic instability - an important quality of microtubules [65]. In the model by Eren *et al.* an attempt was made to investigate the role of the geometry - however, the authors haven't explored sufficiently enough the conditions when it the orientation may happen [70].

Computational methods along with mathematical analysis may provide a powerful tools for description of biological systems and for explanation of the observed phenomena. In this work we are using analytical calculations for exploration of properties of microtubule arrays. We are also using Monte-Carlo simulations for the

investigation of:

- The influence of mechanical stress on the orientation of microtubules;

- The effects of hormones' action on microtubule arrays;

- The combined impact of mechanical stress along with hormones' action on the cortex of microtubules.

2.2. Methods

According to the minimal model described in Ref. [65], a microtubule is a rigid rod that can grow at a plus-end and shorten at a minus-end. The collisions with other microtubules perturb the growth of microtubules, which itself is sufficient to induce a global order in the system without even excluded volume effects that are necessary for ordering in ordinary lyotropic liquid crystals, which comes from purely collective and kinetic interaction between microtubules. However, this model, due to its simplicity, assumes infinite and unrestricted growth of perfectly aligned microtubules, thus the model should include dynamic instability of the plus-end, which would lead to a stationary state of ordered micotubules[67, 68, 72].

Thus, in contrast to Ref. [65], our model is a three-state model, where microtubule may exist in the growing state (g), shrinking state (s) and blocked state (d), which is similar to Refs. [68, 72]. The length and the position of each microtubule change with time. Every time interval Δt the minus-end of each microtubule is shortened by $v_- \Delta t$, where v_- is the speed of shrinkage of the minus-end. The speed of elongation of the plus-end is v_g and the speed of shrinkage is v_s. The plus-end of initially growing microtubule can experience catastrophes with the rate P_c and rescues with the rate P_r, can be blocked due to collisions with the rate P_b and unblocked with the rate P_{ub}, thus providing stochastic oscillations of microtubule length. If the length of a microtubule goes to 0, it disappears, while new microtubules are created with the nucleation rate P_n (Figure Fig. 2.2). The balance between growing and shrinking,
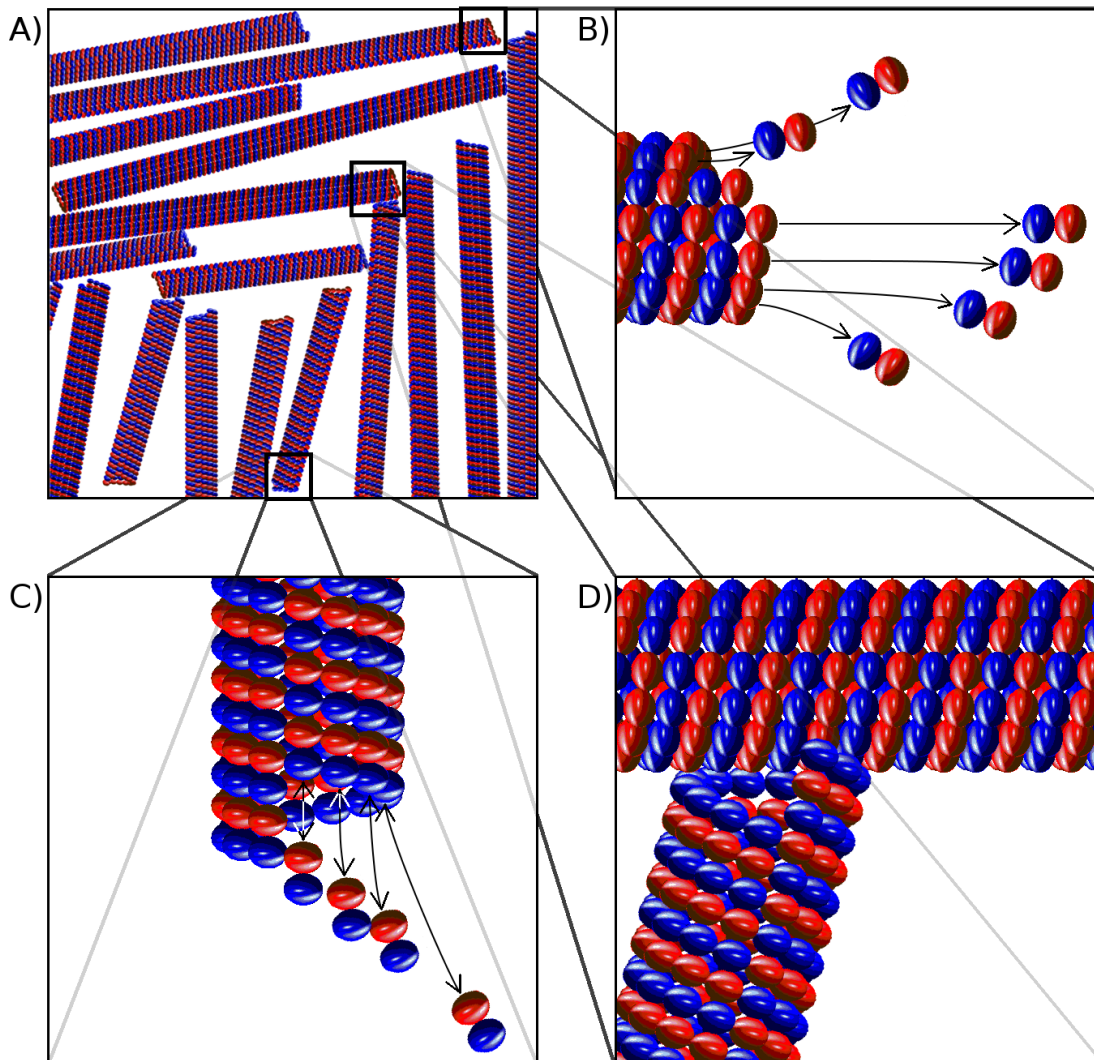
Figure 2.1.: Microtubule dynamics presented in the model. A) Overview of the array of microtubules. B) Minus-end shrinkage. C) Plus-end shrinkage and growing. D) Blocking of the growth of one microtubule by another.

nucleation and disappearing of microtubules in a steady state insures dynamic stability of the average number of microtubules and their average length. The values of parameters are given in Tab. 2.1. If a microtubule occasionally intersects any other microtubule, the growth step is rejected and the microtubule passes from growing to blocked state b. The shrinkage and growth can be reversed stochastically according to the given probabilities. Thus, every time step the length of a microtubule either increases (in state g) by $(v_g - v_-)\Delta t$ or decreases (in state s) by $(v_s + v_-)\Delta t$ or decreases (in state b) by $v_-\Delta t$ in a blocked state (Figure Fig. 2.2). The model by Allard *et al.* [69] includes complex collision rules, requiring the introduction of a critical entrainment angle Θ_z. However, collision-induced catastrophes alone can induce a global ordering and we use such simple description.

Parameter	Dimension	Value
Plus-end growth rate v_g	nm/s	$70 - 100$
Plus-end shortening rate v_s	nm/s	$200 - 230$
Minus-end shortening rate v_-	nm/s	$15 - 40$
Catastrophe probability P_c	1/s	$40 - 80 \times 10^{-3}$
Rescue probability P_r	1/s	124×10^{-3}
Nucleation rate P_n	1/s	5000

Table 2.1.: The parameters used for similations. These parameters are based on experimental data by Dixit *et al.* [61] and Shaw *et al.* [8].

For computations we use Monte-Carlo simulations - a powerful tool for calculations of unknown probabilistic entity, in our case - for estimation of ordering of microtubules. Monte-Carlo methods are widely used in physical or mathematical problems and are most useful when deterministic algorithm can not be implied. They are especially useful for simulating phenomena with significant uncertainty in inputs and systems with a large number of coupled degrees of freedom.

In mathematics, Monte-Carlo methods are used in general to solve various problems by generating suitable random numbers and observing that fraction of the numbers that obeys some property or properties. The most common application of the Monte-Carlo method is Monte-Carlo integration. The method is useful for obtaining numerical solutions to problems too complicated to solve analytically.
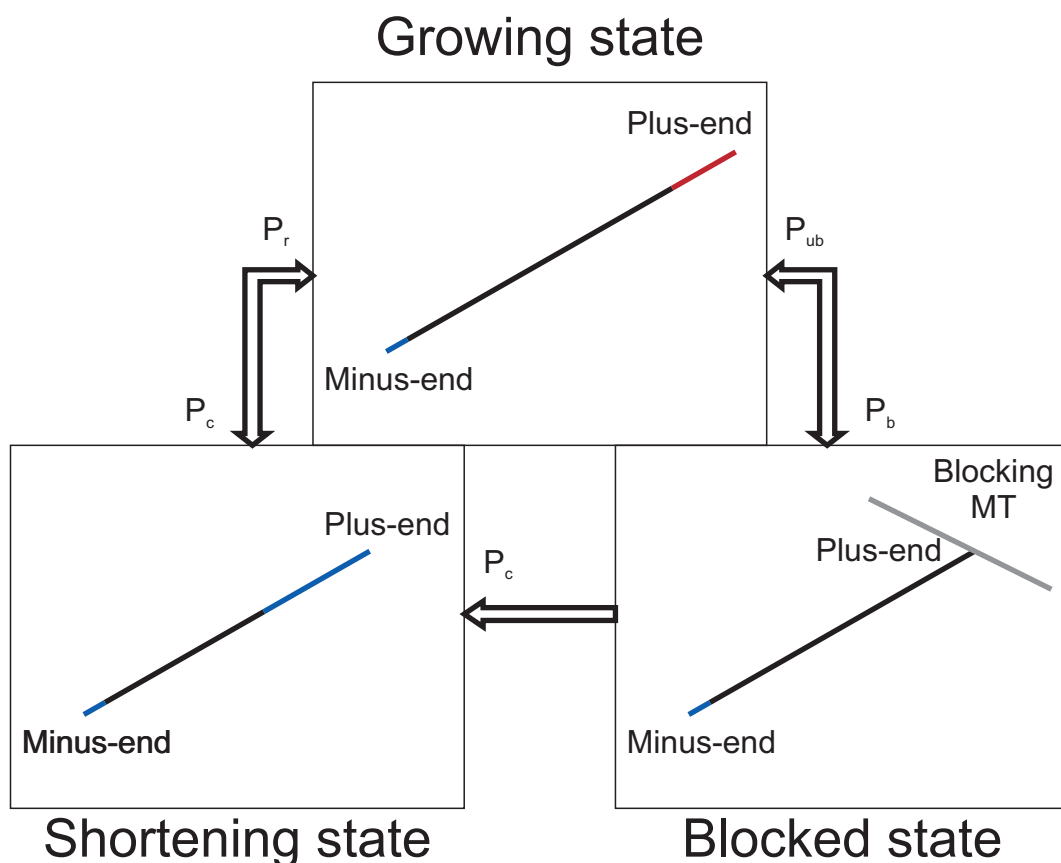
Figure 2.2.: Schematic image of the states in which microtubules persist and switching between the states.

In physics Monte-Carlo simulations are usually used for solving multibody problems. Monte-Carlo methods are very important in computational physics, physical chemistry, and related applied fields, and have diverse applications from complicated quantum chromodynamics calculations to designing heat shields and aerodynamic forms. In statistical physics Monte Carlo molecular modeling is an alternative to computational molecular dynamics, and Monte Carlo methods are used to compute statistical field theories of simple particle and polymer systems[73]. Quantum Monte Carlo methods solve the many-body problem for quantum systems. In experimental particle physics, Monte Carlo methods are used for designing detectors, understanding their behavior and comparing experimental data to theory. In astrophysics, they are used in such diverse manners as to model both the evolution of galaxies [74] and the transmission of microwave radiation through a rough planetary surface [75]. Monte Carlo methods are also used in the ensemble models that form the basis of

23

modern weather forecasting.

In computational biology and biophysics Monte-Carlo methods compete with Molecular Dynamics. Monte-Carlo methods are used for solving problems ranging from microscopic (e.g. studying the properties of proteins or membranes [76, 77]) to mesoscopic (e.g. simulations of ogranelles' movements [78]) and macroscopic scale (e.g. for simulation breast cancer screening programmes [79]).

2.3. Theoretical model

To get more strict mathematical description of the model and to compare it more thoroughly with the other models it is possible to introduce a theoretical "coarse-grained" analysis similar to those described by Baulin *et al.* or by Allard *et al.* We are using it to show similiarities and differences of the models described in sec. 1.3.[1]

We consider that the seeds of new microtubules are nucleated homogeneously and with random angles. Microtubules cannot change their orientation, but they can change their states between growing (g), shortening (s) and blocked (b). Introducing the corresponding surface concentrations, c_g, c_s and c_b, the total length concentration $k(\Theta, t)$ can be written in the following form:

$$k(\Theta, t) = \int\limits_0^\infty ldl[c_g(l, \Theta, t) + c_s(l, \Theta, t) + c_b(l, \Theta, t)]. \tag{2.1}$$

---

[1]Although the words "coarse-grained analysis" may be confusing, as they are usually referred to those models in which aggregates of small molecules are introduced as one big particle ("grain"), we are calling our approach "coarse-grained" following established tradition. See, for example, [68].

2.3 Theoretical model

A set of evolution equations is written as

$$
\frac{\partial c_g}{\partial t} = - v_g \frac{\partial c_g}{\partial l} + P_r c_s - P_c c_g
$$
$$
+ v_- \frac{\partial c_g}{\partial l} - P_b c_g + P_{ub}(c_\sigma, k)c_b, \tag{2.2}
$$
$$
\frac{\partial c_s}{\partial t} = v_s \frac{\partial c_s}{\partial l} - P_r c_s + P_c c_g
$$
$$
+ P_c c_b + v_- \frac{\partial c_s}{\partial l}, \tag{2.3}
$$
$$
\frac{\partial c_b}{\partial t} = v_- \frac{\partial c_b}{\partial l} + P_b c_g - P_c c_b
$$
$$
- P_{ub}(c_\sigma, k)c_b. \tag{2.4}
$$

where $P_r c_s = \Phi_r[c_s]$ and $P_c c_g = \Phi_c[c_g]$ along with $P_c c_b = \Phi_c[c_b]$ are the spontaneous flux terms [72] responsible for rescue and catastrophe respectively; $-v_g \frac{\partial c_g}{\partial l} = \Phi_g[c_g]$, $v_s \frac{\partial c_s}{\partial l} = \Phi_s[c_s]$ and $v_- \frac{\partial c_b}{\partial l} = \Phi_-[c_b]$ describe fluxes caused by growth and shrinkage of plus-end and shortening of minus-end respectively [59, 65, 72, 68]. Blocking term is determined by the collisions between microtubules when a growing microtubule collides with another microtubule with a rate $P_b c_g(\Theta) = v_+ c_g(\Theta) \int d\Theta' \sin |\Theta - \Theta'| k(\Theta') = \Phi_b[c_g, k]$, where $\sin |\Theta - \Theta'|$ defines the cross section of collisions. This term reminds the second virial coefficient of the Onsager theory [80], but has a completely different physical origin. The unblocking term $P_{ub}(c_\sigma, k)c_b$ is connected with the possibility of a previously blocked plus-end of a microtubule to restart its growing due to disassembly of a blocking microtubule, no matter if it is a shrinkage of a plus-end or shortening of a minus-end. It is related to the concentration $c_b(l, t, \Theta)$ as following $P_{ub}(c_\sigma, k)c_b(\Theta) = \Phi_{ub}[c_b, c_\sigma, k]$.

The initial conditions are the following: at $t=0$ the concentration of shortening and blocked microtubules are equal zero $c_s(l, 0, \Theta) = 0$, $c_b(l, 0, \Theta) = 0$ while c_g is connected with the nucleation rate P_n as $(v_g - v_-)c_g(0, t, \Theta) = \frac{P_n(\Theta)}{2\pi}$, $c_g(l > 0, 0, \Theta) = 0$.

The first model [65] lacked dynamic instability, that means it was missing Φ_c and Φ_r terms in eqs. 2.2-2.4, which are responsible for stabilization of the length of microtubules in ordered arrays and thus these terms are essential for the stationary state in ordered arrays. The model by Hawkins at. al. [72] lacks the minus-end disassembly, i.e. terms Φ_-, Φ_b and Φ_{ub}, but it includes $\Phi_{inducedcat.}$, Φ_{zipper} and $\Phi_{reactivation}$. It's possible to connect their population of "inactive" segments with the

25

population of blocked segments. It is noteworthy, that "zippering" in this model is similar to "blocking" described by the present model, where reactivation occurs due to disassembly of a blocking microtubules, in contrast to disassembly of an active segment of the microtubule in zippering event.

To get a control parameter that defines the behavior of the system, eqs. 2.2-2.4 can be rewritten as:

$$\frac{\partial c_g}{\partial t} + (v_g - v_-)\frac{\partial c_g}{\partial l} = -(P_c + P_b)c_g$$
$$+ P_r c_s + P_{ub} c_b, \tag{2.5}$$

$$\frac{\partial c_s}{\partial t} - (v_s + v_-)\frac{\partial c_s}{\partial l} = -P_r c_s + P_c(c_g + c_b), \tag{2.6}$$

$$\frac{\partial c_b}{\partial t} - v_-\frac{\partial c_b}{\partial l} = -(P_c + P_{ub})c_b + P_b c_g. \tag{2.7}$$

The sum of these equations gives

$$\frac{\partial}{\partial t}(c_g + c_s + c_b) + \frac{\partial}{\partial l}((v_g - v_-)c_g - (v_s + v_-)c_s - v_- c_b) = 0. \tag{2.8}$$

The steady state implies time derivatives to be equal to zero, leading to the following flux balance equation

$$(v_g - v_-)c_g(l, \Theta) = (v_s + v_-)c_s(l, \Theta) + v_- c_b(l, \Theta), \tag{2.9}$$

or in a more convenient form

$$v_g c_g - v_s c_s = v_-(c_g + c_s + c_b). \tag{2.10}$$

To simplify these equations even more, we assume that the probabilities P_c and P_r are small (see Tab. 2.1), thus the related terms in eqs. 2.5-2.7 may be neglected. This means that shortening microtubules either do not present ,or their length distribution is constant, thus eq. 2.10 yields in the form

$$(v_g - v_-)c_g(l, \Theta) = v_- c_b(l, \Theta). \tag{2.11}$$

Thus, the dimensionless parameter

$$\alpha = \frac{v_-}{v_g - v_-}, \tag{2.12}$$

2.3 Theoretical model

can be regarded as a control parameter. It coincides with the corresponding control parameter in Ref. [65]. Following the same notations, $v = v_g - v_-$, $\alpha = \frac{v_-}{v}$. Thus, eqs. 2.5-2.7 corresponding to steady state can be rewritten as follows,

$$v\frac{\partial c_g}{\partial l} = -P_b c_g + P_{ub} c_b, \tag{2.13}$$

$$-\alpha v\frac{\partial c_b}{\partial l} = -P_{ub} c_b + P_b c_g. \tag{2.14}$$

Probabilities P_b and P_{ub} are length-independent, thus the solution of this system of differential equations has the following form:

$$c_g(l, \Theta) = A(\Theta)e^{-l/\bar{l}}, \tag{2.15}$$

$$c_b(l, \Theta) = B(\Theta)e^{-l/\bar{l}}, \tag{2.16}$$

where

$$\frac{1}{\bar{l}} = \frac{P_b}{v} - \frac{P_{ub}}{\alpha v}, \tag{2.17}$$

$$A(\Theta) = \alpha B(\Theta). \tag{2.18}$$

It is noteworthy that $1/\bar{l}$ is similar to the growth parameter introduced by Hawkins *et al.* [68, 72].

As it was possible to separate the variables in the solution for the steady state in this simplified model, one can actually show that the changes in the shape of the cell lead to anisotropy. In the work of Baulin [65] it was shown that growth parameter causes the system to persist in different regimes depending on its value: chaotic or ordered; it also accounts for the model presented above. Anisotropy of the cell will cause the angle dependence of both blocking rate P_b and nucleation rate P_n. The unblocking probability P_{ub} is angle-independent. This inhomogeneity will yield different growth parameters g for different angles, causing even different regimes of system's persistence at different angles. This different regimes may compete with each other, but one of them will inevitably be in a preferred position due to anisotropy of nucleation.

In the model by Hawkins *et al.* [65, 72, 68] the minus-end shrinkage speed equals

27

to zero, hence eq. 2.10 yields in the following form

$$v_g c_g(l, \Theta) = v_s c_s(l, \Theta). \tag{2.19}$$

This equation along with the equations, describing the evolution of the system, gives the growth parameter g:

$$g = \frac{P_r}{v_s} - \frac{P_c}{v_g}, \tag{2.20}$$

which characterizes the noninteracting system. This expression corresponds to eq. 2.17 up to notations. "Rescue" is effectively corresponds to unblocking in our model, while "blocking" corresponds to catastrophes.

3. Results

3.1. Influence of a mechanical stress on the ordering of microtubules

Cortex microtubules attached to the cell wall may form stationary states of oriented domains or stay in disordered state depending on the rates of growth and shrinkage, catastrophe rates and concentration[67, 68, 72]. Mechanical stretching or compression of the cell wall anisotropically changes the distance between the microtubules, thus affecting the concentration in the direction of applied force. This, in turn, may induce orientation in disordered arrays or reorient microtubules in ordered arrays. In the following, we investigate the effect of stretching and compression on these two initial stationary states, (i) isotropically oriented, disordered array of microtubules and (ii) oriented domains of microtubules are then subject to stretching and compression (See Fig. 1.8).

3.1.1. Compression-induced orientation in disordered arrays

Set of parameters corresponding to initially disordered arrays (Table Tab. 3.1) leads to formation of stationary disordered state, characterized by the balance between growing, shrinking and blocked microtubules. Thus, stationary average total number of microtubules is provided by the balance between microtubules, that disappear due to collisions with other microtubules or due to catastrophes events, and new-born microtubules appearing with random directions. Freshly appearing microtubules correspond to nucleation sites that are fixed in the cortex, thus we assume that the total number of new-born microtubules per time step and per area is kept constant. However, stretching or compression change the distance between nucleation sites and thus, the nucleation rate, being inversely proportional to the area, may vary with the direction.

Parameter	Dimension	Value
Plus-end growth rate v_g	nm/s	70
Plus-end shortening rate v_s	nm/s	225
Minus-end shortening rate v_-	nm/s	15
Catastrophe probability P_c	1/s	64×10^{-3}
Rescue probability P_r	1/s	124×10^{-3}
Nucleation rate P_n	1/s	5000

Table 3.1.: The parameters used for similations of a disordered array. These parameters are based on experimental data by Dixit *et al.* [61] and Shaw *et al.* [8].

Stationary disordered array of $10 \times 10 \mu m^2$ (Fig. 3.1A)) is compressed in one direction by two times (Fig. 3.1B)). This compression provokes orientation of microtubules in the direction of compression. In contrast, the stretching by two times of the array does not lead to orientation. This goes inline with the observations of microtubule orientation perpendicular to the gravity vector in gravitropism in roots [40] and may be related to coordinated patterns of microtubule arrays governed by mechanical stress [29].

The degree of microtubule orientation can be described by the nematic order parameter, which is proportional to the cost function $\sigma(\Theta) = \overline{\cos^2(\Omega - \Theta)}$, where Θ is the direction of the director and Ω is the direction of individual microtubule and the bar signifies the ensemble average. However, microtubules has intermittent length and the ordering of the domains is determined by long microtubules [65]. Thus, the cost function should include the length and we use the following function [65]

$$\sigma_l(\Theta) = \overline{l^2 cos^2(\Omega - \Theta)}. \tag{3.1}$$

With this, an anisotropy ratio S_l can be defined as [65]:

$$S_l = \frac{\sigma(\Theta_{max}) - \sigma(\Theta_{min})}{\sigma(\Theta_{max}) + \sigma(\Theta_{min})} \tag{3.2}$$
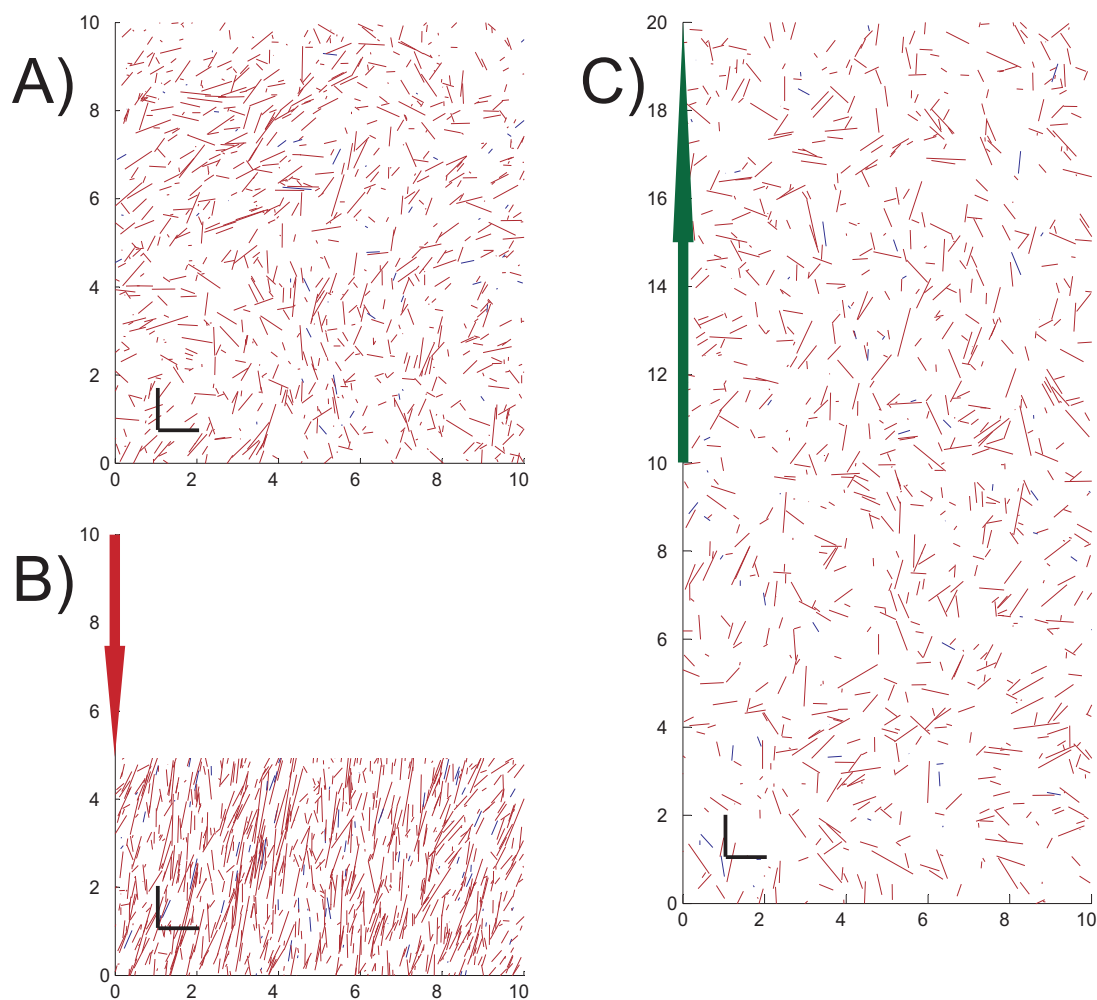
Figure 3.1.: Snapshots of microtubule arrays (only 1000 longest microtubules are shown) evolving from A) initially homogeneous and isotropic array $10 \times 10 \mu m$ under B) compression and C) stretching. Shrinking microtubules (state s) are shown in blue, other microtubules (state b and g) are shown in red. Bar indicates $1 \mu m$.
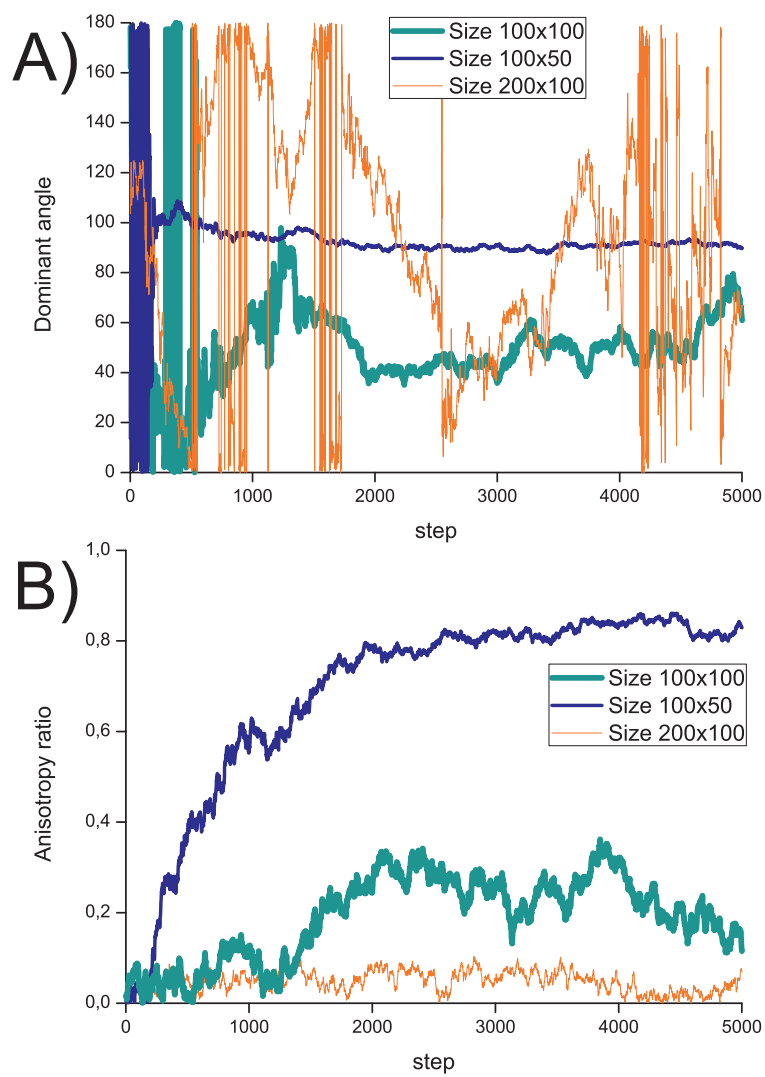
Figure 3.2.: For initially isotropic array in Fig. 3.1: A) Dominaiting angle versus simulation timestep; B) Anisotropy ratio versus simulation timestep.

3.1 Influence of a mechanical stress on the ordering of microtubules

and the dominant angle is given by [65]:

$$tan2\Theta_l = \frac{\overline{l^2 sin2\Omega}}{\overline{l^2 cos2\Omega}}.$$

(3.3)

The anisotropy ratio S_l and the dominant angle Θ_l as function of time are given in Fig. 3.2A) and B).

3.1.2. Stretching-induced disorientation in ordered arrays

Parameter	Dimension	Value
Plus-end growth rate v_g	nm/s	80
Plus-end shortening rate v_s	nm/s	200
Minus-end shortening rate v_-	nm/s	40
Catastrophe probability P_c	1/s	64×10^{-3}
Rescue probability P_r	1/s	124×10^{-3}
Nucleation rate P_n	1/s	5000

Table 3.2.: The parameters used for similations of an ordered array. These parameters are based on experimental data by Dixit *et al.* [61] and Shaw *et al.* [8].

Once a stationary ordered array is formed (Fig. 3.3A)), the orientation of the array is governed by longest microtubules [65], which are also the oldest microtubules, and thus having biggest life expectancy and hence more persistent. Since the angles of microtubules in this model are irrevocably fixed during the life cycle, changing the direction of the ordered array implies disassemble of these leading microtubules, which may require collisions with domains with even longer microtubules. Thus, compression of the ordered arrays only increases the distance between microtubules, that may increase the order, but may not lead to disassemble of microtubules. This is shown in Fig. 3.3B) and the corresponding plot of the dominant angle and anisotropy ratio S_l, Fig. 3.4.

In turn, stretching of the cortex increase the distance between microtubules, thus new-born microtubules may grow longer before they collide with the dominant microtubules and bring more random orientations into arrays. Fig. 3.3C) and Fig. 3.4

33
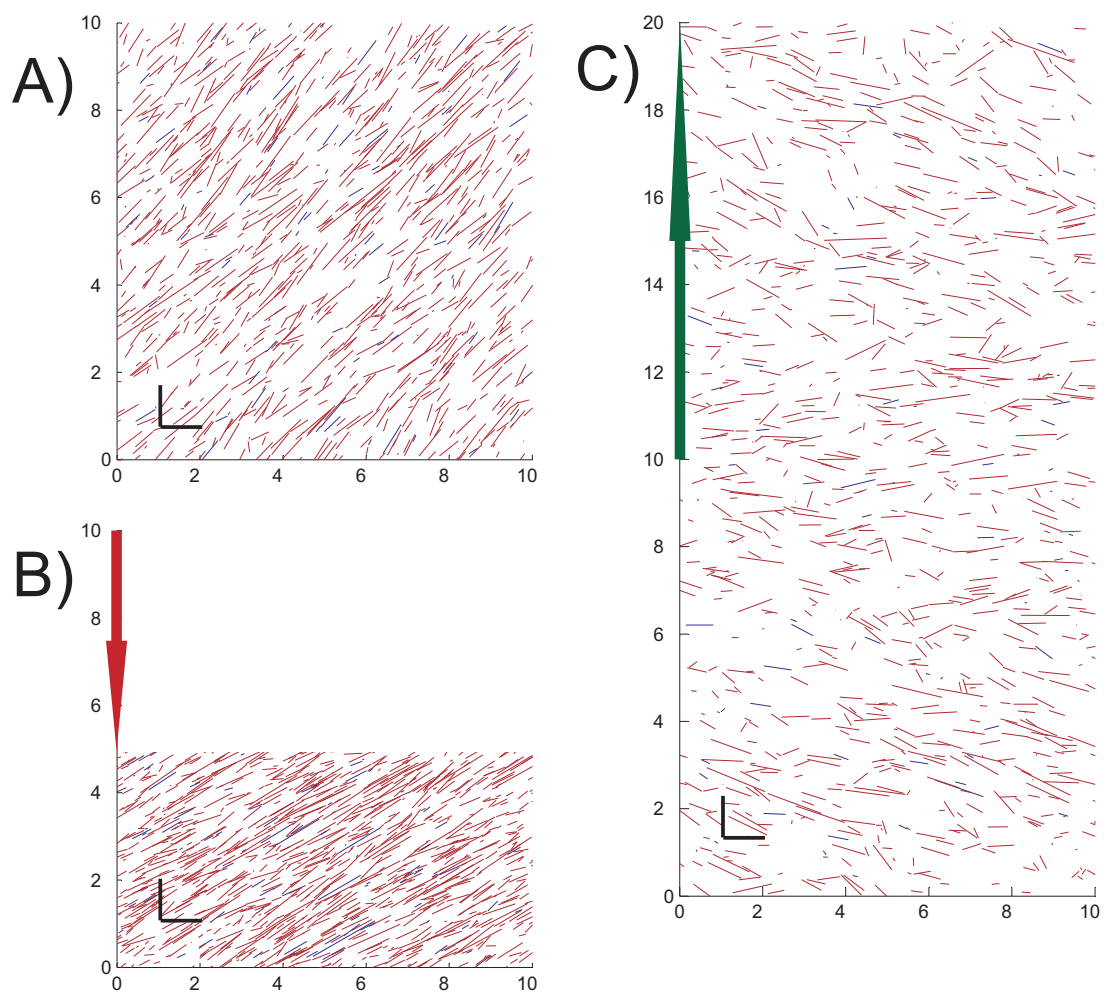
Figure 3.3.: Snapshots of microtubule arrays (only 1000 longest microtubules are shown) evolving from A) ordered array $10 \times 10\mu m$ under B) compression and C) stretching. Shrinking microtubules (state s) are shown in blue, other microtubules (state b and g) are shown in red. Bar indicates $1\mu m$.

3.1 Influence of a mechanical stress on the ordering of microtubules

show that stretching may considerably reduce the order in the arrays, and, in principle, may lead to complete disorientation of the arrays.

Both effects, disorientation of the arrays due to stretching and orientation induced by compression, may work together to help to reorient microtubule arrays in response to mechanical stress on the cortex.

3.1.3. Length distribution

The detailed balance model introduced in sec. 2.3 shows that the length distribution of microtubules in steady state is exponential which is consistent with the previous model [65].

Simulations also show the exponential length distribution, Fig. 3.5. The lengths in disordered array (squares) are shorter than in ordered array (circles). This is the manifestation of the fact that microtubules in ordered arrays are more aligned parallel to each other and hence have less mutual collisions, that reduce their lengths.

Now we are able to compare the results of simulations with theoretical predictions. In ordered arrays $\alpha = v_-/(v_g - v_-) = 0.9$. Parameters listed in Tab. 3.2 lead to $P_b = 0.3$ and $P_{ub} = 4 \times 10^{-2}$ and thus $1/\bar{l} = \frac{P_b}{v_g - v_-} - \frac{P_{ub}}{v_-} = -0.6$. Meanwhile the slope in Fig. 3.5 (circles) is -0.5. Theoretical analysis shows that α defines the quotient of blocked microtubules to growing microtubules, thus the value $1/(1 + \alpha)$ describes the percentage of blocked microtubules in the general number of microtubules (the number of shortening microtubules is still considered negligible). This rate in simulations is estimated as 0.6, while detailed balance estimation gives 0.52. The values of P_b and P_{ub} are comparable with the values of catastrophe and rescue rates P_c and P_r, thus the difference between theoretical and experimental data may be explained.

In disordered arrays the values for P_b and P_{ub} are estimated as 0.2 and 4×10^{-2} correspondingly. It is notable that these possibilities do not differ much from those obtained for ordered arrays - that means that difference in regimes is primarily determined by dynamic properties of microtubules. Detailed balance estimation

35
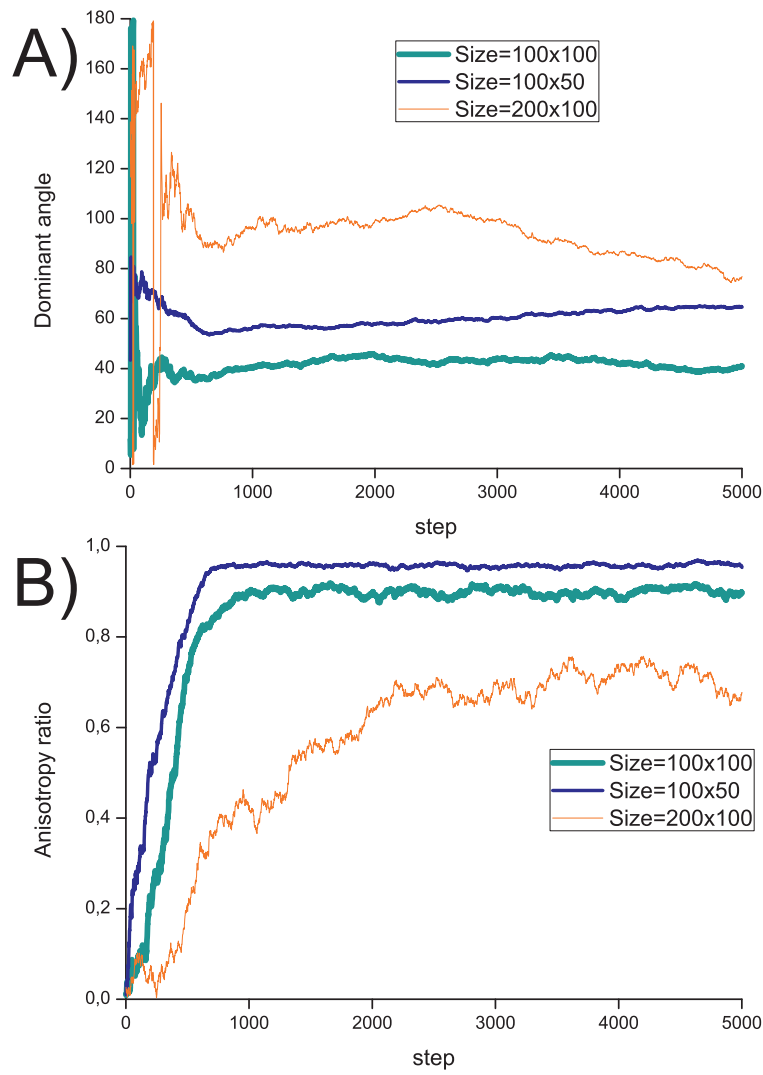
Figure 3.4.: For initially isotropic array in Fig. 3.3: A) Dominaiting angle versus simulation timestep; B) Anisotropy ratio versus simulation timestep.
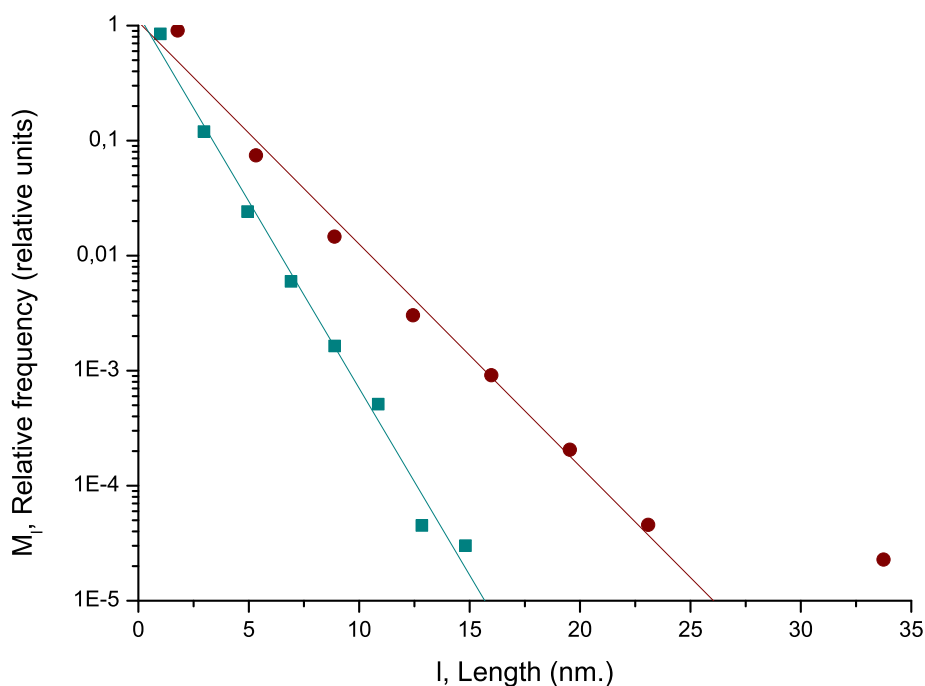
Figure 3.5.: Length distribution of microtubules for ordered (circles) and disordered (squares) states. Linear fitting shows exponential dependence.

gives $1/(1 + \alpha) = 0.8$, $1/\bar{l} = 0.1$ for disordered array, while simulation give 0.7 and 0.8 respectively. The discrepancy is due to catastrophes and rescues rates that are neglected in detailed balance estimates, but are more important than in ordered state.

3.2. Chemical effects on the ordering of microtubules

Chemical agents, such as hormones (e.g. auxin [41]) or ethylene, are often reported to modify microtubule dynamics. The nature of this event is not yet clear, but it may be suggested that chemical agents catalyse or inhibit the action of microtubule-associated proteins (MAPs), and this changes are connected with concentrational gradients. These proteins change dynamic parameters of microtubules, generally affecting growth velocities or catastrophe rates. The action of chemical agents may form different paterns within a plant cell, leading to assymetric growth. Although previously it has been shown that changes in dynamic instability parameters are not

37

sufficient to generate oblique microtubule arrays [70], we try to test this hypothesis once again, as we believe that former negative result was connected with the complexity of the model.

We propose that chemical agents influence dynamic instability parameters, such as catastrophe rate. Concentrational gradient of chemical agent leads to polarity and anisotropy in the values of catastrophe rate. It becomes higher in the direction along concentrational gradient. This idea is actually consistent with experimental data presented in literature: for instance, auxin has been identified to generate polarity in distribution of auxin transporters, proteins of PIN family [51]. These proteins are linked with microtubule orientation regulator CLASP [81, 82, 83] and with microtubule-associated protein MAP65 [84]. Such a mechanism may regulate correlation between orientation of cortical microtubules and concentrational gradient.

3.2.1. Orientation and reorientation of microtubules due to the action of chemical agents

Two sets of parameters are picked to provoke spontaneous organization of microtubulesTab. 3.3. An increase in catastrophe rate along one chosen direction eliminates old microtubules oriented in this selected direction, while microtubules oriented in the opposite direction are expected to persist for longer time. Oldest microtubules are also the longest ones, thus guiding the orientation of the whole array. To test this more thoroughly we change the polarity of chemical agent once the orientation is established. This change indeed leads to reorientation, what is shown in Fig. 3.6 and Fig. 3.7.

Parameter	Dimension	Value	
Plus-end growth rate v_g	nm/s	100	
Plus-end shortening rate v_s	nm/s	200	225
Minus-end shortening rate v_-	nm/s	40	15
Catastrophe probability P_c	1/s	$45 - 85 \times 10^{-3}$	
Rescue probability P_r	1/s	124×10^{-3}	
Nucleation rate P_n	1/s	5000	

Table 3.3.: The parameters used for similations. These values are based on experimental data by Dixit *et al.* [61] and Shaw *et al.* [8].

38

3.2 Chemical effects on the ordering of microtubules

First set of parameters lead to slower reorientation: although anisotropy ratio soon recovers its high value (See Fig. 3.7B)), it takes a lot of time for microtubules to reorient, as it may be seen in the Fig. 3.7A). Eventually the system reaches the state shown on Fig. 3.6B), but takes around 10000 steps.

An important conclusion can be made: as shortening microtubules shrink with the same rate $v_s + v_- = 240$ nm/s, the difference in reorientation behaviour is primarily defined by populations of blocked and growing microtubules. Thus, as it has been predicted by theoretical analysis, parameter $\alpha = \frac{v_-}{v_g - v_-}$ serves as critical in this case.

On the graph of anisotropy ratio (Fig. 3.7A)) an intermediate state is clearly seen. It corresponds to the state when old orientation has already been destroyed and a new one has not yet been formed. This state may be particulary interesting as microtubules in such state may form domains, as it was shown in [65]. We analyse domain existence for both sets of parameters. For second set , as it can be easily seen, domains ao not exist (See Fig. 3.8B)). Results for first set we analyse with introducing of the space anisotropy ratio. For its calculaton we split our simulation box to smaller "cells" and then calculate anisotropy ratio inside each "cell", taking into account only the microtubules inside it. The results are present on Fig. 3.8.

This results mean that polar action of chemical agents may lead to orientation of microtubue array, and the change in this action may lead to reorientation. The process of reorientation involves the formation of domains.

3.2.2. Pattern formation

Another interesting case is the formation of local patterns for an anisotropic cell growth. To investigate such a case we generate a concentrational gradient only locally, not covering all the simulation area. In that specific area a domain's creation will be provoked.

We investigate a case when concentrational gradient provokes the emergence of a circular domain, i.e. a domain where microtubules are aligned along tangents to
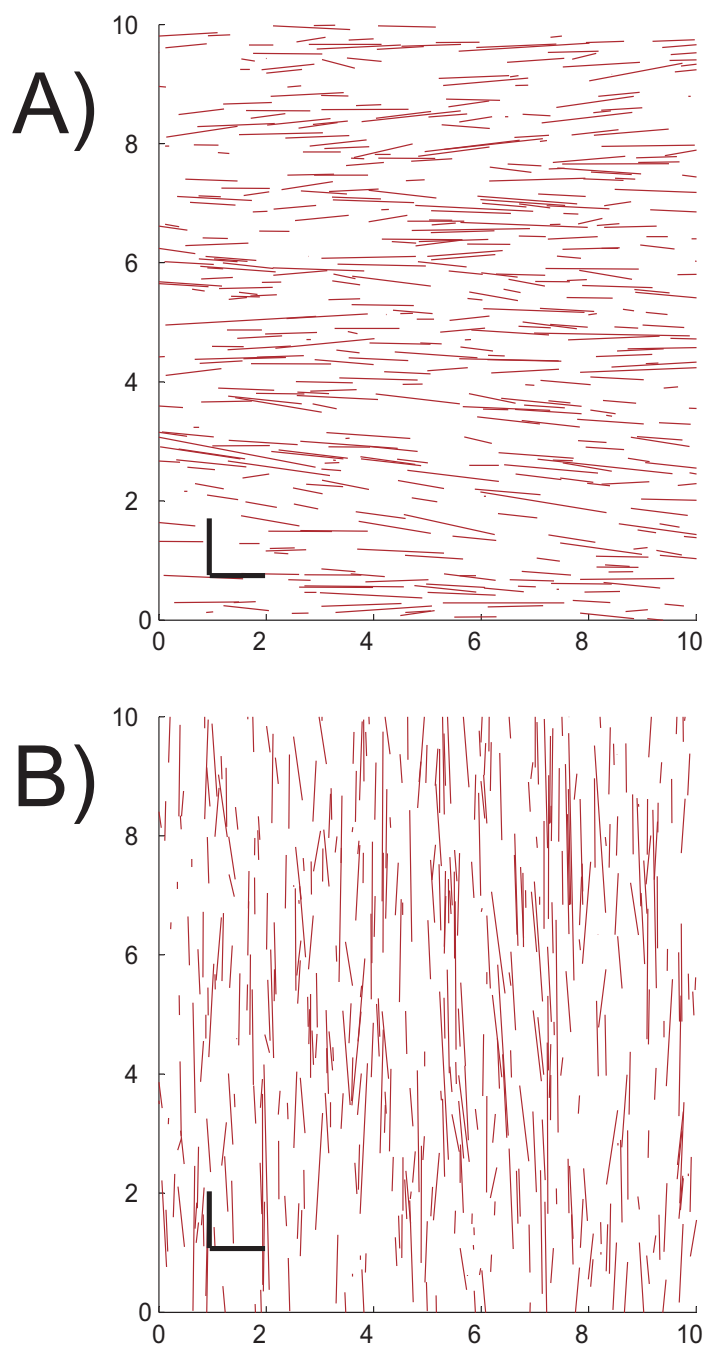
Figure 3.6.: Microtubules A) before and B) after reorientation. Only 1000 longest microtubules are shown. Bar indicates $1\mu m$.

3.2 Chemical effects on the ordering of microtubules
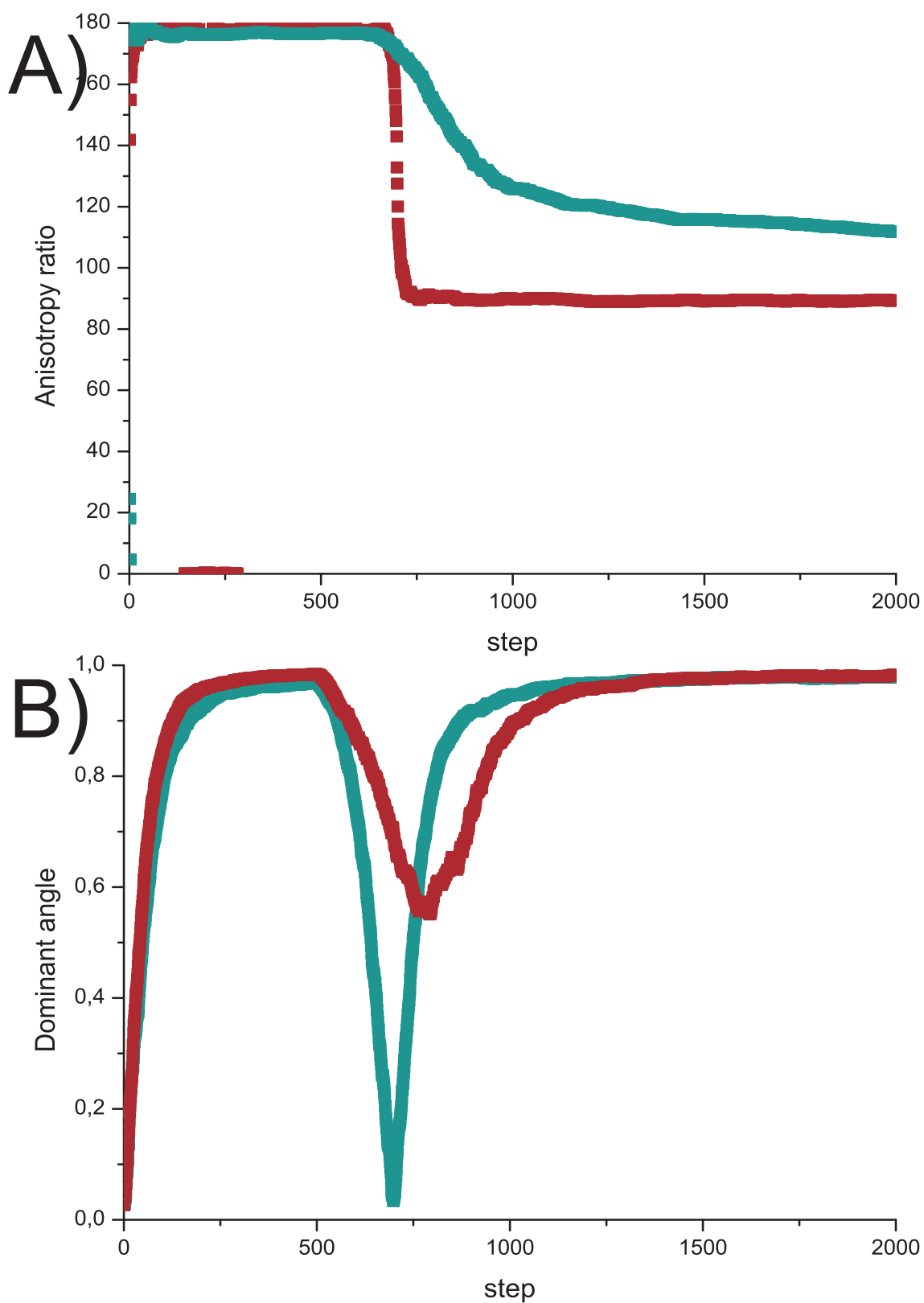
Figure 3.7.: For two sets of parameters in Tab. 3.3A) Dominant angle versus simulation timestep; B) Anisotropy ratio versus simulation timestep. First set of parameters is represented by wine dots, second - by cyan dots.
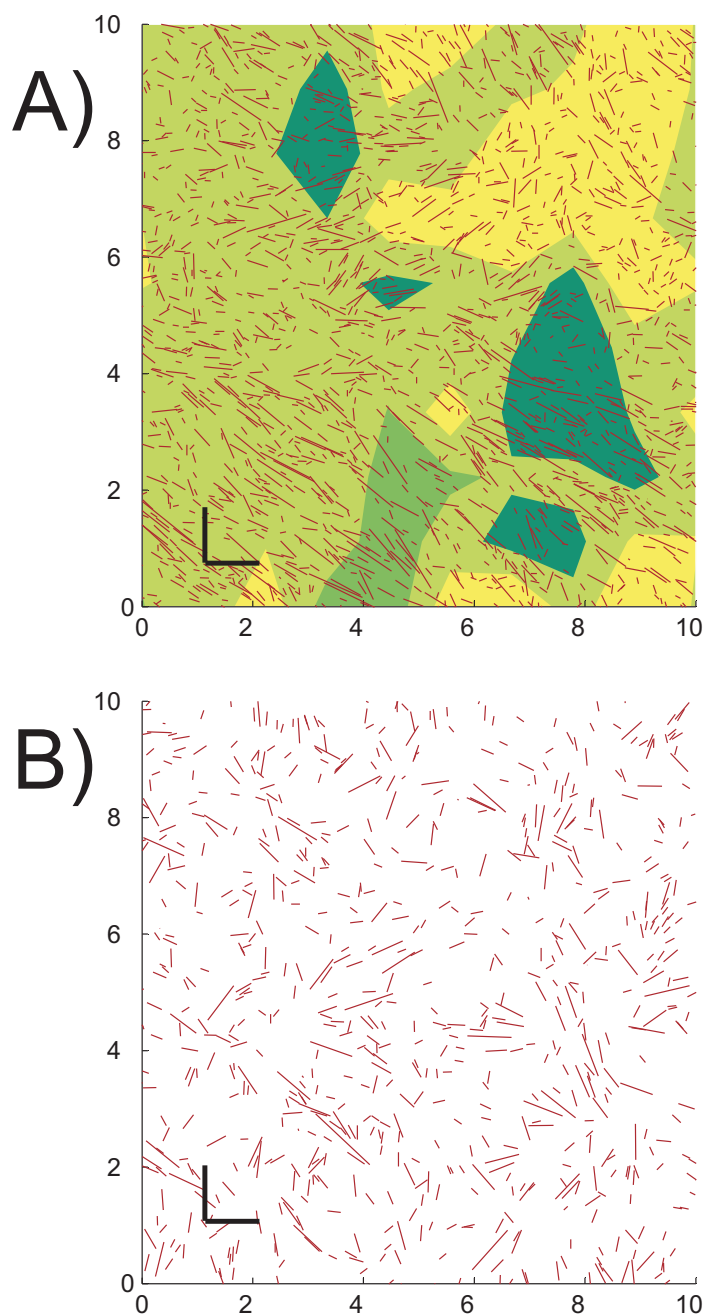
Figure 3.8.: A snapshot of an intermediate state of microtubules' array reorientation for: A) First set of parameters from Tab. 3.3. Greener areas correspond to areas with higher anisotropy ratio; B) Second set of parameters from Tab. 3.3. All microtubules are shown. Bar indicates $1\mu m$.
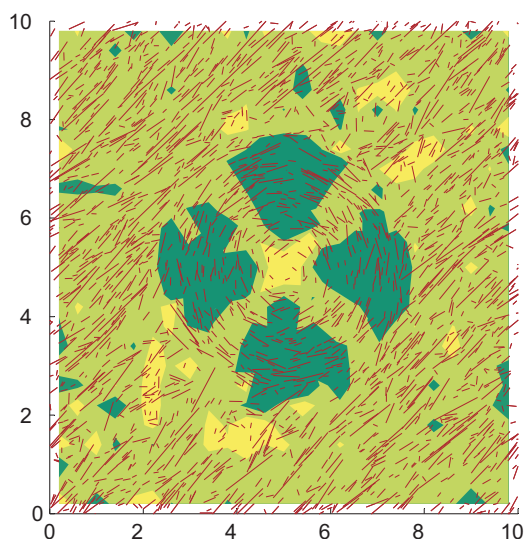
Figure 3.9.: A snapshot of microtubule array with a circular pattern. Greener areas correspond to areas with higher anisotropy ratio.

a circle. Typical results are shown on Fig. 3.9. Circular gradient is distinguished by space anisotropy ratio. A global orientation of microtubules is provoked spontaneously in the area where concentrational gradient is not present and it is not perturbed by circularly oriented microtubules, i.e. there is no orientation transduction in the system.

3.3. Combined action of dynamic instability changes and mechanical stress on the ordering of microtubules

As it was shown in sec. 3.1 and sec. 3.2, mechanical stress and changes in dynamic instability conditioned by external stimuli are alone sufficient enough to provoke ordering. Their combined action is also interesting to be studied as in real cells these effects are present simultaneously. Here we consider that chemical agents change growth and shrinkage velocities of microtubules and we use parameters form Tab. 3.1 and Tab. 3.2.

First set of parameters for an array of $10 \times 5 \mu m^2$ yields an ordered array with pre-defined dominant angle. The changes in dynamic instability lead to faster and

43

Parameter	Dimension	Value from Tab. 3.1	Value from Tab. 3.2
Plus-end growth rate v_g	nm/s	70	80
Plus-end shortening rate v_s	nm/s	225	200
Minus-end shortening rate v_-	nm/s	15	40
Catastrophe probability P_c	1/s	64×10^{-3}	
Rescue probability P_r	1/s	124×10^{-3}	
Nucleation rate P_n	1/s	5000	

Table 3.4.: The parameters used for similations of combined effect of mechanical stress and dynamic instability changes. These parameters are based on experimental data by Dixit *et al.* [61] and Shaw *et al.* [8].

greater ordering (Fig. 3.10). However, in this case the role of small fluctuations becomes greater as ordering happens faster, so dominant angle is no longer pre-defined, and an oblique array can be formed.

For an array of $20 \times 10 \mu m^2$ the parameters from first column of Tab. 3.4 yield a highly unordered array (Consult Fig. 3.1C)). The increases in plus-end growth rate and minus-end shrinkage rate along with slight decrease in plus-end shortening rate lead to formation of an ordered array with defined orientation (Fig. 3.11).

3.3 Combined action of dynamic instability changes and mechanical stress on the ordering of microtubules
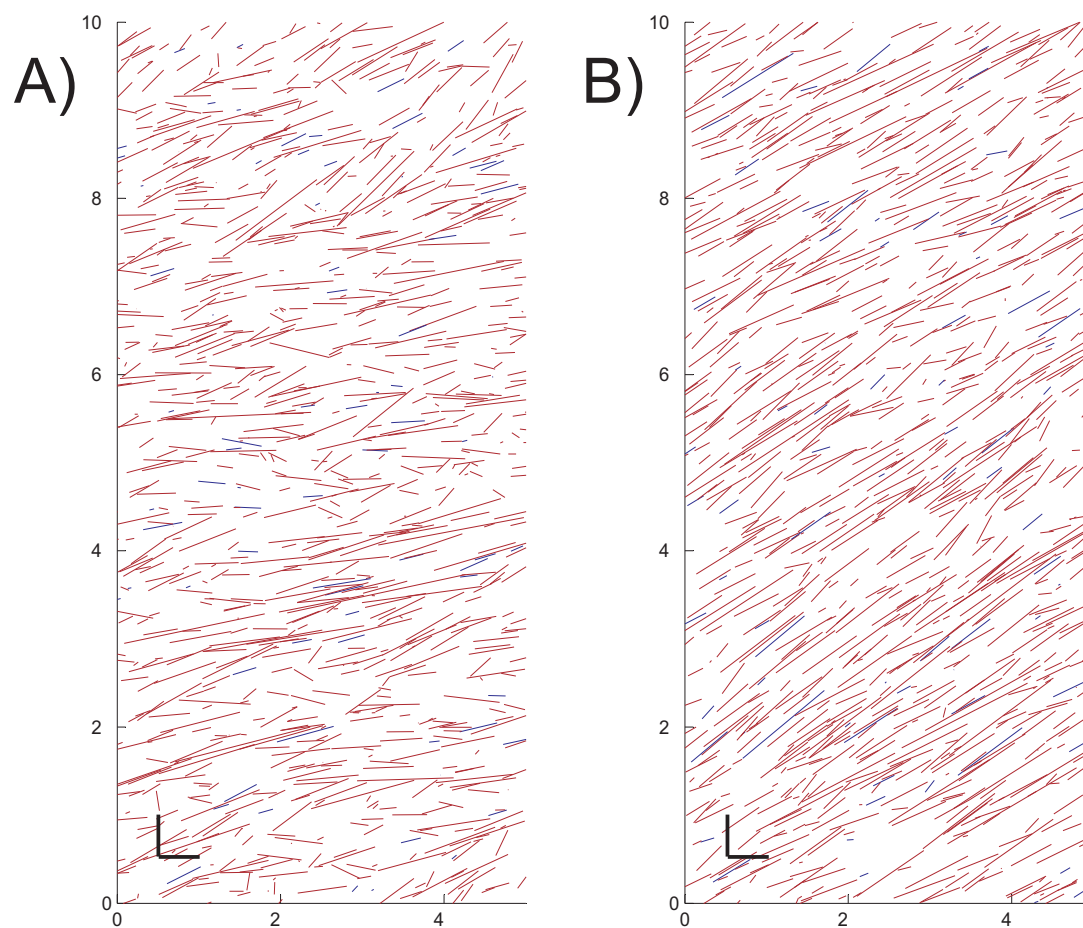
Figure 3.10.: Snapshots of microtubule arrays (only 1000 longest microtubules are shown) of $10 \times 5\mu m^2$: A) Ordered array with pre-defined dominant angle; B) Ordered array without pre-defined dominant angle.
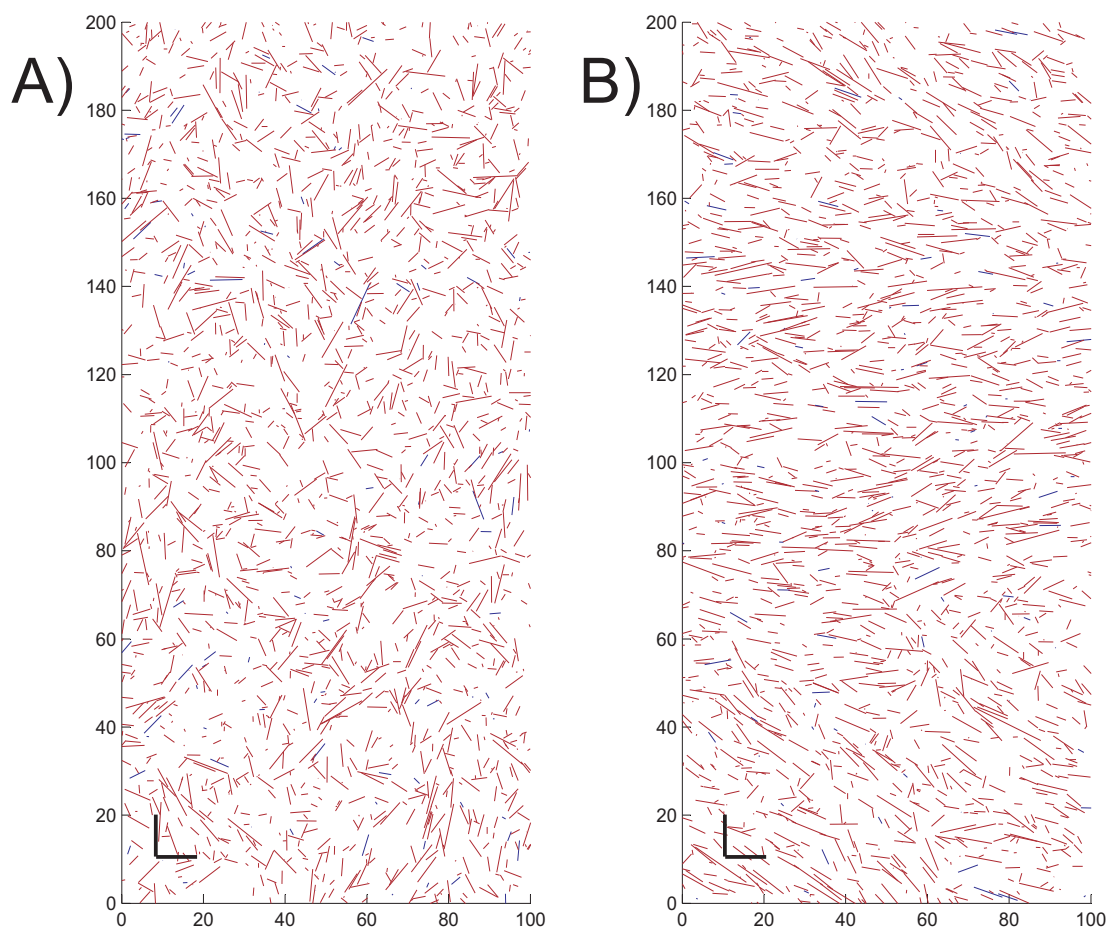
Figure 3.11.: Snapshots of microtubule arrays (only 1000 longest microtubules are shown) of $20 \times 10 \mu m^2$: A) Unrdered array; B) Ordered array with pre-defined dominant angle.

4. Conclusions

1. The model of kinetic orientation of microtubules arrays due to collisions was used to study the effect of mechanical deformation (compression and stretching) of the cortex in plant cells. Such deformations may arise from the elongation of the cell due to growth influenced by the external stimuli such as gravitational field, transduct by sedimenting amyloplasts or light in phototropic growth. The mechanical compression and stretching of the cell is also important in morphogenesis. We have shown that the compression of initially disordered microtubule arrays itself may induce a global order, where microtubules are oriented along the action of mechanical stress.

2. The same model was also applied to investigate the effects of modifying of dynamic instability parameters, such as microtubule's growth rate and catastrophe probability. Such changes may be caused by the action of different chemical agents creating intracellular polarity. This polarity is thereover transferred to forced microtubule array reorientation, possibly by promoting or inhibiting microtubule-associated proteins' action. We have shown that such mechanism is easily obtained and microtubules form different arrays ranging from simply oriented to highly patterned.

3. Combined action of two factors has also been studied in this work. We have managed to show that mechanical stass may compement the action of chemical agents and vice versa.

4. Ordered microtubule arrays, in turn, can direct cellulose microfibrils assembly, thus resulting in oriented microfibrils growth. Orientation of cellulose microfibrils in a certain direction consequently leads to anisotropy of the cell wall, which, in turn, combined with turgor pressure indicates the direction of cell growth.

A. How gravitropic stimulus and mechanical stress induce microtubule orientation

The Plant Journal

the plant journal

How gravitropic stimulus and mechanical stress induce microtubule orientation

SCHOLARONE™
Manuscripts

SUBMITTED MANUSCRIPT

Research Article

How gravitropic stimulus and mechanical stress induce microtubule orientation

Alexander Muratov and Vladimir Baulin

Departament d'Enginyeria Quimica, Universitat Rovira i Virgili 26 Av. dels Paisos Catalans, 43007 Tarragona, Spain

Corresponding author: Vladimir Baulin

Corresponding author's address: Departament d'Enginyeria Quimica, Universitat Rovira i Virgili 26 Av. dels Paisos

Catalans, 43007 Tarragona, Spain

Corresponding author's phone and fax: +34644448558

Corresponding author's e-mail address: vladimir.baulin@urv.cat

Running head: Tropisms, mechanical stress and plant cell cortex

Keywords: microtubules | plant cells | cytoskeleton | cortex | orientation

Number of words in summary: 179

Number of words in introduction: 1339

Number of words in materials and methods: 1464

Number of words in results and discussion: 1026

Number of words in conclusions: 141

Number of words in introduction: 1339

Number of words in references: 1481

Number of words in table legend: 14

Number of words in figure legends: 238

Number of words in main text: 5882

Number of figures: 4

Number of tables: 1

ABSTRACT (limit 250 words)

Directional growth caused by gravitropism and corresponding bending of plant cells has been explored since 19th century, however, many aspects of mechanisms underlying the perception of gravity at the molecular level are still not well known. Perception of gravity in root and shoot gravitropisms is usually attributed to gravisensitive cells, called statocytes, which exploit sedimentation of macroscopic and heavy organelles, amyloplasts, to sense the direction of gravity. Gravity stimulus is then transduced into distal elongation zone which is several mm far from statocytes. It is suggested that gravity stimulus is conveyed by gradients in auxin flux. We propose a theoretical model that may explain how concentration gradients can affect the global orientation of cortical microtubules, attached to the cell membrane and induce their dynamic reorientation perpendicular to the gradients. In turn, oriented microtubules arrays direct the growth and orientation of cellulose microfibrils, forming part of the cell external skeleton and determine the shape of the cell. Reorientation of microtubules is also observed in reaction to light in phototropism and mechanical bending, thus suggesting certain universality of the proposed mechanism.

INTRODUCTION

The main ingredients of external skeleton in plant cells are cellulose microfibrils (Alberts *et al.*, 2002). They help to maintain the shape of cells and prevent plant cells from bursting due to high internal turgor pressure (Alberts *et al.*, 2002; Hamant and Traas, 2010). Cellulose microfibrils have high tensile strength and provide the cell wall mechanical strength and stiffness (Hamant and Traas, 2010). Since cellulose arrays are naturally anisotropic, the anisotropy of the cell growth is controlled by the orientation of the cellulose microfibrils arrays (Nick *et al.*, 1997). In turn, the deposition of cellulose microfibrils is directed by highly aligned microtubules (MTs) arrays (Wymer *et al.*, 1996), which serve as a template for directed growth of cellulose microfibrils (Wymer *et al.*, 1996).

MTs are hollow cylinders of 25 nm external and 15 nm internal diameters (Alberts *et al.*, 2002) and the length ranged from few nm to several microns. They are highly dynamic by their nature (Desai and Mitchison, 1997), and MT ends are constantly switching between polymerization and depolymerization, thus making the length of MTs intermittent. This property of MTs is called dynamic instability (Mitchison and Kirschner, 1984; Dogterom and Leibler, 1993; Desai and Mitchison, 1997); a plus-end of a MT is usually more dynamic than a minus-end (Mitchison and Kirschner, 1984; Gildersleeve *et al.*, 1992; VanBuren *et al.*, 2002).

Cortex MTs in plant cells are organized in parallel arrays adjacent to the cell membrane (Lloyd *et al.*, 2000). There is a direct evidence (Yuan *et al.*, 1994; Paredez *et al.*, 2006) that cellulose microfibrils are deposed in the same direction as cortical MTs during the plant growth. Depolymerizing drugs, ethylene and various agents (Baskin *et al.*, 1994; Yuan *et al.*, 1994; Corson *et al.*, 2009) affecting orientation of MTs, change also the orientation of cellulose microfibrils arrays (Green, 1962). Aligned cellulose microfibrils provide anisotropy to the cell wall, which is more rigid in the direction parallel to cellulose arrays than in perpendicular direction. This anisotropy allows to transduce the isotropic turgor pressure into a directional cell growth (Ledbetter and Porter, 1963; Yuan *et al.*, 1994; Hamant *et al.*, 2008; Hamant *et al.*, 2011).

Thus, anisotropy in plant cell wall rigidity irrevocably fixes the direction of growth of the cell leading to irreversibility of the processes such as cell division and cell elongation (Chan *et al.*, 2007; Sassi and Vernoux, 2013). We focus in particular, on gravitropism and phyllotaxis, although the biochemical background is similar to other types of tropisms, such as phototropism or chemitropism (Fischer and Schopfer, 1998).

Cell constituents, molecules and their aggregates, are too small to sense the gravitational field directly, however roots of many plants are able to sense the direction of gravity with the help of statocytes, specific cells located in the growing tip of roots or shoots (Sack, 1991). Statocytes can efficiently perceive the direction of the gravity and direct plant growth along the gravity vector. Directed growth is observed only in the presence of gravitational or centrifugal force and disappear in the absence of gravity or when the direction of gravity is altered (Baluska and Hasenstein, 1997; Hamant and Traas, 2010). The perception of gravity in statocytes is usually attributed to amyloplasts, macroscopic, heavy organelles that sediment in a lower part of the cell (Sack, 1991; Baluska and Hasenstein, 1997; Hashiguchi *et al.*, 2012) in root gravitropism and can exhibit saltatory upward movements in shoot gravitropism (Nick *et al.*, 1997; Hashiguchi *et al.*, 2012).

Sedimenting amyloplasts inside statocytes are probably the main driving force for root gravitropism. Since the radius of amyloplasts, r, is about few microns (Smith *et al.*, 1997; Vitha *et al.*, 2007), their concentration corrected for buoyancy is $\sim\Delta\rho=0.5$ *g/ml* (Wayne *et al.*, 1990) and $g\approx 9.8$ *m/s^2*, the resulting sedimentation force of one amyloplast at the bottom of the cell is $\Delta\rho g(4/3)\pi r^3\sim 1$ *pN* (Yoder *et al.*, 2001). However, the elongation growth occurs in epidermis, where MTs reorientation takes place. The distance between elongation zone and root cap is several mm, or ~ 20 cell layers (Blancaflor and Masson, 2003; Perrin, 2005; Hashiguchi *et al.*, 2012). Amyloplast sedimentation causes alternation of auxin flux, which causes reorientation of microtubules (Himmelspach and Nick, 2001; Bisgrove, 2008; Korasick *et al.*, 2014; Xu *et al.*, 2014) supported by other signals, such as Ca^{+2} ions (Leitz *et al.*, 2009). Most probably, gradients in hormonal fluxes change the stability of MTs depending on their direction (Wiesler *et al.*, 2002; Akhmanova and Steinmetz, 2008; Korasick *et al.*, 2014).

In turn, there is an evidence that MTs respond directly to mechanical stress of the cell (Ikushima and Shimmen, 2005; Hamant and Traas, 2010). It can be directly observed during phyllotaxis in shoot apical meristem (Hamant *et al.*, 2008; Hamant *et al.*, 2010; Sassi and Vernoux, 2013). This suggests that MTs might feel mechanical stress and reorient themselves inducing anisotropic cellulose deposition. Such mechanism is also observed in the experiments with shoot apical meristem compression, laser ablations of its cells or weakening of the cell wall (Hamant *et al.*, 2008; Heisler *et al.*, 2010; Uyttewaal *et al.*, 2012).

Here we provide a theoretical basis for MT reorientation caused by concentration gradients of chemical agents or mechanical cell elongation. Our model is based on the mechanism of collective self-orientation of cortical MTs

induced by mutual collisions and re-growing of individual MTs. This mechanism was first proposed in Baulin *et al.* (2007). It was shown that collisions between individual MTs may spontaneously lead to orientation domains with highly aligned MTs from initially disordered array. This simple model assumes a MT as a rigid rod that can grow at a plus-end and shorten at a minus-end, while the rate of shrinkage at a plus end is altered by the collisions with other MTs. It was shown that the anisotropy in the rates of catastrophes at a plus end due to collisions is enough to induce collective phenomena of MT self-ordering into aligned domains with preferential orientation. The selection of preferential orientation in the domains is similar to evolution selection, where MTs with "incorrect" orientation disassemble and disappear, leaving space to "correctly" aligned and thus, longer and older MTs (Baulin *et al.*, 2007).

This minimal model based on age and length discrimination was further extended and improved in consequent theoretical models (Allard *et al.*, 2010; Eren *et al.*, 2010; Hawkins *et al.*, 2010; Shi and Ma, 2010; Tindemans *et al.*, 2010). The models consider two dimensional (2D) movements because cortex MTs in plant cells are attached to plasma membrane forming a 2D array (Alberts *et al.*, 2002; Hamant and Traas, 2010). Since the movements in 2D are much more restricted than in 3D, the probability of collisions is high even for relatively low concentrations. Direct observation of collisions between MTs in the cortex array and measure of collision rates (Dixit and Cyr, 2004) have shown that the probabilities of catastrophes and consequent shrinkage of MTs, rescue and continuation of growth depends on angles of collisions. Shallow angles favor continuation of growth, while perpendicular collisions may provoke catastrophe and disassembling of the MT (Dixit and Cyr, 2004). The models based on these results (Allard *et al.*, 2010; Eren *et al.*, 2010) predict the self-orientation induced by collisions and show that zippering between MTs with similar orientation play an important role in onset of ordering. Another model of collision induced reorientation of MTs (Shi and Ma, 2010) focuses on phase transitions in MT arrays and predicts the existence of three phases: isotropic phase, weakly ordered nematic phase and highly ordered nematic phase. A similar model (Hawkins *et al.*, 2010; Tindemans *et al.*, 2010) includes explicitly dynamic instability of a plus end and uses more realistic parameters for growth and shrinkage rates of MT ends. In addition, this model implements a set of rules driving MTs in case of their collisions: induced catastrophe, plus-end entrainment (zippering) and intersection are possible depending on the angle between colliding MTs (Hawkins *et al.*, 2010; Tindemans *et al.*, 2010). This model predicts orientation induced by collisions and competition between domains with different orientations.

SUBJECTS/MATERIALS AND METHODS

Here we use a modified model of collision induced ordering in 2D MTs arrays that incorporates essential parts of the previous models. We model MTs as rigid rods which can switch between shrinking at their minus-end and growing at their plus-end (Mitchison and Kirschner, 1984; Shaw *et al.*, 2003). Switching between polymerization and depolymerization on a plus end happens according to preset catastrophe and rescue rates. In case of collision with another MT the plus-end of a MT stops growing (Sumino *et al.*, 2012); however, it may still experience catastrophe with a preset rate and start shrinking (Mitchison and Kirschner, 1984). This model is summarized at Figure 2 and the parameters (Table 1) describing individual MT dynamics correspond to other models and to experimental data. Each MT is characterized by its length, position and orientation. We consider that orientation is set while MT is nucleated and does not change during its lifetime. The only way to reorient an array of MTs is to eliminate by complete disassembly the MTs with "incorrect" orientation and inject new MTs with "correct" orientations. Zippering effect for shallow contact angles (Dixit and Cyr, 2004; Allard *et al.*, 2010; Eren *et al.*, 2010) would only enhance the suggested mechanism and lead to faster ordering.

According to the minimal model described in Baulin *et al.* (2007), a MT is a rigid rod that can grow at a plus-end and shorten at a minus-end. The collisions with other MTs perturb the growth of MTs, which itself is sufficient to induce a global order in the system without even excluded volume effects that are necessary for ordering in ordinary lyotropic liquid crystals, which comes from purely collective and kinetic interaction between MTs. However, this model, due to its simplicity, assumes infinite and unrestricted growth of perfectly aligned MTs, thus the model should include dynamic instability of the plus end, which would lead to a stationary state of ordered MTs (Hawkins *et al.*, 2010; Shi and Ma, 2010; Tindemans *et al.*, 2010).

Thus, in contrast to Baulin *et al.* (2007), our model is a three-state model, where MT may exist in the growing state (g), shrinking state (s) and blocked state (d), which is similar to Hawkins *et al.* (2010) and Tindemans *et al.* (2010). The length and the position of each MT change with time. Every time interval Δt the minus-end of each MT is shortened by $v\_\Delta t$, where $v\_$ is the speed of shrinkage of the minus-end. The speed of elongation of the plus-end is v_g and the speed of shrinkage is v_s. The plus-end of initially growing MT can experience catastrophes with the rate P_c and rescues with the rate P_r, can be blocked due to collisions with the rate P_b and unblocked with the rate P_{ub}, thus providing stochastic oscillations of MT length. If the length of a MT goes to 0, it disappears, while new MTs are created with the nucleation

rate P_n (Figure 2). The balance between growing and shrinking, nucleation and disappearing of MTs in a steady state insures dynamic stability of the average number of MTs and their average length. The values of parameters are given in Table 1. If a MT occasionally intersects any other MT, the growth is rejected and the MT passes from growing to blocked state b. The shrinkage and growth can be reversed stochastically according to the given probabilities. Thus, every time step the length of a MT either increases (state g) by $(v_g\text{-}v_-)$ Δt or decreases (state s) by $(v_s\text{+}v_-)$ Δt or decreases (state b) by $v_-\Delta t$ in a blocked state (Figure 2). The model by Allard *et al.* (2010) includes complex collision rules, requiring the introduction of a critical entrainment angle Θ_z. However, collision-induced catastrophes alone can induce a global ordering and we use such simple description.

We consider that the seeds of new MTs are nucleated homogeneously and with random angles. MTs cannot change their orientation, but they can change their states between growing (g), shortening (s) and blocked (b). Introducing the corresponding surface concentrations, c_g, c_s and c_b, the total length concentration $k(\Theta,t)$ can be written in the following form:

$$k(\theta, t) = \int l\big[c_g(l,\theta,t) + c_s(l,\theta,t) + c_b(l,\theta,t)\big]dl \, . (1)$$

A set of evolution equations are written as

$$\frac{\partial c_g}{\partial t} = -v_g\frac{\partial c_g}{\partial l} + P_r c_s - P_c c_g + v_-\frac{\partial c_g}{\partial l} + P_{ub}c_b - P_b c_g, (2)$$

$$\frac{\partial c_s}{\partial t} = v_s\frac{\partial c_s}{\partial l} - P_r c_s + P_c c_g + P_c c_b + v_-\frac{\partial c_g}{\partial l}, (3)$$

$$\frac{\partial c_b}{\partial t} = v_-\frac{\partial c_g}{\partial l} - P_{ub}c_b + P_b c_g - P_c c_b. (4)$$

where $P_r c_s = \Phi_r[c_s]$ and $P_c c_g = \Phi_c[c_g]$ along with $P_c c_b = \Phi_c[c_b]$ are the spontaneous flux terms (Hawkins *et al.*, 2010) responsible for rescue and catastrophe respectively; $-v_g(\partial c_g/\partial l) = \Phi_g[c_g]$, $vs(\partial c_s/\partial l) = \Phi_s[c_s]$ and $v_-(\partial c_g/\partial l) = \Phi_-[c_g]$ describe growth and shrinkage of plus-end and shortening of minus-end respectively (Dogterom and Leibler, 1993; Baulin *et al.*, 2007; Hawkins *et al.*, 2010; Tindemans *et al.*, 2010). Blocking term is determined by the collisions between MTs when a growing MT collides with another MT with a rate $P_b c_g(\Theta) = v_g c_g(\Theta) \int d\theta' \, sin|\theta - \theta'|k(\theta') = \Phi_b[c_g, k]$, where $sin|\Theta\text{-}\Theta'|$ defines the cross section of collisions. This term reminds the second virial coefficient of the Onsager theory (Onsager, 1949), but has a completely different physical origin. The unblocking term $P_{ub}(c_g,k)c_b$ is connected with the possibility of a previously blocked plus-end of a MT to restart its growing due to disassembly of a

blocking MT, no matter if it is a shrinkage of a plus-end or shortening of a minus-end. It is related to the concentration $c_b(l,t,\Theta)$ as following $P_{ub}(c_\sigma,k)c_b(\Theta)=\Phi_{ub}[c_b,c_\sigma,k]$.

The initial conditions are the following: at $t=0$ the concentration of shortening and blocked MTs are equal zero $c_s(l,0,\Theta)=0$, $c_b(l,0,\Theta)=0$ while c_g is connected with the nucleation rate P_n as $(v_g\text{-}v_\text{-})c_g(0,t,\Theta)= P_n(\Theta)/2\pi$, $c_g(l>0,0,\Theta)=0$.

The first model (Baulin *et al.*, 2007) lacked dynamic instability, i.e. missed Φ_c and Φ_r terms in eqs. \ref{eq:2} and \ref{eq:4}, which are responsible for stabilization of the length of MTs in ordered arrays and thus these terms are essential for the stationary state in ordered arrays. The model by Hawkins *et al.* (2010) lacks the minus-end disassembly, i.e. terms $\Phi_\text{-}$, Φ_b and Φ_{ub}, but it includes $\Phi_{inducedcat.}$, Φ_{zipper} and $\Phi_{reactivation}$. It's possible to connect their population of "inactive" segments with the population of blocked segments. It is noteworthy, that "zippering" in this model is similar to "blocking" described by the present model, where reactivation occurs due to disassembly of blocking MTs, in contrast to disassembly of an active segment of the MT in zippering event.

To get a control parameter that defines the behavior of the system, eqs. (2)-(4) can be rewritten as:

$$\frac{\partial c_g}{\partial t} + \left(v_g - v_-\right)\frac{\partial c_g}{\partial l} = -(P_c + P_b)c_g + P_{ub}c_b - P_rc_s, \text{(5)}$$

$$\frac{\partial c_s}{\partial t} - (v_s + v_-)\frac{\partial c_s}{\partial l} = -P_rc_s + P_c(c_g + c_b), \text{(6)}$$

$$\frac{\partial c_b}{\partial t} - v_-\frac{\partial c_g}{\partial l} = -(P_{ub} + P_c)c_b + P_bc_g. \text{(7)}$$

The sum of these equations gives

$$\frac{\partial}{\partial t}\left(c_g + c_s + c_b\right) + \frac{\partial}{\partial l}\left((v_g - v_-)c_g - (v_s + v_-)c_s - v_-c_b\right) = 0. \text{(8)}$$

The steady state implies time derivatives to be equal to zero, leading to the following flux balance equation

$$\left(v_g - v_-\right)c_g(l,\theta) = (v_s + v_-)c_s(l,\theta) + v_-c_b(l,\theta), \text{(9)}$$

or in a more convenient form

$$v_gc_g - v_sc_s = v_-\left(c_g + c_s + c_b\right). \text{(10)}$$

To simplify these equations even more, we assume that the probabilities P_c and P_r are small (see Table 1), thus the related terms in eqs. (5)-(7) may be neglected. This means that shortening MTs either do not present, or their length distribution is constant, thus eq. (9) yields in the form

$$\left(v_g - v_-\right)c_g(l, \theta) = v_- c_b(l, \theta), (11)$$

Thus, the dimensionless parameter

$$\alpha = \frac{v_-}{v_g - v_-}, (12)$$

can be regarded as a control parameter. It coincides with the corresponding control parameter in Baulin *et al.* (2007). Following the same notations, $v = v_g - v_-$, $\alpha = v/v$. Thus, eqs. (5)-(7) corresponding to steady state can be rewritten as follows,

$$v \frac{\partial c_g}{\partial l} = -P_b c_g + P_{ub} c_b, (13)$$
$$-\alpha v \frac{\partial c_g}{\partial l} = -P_{ub} c_b + P_b c_g. (14)$$

Probabilities P_b and P_{ub} are length-independent, thus the solution of this system of differential equations has the following form:

$$c_g(l, \theta) = A(\theta)e^{-l/\bar{l}}, (15)$$
$$c_b(l, \theta) = B(\theta)e^{-l/\bar{l}}, (16)$$

where

$$\frac{1}{\bar{l}} = \frac{P_b}{v} - \frac{P_{ub}}{\alpha v}, (17)$$
$$A(\theta) = \alpha B(\theta). (18)$$

It is noteworthy that $1/\bar{l}$ is similar to the growth parameter introduced by Hawkins *et al.* (2010).

As it was possible to separate the variables in the solution for the steady state in this simplified model, one can actually show that the changes in the shape of the cell lead to anisotropy. In the work of Baulin *et al.* (2007) it was

shown that growth parameter causes the system to persist in different regimes depending on its value: chaotic or ordered; it also accounts for the model presented above. Anisotropy of the cell will cause the angle dependence of both blocking rate P_b and nucleation rate P_n. The unblocking probability P_{ub} is angle-independent. This inhomogeneity will yield different growth parameters $1/\bar{l}$ for different angles, causing even different regimes of system's persistence at different angles. These different regimes may compete with each other, but one of them will inevitably be in a preferred position due to anisotropy of nucleation.

In the model by Hawkins *et al.* (2010) the minus-end shrinkage speed equals to zero, hence eq. (9) yields in the following form

$$v_g c_g(l, \theta) = v_s c_s(l, \theta). \, (19)$$

This equation along with the equations, describing the evolution of the system, gives the growth parameter g:

$$g = \frac{P_r}{v_s} - \frac{P_c}{v_g}, \, (20)$$

which characterizes the noninteracting system. This expression corresponds to eq. (17) up to notations. "Rescue" is effectively corresponds to unblocking in our model, while "blocking" corresponds to catastrophes.

RESULTS AND DISCUSSION

We performed two types of simulations: microtubule orientation in response to concentration gradients and mechanical stress of the cortex. Both stimulus may induce oriented self-organization of MTs.

Orientation of MTs induced by concentration gradients

Chemical agents, e.g. hormone of growth auxin or ethylene, are often reported to modify MT dynamics (Bisgrove, 2008). The mechanism of such influence is not well understood. It is suggested (Akhmanova and Steinmetz, 2008) that chemical agents catalyse or inhibit the action of microtubule-associated proteins (MAPs). These proteins change dynamic parameters of MTs, and generally affect the growth velocities or catastrophe rates (Akhmanova and Steinmetz, 2008). Concentration gradients thus may affect global dynamics of MTs.

We assume that chemical agents influence dynamic instability parameters, such as catastrophe rate, which becomes higher in the direction of the concentration gradient. This assumption is consistent with experimental data showing that auxin can generate polarity in distribution of auxin transporters, proteins of PIN family (Heisler *et al.*, 2010). These proteins are linked with MT orientation regulator CLASP (Ambrose *et al.*, 2011; Ambrose *et al.*, 2013; Zhang *et al.*, 2013) and with microtubule-associated protein MAP65 (Kakar *et al.*, 2013).

Two sets of parameters are selected to induce spontaneous organization of MTs (Table 1). An increase in catastrophe rate in one direction breaks the symmetry between MTs oriented along the gradient and against it. This asymmetry may induce global order of MT arrays in one direction. To investigate this phenomenon in detail we change the gradient of catastrophe rate. This change indeed leads to reorientation of already formed MT arrays, as shown in Figure 3.

First set of parameters lead to slower reorientation: although anisotropy ratio soon recovers its high value (See Figure 3D)), it takes more time for MTs to reorient, as depicted in Figure 3C). Eventually the system reaches the state shown on Figure 3B), but takes around 10000 steps. Thus, the difference in reorientation behavior is primarily controlled by the populations of blocked (*b*) and growing (*g*) MTs, while shortening MTs (*s*) shrink with the same rate $v_s + v_- = 240$ *nm/s*.

Compression-induced orientation in disordered arrays

Cortex MTs attached to the cell wall may form stationary states of oriented domains or stay in disordered state depending on the rates of growth and shrinkage, catastrophe rates and concentration (Hawkins *et al.*, 2010; Shi and Ma, 2010; Tindemans *et al.*, 2010). Mechanical stretching or compression of the cell wall anisotropically changes the

distance between the MTs, thus affecting the concentration in the direction of applied force. This, in turn, may induce orientation in disordered arrays or reorient MTs in ordered arrays. In the following, we investigate the effect of stretching and compression on these two initial stationary states, (i) isotropically oriented, disordered array of MTs and (ii) oriented domains of MTs are then subject to stretching and compression (Figure 1).

Set of parameters corresponding to initially disordered arrays (Table 1) leads to formation of stationary disordered state, characterized by the balance between growing, shrinking and blocked MTs. Thus, stationary average total number of MTs is provided by the balance between MTs that disappear due to collisions with other MTs or due to catastrophes events, and new-born MTs appearing with random directions. Freshly appearing MTs correspond to nucleation sites that are fixed in the cortex, thus we assume that the total number of new-born MTs per time step and per area is kept constant. However, stretching or compression change the distance between nucleation sites and thus, the nucleation rate, being inversely proportional to the area, may vary with the direction.

Stationary disordered array of $10x10 \ \mu m^2$ (Figure 4A)) is compressed in one direction by two times (Figure 4B)). This compression provokes orientation of MTs in the direction of compression. In contrast, the stretching by two times of the array does not lead to orientation. This goes inline with the observations of MT orientation perpendicular to the gravity vector in gravitropism in roots (Himmelspach and Nick, 2001) and may be related to coordinated patterns of MT arrays governed by mechanical stress (Hamant *et al.*, 2011).

The degree of MT orientation can be described by the nematic order parameter, which is proportional to the cost function $\sigma(\Theta) = \overline{\cos^2(\Omega - \Theta)}$, where Θ is the direction of the director and Ω is the direction of individual MT and the bar signifies the ensemble average. However, MTs has intermittent length and the ordering of the domains is determined by long MTs (Baulin *et al.*, 2007). Thus, the cost function should include the length and we use the following function (Baulin *et al.*, 2007)

$$\sigma(\Theta) = \overline{l^2 \cos^2 \theta}$$

With this, an anisotropy ratio S_l can be defined as (Baulin *et al.*, 2007):

$$s_l = \frac{\sigma(\theta_{max}) - \sigma(\theta_{min})}{\sigma(\theta_{max}) + \sigma(\theta_{min})}$$

and the dominant angle is given by (Baulin *et al.*, 2007):

$$\tan 2\theta_l = \frac{\overline{l^2 \sin^2 2\Omega}}{\overline{l^2 \cos^2 2\Omega}}.$$

The anisotropy ratio S_l and the dominant angle Θ_l as function of time are given in Figure 4G) and H).

Stretching-induced disorientation in ordered arrays

Once a stationary ordered array is formed (Figure 4D)), the orientation of the array is governed by longest MTs (Baulin *et al.*, 2007), which are also the oldest MTs, and thus having biggest life expectancy and hence more persistent. Since the angles of MTs in this model are irrevocably fixed during the life cycle, changing the direction of the ordered array implies disassemble of these leading MTs, which may require collisions with domains with even longer MTs. Thus, compression of the ordered arrays only increases the distance between MTs that may increase the order, but may not lead to disassemble of MTs. This is shown in Figure 4E) and the corresponding plot of the dominant angle and anisotropy ratio S_l, Figure 4I-J).

In turn, stretching of the cortex increase the distance between MTs, thus new-born MTs may grow longer before they collide with the dominant MTs and bring more random orientations into arrays. Figures 4F) and I-J) show that stretching may considerably reduce the order in the arrays, and, in principle, may lead to complete disorientation of the arrays.

Both effects, disorientation of the arrays due to stretching and orientation induced by compression, may work together to help to reorient MT arrays in response to mechanical stress on the cortex.

CONCLUSIONS

The model of kinetic orientation of microtubules arrays due to collisions was used to study the effects of concentration gradients of hormones and mechanical deformation (compression and stretching) of the cortex in plant cells. In gravitropic response, concentration gradients of auxin influence catastrophe and growth rate of MTs, which in turn may lead to reorientation of MT arrays transverse to the direction of the gradient. In phyllotactic arrangement of leafs on stem, the mechanical stretching of initially disordered MT arrays itself may induce a global order, where MTs are oriented along the action of mechanical stress. Ordered MT arrays, in turn, can direct cellulose microfibrils assembly, thus resulting in oriented microfibrils growth. Orientation of cellulose microfibrils in a certain direction consequently leads to anisotropy of the cell wall, which, in turn, combined with turgor pressure indicates the direction of cell growth.

REFERENCES

Akhmanova, A. and Steinmetz, M.O. (2008) Tracking the ends: a dynamic protein network controls the fate of microtubule tips. *Nat. Rev. Mol. Cell Biol.*, **9**, 309–322. Available at: [Accessed April 1, 2014].

Alberts, B., Johnson, A., Lewis, J., Raff, M., Roberts, K. and Walter, P. (2002) *Molecular Biology of the Cell* 4th ed., Garland Science.

Allard, J.F., Wasteneys, G.O. and Cytrynbaum, E.N. (2010) Mechanisms of Self-Organization of Cortical Microtubules in Plants Revealed by Computational Simulations. *Mol. Biol. Cell*, **21**, 278–286.

Ambrose, C., Allard, J.F., Cytrynbaum, E.N. and Wasteneys, G.O. (2011) A CLASP-modulated cell edge barrier mechanism drives cell-wide cortical microtubule organization in Arabidopsis. *Nat. Commun.*, **2**, 430. Available at: [Accessed February 17, 2014].

Ambrose, C., Ruan, Y., Gardiner, J., Tamblyn, L.M., Catching, A., Kirik, V., Marc, J., Overall, R. and Wasteneys, G.O. (2013) CLASP Interacts with Sorting Nexin 1 to Link Microtubules and Auxin Transport via PIN2 Recycling in Arabidopsis thaliana. *Dev. Cell*, **24**, 649–659. Available at: [Accessed February 17, 2014].

Baluska, F. and Hasenstein, K.H. (1997) Root cytoskeleton: its role in perception of and response to gravity. *Planta*, **203**, S69–S78.

Baskin, T.I., Wilson, J.E., Cork, A. and Williamson, R.E. (1994) Morphology and microtubule organization in Arabidopsis roots exposed to oryzalin or taxol. *Plant Cell Physiol.*, **35**, 935–942.

Baulin, V.A., Marques, C.M. and Thalmann, F. (2007) Collision induced spatial organization of microtubules. *Biophys. Chem.*, **128**, 231 – 244.

Bisgrove, S.R. (2008) The roles of microtubules in tropisms. *Plant Sci.*, **175**, 747–755. Available at: [Accessed September 30, 2013].

Blancaflor, E.B. and Masson, P.H. (2003) Plant gravitropism. Unraveling the ups and downs of a complex process. *Plant Physiol.*, **133**, 1677–1690.

Chan, J., Calder, G., Fox, S. and Lloyd, C. (2007) Cortical microtubule arrays undergo rotary movements in Arabidopsis hypocotyl epidermal cells. *Nat. Cell Biol.*, **9**, 171–175. Available at: [Accessed February 27, 2014].

Corson, F., Hamant, O., Bohn, S., Traas, J., Boudaoud, A. and Couder, Y. (2009) Turning a plant tissue into a living cell froth through isotropic growth. *Proc. Natl. Acad. Sci. U. S. A.*, **106**, 8453–8458.

Desai, A. and Mitchison, T.J. (1997) Microtubule polymerization dynamics. *Annu Rev Cell Dev Biol*, **13**, 83–117.

Dixit, R. and Cyr, R. (2004) Encounters between dynamic cortical microtubules promote ordering of the cortical array through angle-dependent modifications of microtubule behavior. *Plant Cell*, **16**, 3274–3284.

Dogterom, M. and Leibler, S. (1993) Physical aspects of the growth and regulation of microtubule structures. *Phys. Rev. Lett.*, **70**, 1347–1350. Available at: [Accessed September 13, 2012].

Eren, E.C., Dixit, R. and Gautam, N. (2010) A Three-Dimensional Computer Simulation Model Reveals the Mechanisms for Self-Organization of Plant Cortical Microtubules into Oblique Arrays. *Mol. Biol. Cell*, **21**, 2674–2684.

Fischer, K. and Schopfer, P. (1998) Physical strain-mediated microtubule reorientation in the epidermis of gravitropically or phototropically stimulated maize coleoptiles. *Plant J. Cell Mol. Biol.*, **15**, 119–123.

Gildersleeve, R.F., Cross, A.R., Cullen, K.E., Fagen, A.P. and Williams, R.C. (1992) Microtubules grow and shorten at intrinsically variable rates. *J. Biol. Chem.*, **267**, 7995–8006.

Green, P.B. (1962) Mechanism for Plant Cellular Morphogenesis. *Science*, **138**, 1404–1405.

Hamant, O., Heisler, M.G., Jonsson, H., et al. (2008) Developmental Patterning by Mechanical Signals in Arabidopsis. *Science*, **322**, 1650–1655. Available at: [Accessed June 26, 2013].

Hamant, O., Meyerowitz, E.M. and Traas, J. (2011) Is cell polarity under mechanical control in plants? *Plant Signal. Behav.*, **6**, 137–139.

Hamant, O. and Traas, J. (2010) The mechanics behind plant development. *New Phytol.*, **185**, 369–385. Available at: [Accessed July 9, 2012].

Hamant, O., Traas, J. and Boudaoud, A. (2010) Regulation of shape and patterning in plant development. *Curr. Opin. Genet. Dev.*, **20**, 454–459. Available at: [Accessed April 1, 2014].

Hashiguchi, Y., Tasaka, M. and Morita, M.T. (2012) Mechanism of Higher Plant Gravity Sensing. *Am. J. Bot.*, **100**, 91–100. Available at: [Accessed September 16, 2013].

Hawkins, R.J., Tindemans, S.H. and Mulder, B.M. (2010) Model for the orientational ordering of the plant microtubule cortical array. *Phys Rev E*, **82**, 011911.

Heisler, M.G., Hamant, O., Krupinski, P., Uyttewaal, M., Ohno, C., Jönsson, H., Traas, J. and Meyerowitz, E.M. (2010) Alignment between PIN1 Polarity and Microtubule Orientation in the Shoot Apical Meristem Reveals a Tight Coupling between Morphogenesis and Auxin Transport O. Leyser, ed. *PLoS Biol.*, **8**, e1000516. Available at: [Accessed December 11, 2013].

Himmelspach, R. and Nick, P. (2001) Gravitropic microtubule reorientation can be uncoupled from growth. *Planta*, **212**, 184–189.

Ikushima, T. and Shimmen, T. (2005) Mechano-sensitive orientation of cortical microtubules during gravitropism in azuki bean epicotyls. *J. Plant Res.*, **118**, 19–26. Available at: [Accessed October 29, 2013].

Kakar, K., Zhang, H., Scheres, B. and Dhonukshe, P. (2013) CLASP-mediated cortical microtubule organization guides PIN polarization axis. *Nature*, **495**, 529–533. Available at: [Accessed February 17, 2014].

Korasick, D.A., Westfall, C.S., Lee, S.G., Nanao, M.H., Dumas, R., Hagen, G., Guilfoyle, T.J., Jez, J.M. and Strader, L.C. (2014) Molecular basis for AUXIN RESPONSE FACTOR protein interaction and the control of auxin response repression. *Proc. Natl. Acad. Sci.* Available at: http://www.pnas.org/cgi/doi/10.1073/pnas.1400074111 [Accessed March 26, 2014].

Ledbetter, M.C. and Porter, K.R. (1963) A "microtubule" in plant cell fine structure. *J. Cell Biol.*, **19**, 239–250.

Leitz, G., Kang, B.-H., Schoenwaelder, M.E.A. and Staehelin, L.A. (2009) Statolith Sedimentation Kinetics and Force Transduction to the Cortical Endoplasmic Reticulum in Gravity-Sensing Arabidopsis Columella Cells. *PLANT CELL ONLINE*, **21**, 843–860. Available at: [Accessed September 30, 2013].

Lloyd, C.W., Himmelspach, R., Nick, P. and Wymer, C. (2000) Cortical microtubules form a dynamic mechanism that helps regulate the direction of plant growth. *Grav Space Biol Bull*, **13**, 59–66.

Mitchison, T. and Kirschner, M. (1984) Dynamic instability of microtubule growth. *Nature*, **312**, 237–242. Available at: [Accessed September 13, 2012].

Nick, P., Godbole, R. and Wang, Q.Y. (1997) Probing rice gravitropism with cytoskeletal drugs and cytoskeletal mutants. *Biol. Bull.*, **192**, 141–143.

Onsager, L. (1949) The effects of shape on the interaction of colloidal particles. *Ann. N. Y. Acad. Sci.*, **51**, 627–659. Available at: [Accessed December 2, 2013].

Paredez, A.R., Somerville, C.R. and Ehrhardt, D.W. (2006) Visualization of cellulose synthase demonstrates functional association with microtubules. *Science*, **312**, 1491–1495.

Perrin, R.M. (2005) Gravity Signal Transduction in Primary Roots. *Ann. Bot.*, **96**, 737–743. Available at: [Accessed September 30, 2013].

Sack, F.D. (1991) Plant gravity sensing. *Int. Rev. Cytol.*, **127**, 193–252.

Sassi, M. and Vernoux, T. (2013) Auxin and self-organization at the shoot apical meristem. *J. Exp. Bot.*, **64**, 2579–2592. Available at: [Accessed February 27, 2014].

Shaw, S.L., Kamyar, R. and Ehrhardt, D.W. (2003) Sustained Microtubule Treadmilling in Arabidopsis Cortical Arrays. *Science*, **300**, 1715–1718.

Shi, X. and Ma, Y. (2010) Understanding phase behavior of plant cell cortex microtubule organization. *Proc. Natl. Acad. Sci.*, **107**, 11709–11714.

Smith, J.D., Todd, P. and Staehelin, L.A. (1997) Modulation of statolith mass and grouping in white clover (Trifolium repens) growth in 1-g, microgravity and on the clinostat. *Plant J. Cell Mol. Biol.*, **12**, 1361–1373.

Sumino, Y., Nagai, K.H., Shitaka, Y., Tanaka, D., Yoshikawa, K., Chaté, H. and Oiwa, K. (2012) Large-scale vortex lattice emerging from collectively moving microtubules. *Nature*, **483**, 448–452. Available at: [Accessed September 13, 2012].

Tindemans, S.H., Hawkins, R.J. and Mulder, B.M. (2010) Survival of the Aligned: Ordering of the Plant Cortical Microtubule Array. *Phys Rev Lett*, **104**, 058103.

Uyttewaal, M., Burian, A., Alim, K., et al. (2012) Mechanical Stress Acts via Katanin to Amplify Differences in Growth Rate between Adjacent Cells in Arabidopsis. *Cell*, **149**, 439–451. Available at: [Accessed April 1, 2014].

VanBuren, V., Odde, D.J. and Cassimeris, L. (2002) Estimates of lateral and longitudinal bond energies within the microtubule lattice. *Proc. Natl. Acad. Sci.*, **99**, 6035–6040.

Vitha, S., Yang, M., Sack, F.D. and Kiss, J.Z. (2007) Gravitropism in the starch excess mutant of Arabidopsis thaliana. *Am. J. Bot.*, **94**, 590–598. Available at: [Accessed September 30, 2013].

Wayne, R., Staves, M.P. and Leopold, A.C. (1990) Gravity-dependent polarity of cytoplasmic streaming in Nitellopsis. *Protoplasma*, **155**, 43–57.

Wiesler, B., Wang, Q.-Y. and Nick, P. (2002) The stability of cortical microtubules depends on their orientation. *Plant J. Cell Mol. Biol.*, **32**, 1023–1032.

Wymer, C.L., Wymer, S.A., Cosgrove, D.J. and Cyr, R.J. (1996) Plant cell growth responds to external forces and the response requires intact microtubules. *Plant Physiol.*, **110**, 425–430.

Xu, T., Dai, N., Chen, J., et al. (2014) Cell Surface ABP1-TMK Auxin-Sensing Complex Activates ROP GTPase Signaling. *Science*, **343**, 1025–1028. Available at: [Accessed April 1, 2014].

Yoder, T.L., Zheng, H.Q., Todd, P. and Staehelin, L.A. (2001) Amyloplast sedimentation dynamics in maize columella cells support a new model for the gravity-sensing apparatus of roots. *Plant Physiol.*, **125**, 1045–1060.

Yuan, M., Shaw, P.J., Warn, R.M. and Lloyd, C.W. (1994) Dynamic reorientation of cortical microtubules, from transverse to longitudinal, in living plant cells. *Proc. Natl. Acad. Sci. U. S. A.*, **91**, 6050–6053.

Zhang, C., Raikhel, N.V. and Hicks, G.R. (2013) CLASPing microtubules and auxin transport. *Dev. Cell*, **24**, 569–571.

TABLES

The parameters used in the model. These parameters are based on experimental data by Shaw *et al.* (2003) and Dixit and Cyr (2004).

Parameter	Disordered state	Disordered state
Plus-end growth rate v_g, *nm/s*	70	80
Plus-end shortening rate v_s, *nm/s*	225	200
Minus-end shortening rate v_-, *nm/s*	15	40
Catastrophe probability P_c, *1/s*	64×10^{-3}	
Rescue probability P_r, *1/s*	124×10^{-3}	
Nucleation rate P_n, *1/s*	5000	

FIGURE LEGENDS

Figure 1. Cell elongation caused by gravity-induced sedimentation of amyloplasts. Cell stretching induces reorientation of MTs perpendicular to deformation direction.

Figure 2. A) Schematic representation of interacting MTs in cell cortex. Schematic picture of B) a minus-end disassembly; C) a plus-end assembly and disassembly; D) a growing MT blocked by another one. E) The model: P_c and P_r are the catastrophe and rescue rates, P_b and P_{ub} are probabilities of blocking and unblocking respectively, v_g, v_s and v_- are the speeds of plus-end growing and shortening and minus-end shortening relatively.

Figure 3. MTs A) before and B) after reorientation. Only 1000 longest MTs are shown. Bar indicates 1 μm. C) For two sets of parameters in Table 1 C) Dominant angle versus simulation timestep; D) Anisotropy ratio versus simulation timestep. First set of parameters is represented by wine line, second - by cyan line.

Figure 4. Snapshots of MT arrays (only 1000 longest MTs are shown) evolving from A) initially homogeneous and isotropic array 10x10 μm under B) compression and C) stretching. Shrinking MTs (state s) are shown in blue, other MTs (state b and g) are shown in red. Bar indicates 1μm. D-F) Snapshots of MT arrays evolving D) from ordered array 10x10 μm under E) compression and F) stretching. Dominaiting angle versus simulation timestep G) for initially isotropic array in A-C) and I) oriented array in D-F). Anisotropy ratio versus simulation timestep H) for initially isotropic array in A-C) and J) oriented array in D-F).

.

1
2
3
4
5
6
7
8
9
10
11
12
13
14
15
16
17
18
19
20
21
22
23
24
25
26
27
28
29
30
31
32
33
34
35
36
37
38
39
40
41
42
43
44
45
46
47
48
49
50
51
52
53
54
55
56
57
58
59
60
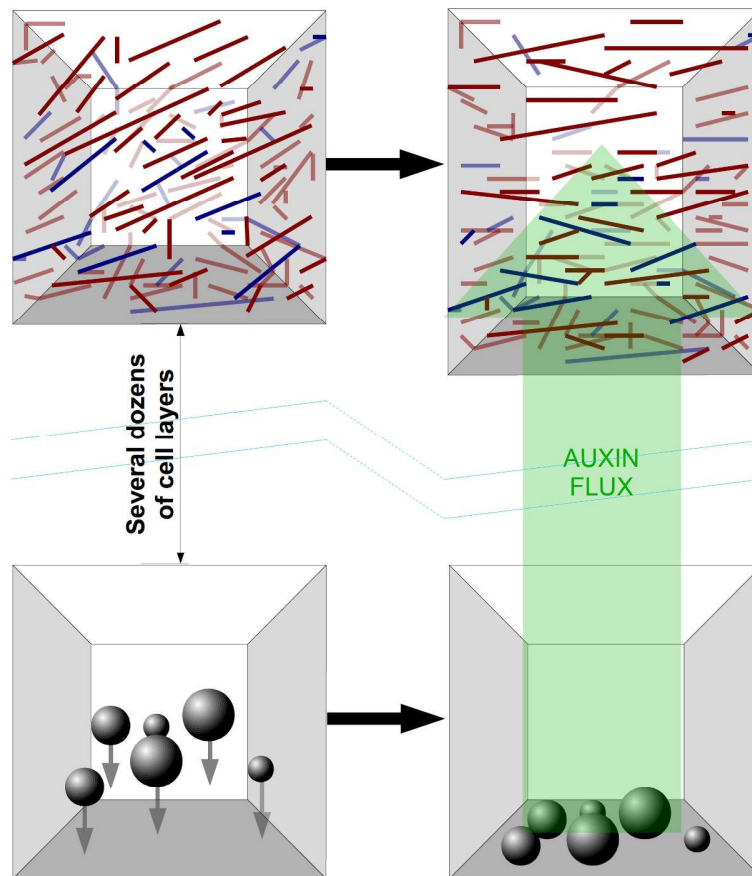
297x420mm (300 x 300 DPI)

279x361mm (300 x 300 DPI)

UNIVERSITAT ROVIRA I VIRGILI
MODELING OF SELF-ORGANIZATION OF MICROTUBULES IN PLANT CELLS
Alexander Muratov
Dipòsit Legal: T 966-2014

Page 23 of 24   **The Plant Journal**

148x123mm (300 x 300 DPI)

UNIVERSITAT ROVIRA I VIRGILI
MODELING OF SELF-ORGANIZATION OF MICROTUBULES IN PLANT CELLS
Alexander Muratov
Dipòsit Legal: T 966-2014

The Plant Journal   **Page 24 of 24**

1
2
3
4
5
6
7
8
9
10
11
12
13
14
15
16
17
18
19
20
21
22
23
24
25
26
27
28
29
30
31
32
33
34
35
36
37
38
39
40
41
42
43
44
45
46
47
48
49
50
51
52
53
54
55
56
57
58
59
60
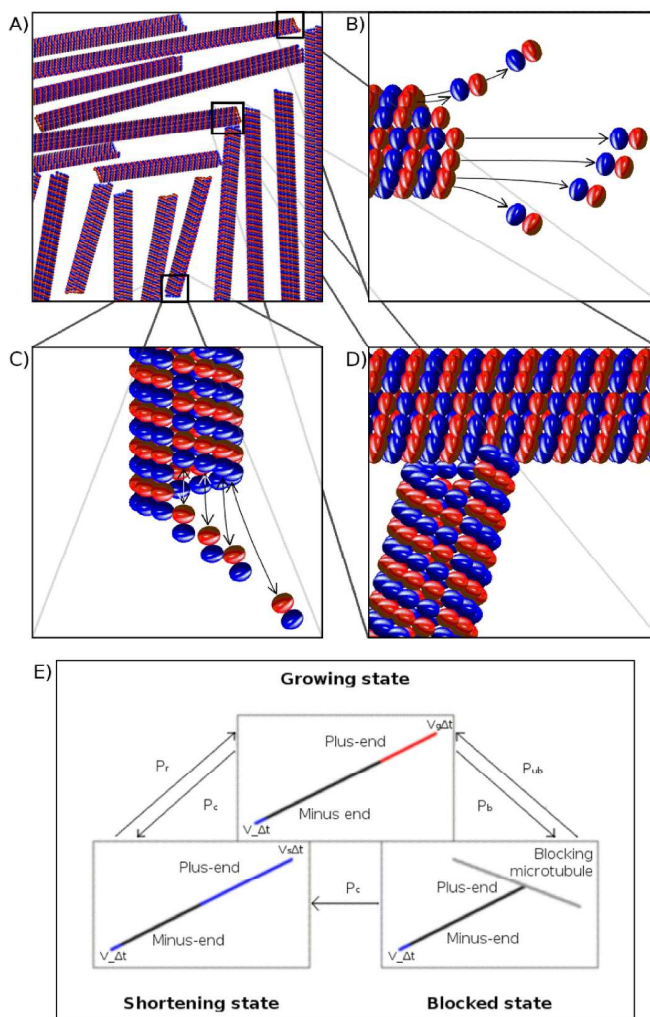
297x420mm (300 x 300 DPI)

A. Degradation versus Self-Assembly of Block Co-Polymer Micelles

Langmuir

Degradation versus Self-Assembly of Block Co-polymer Micelles

Alexander Muratov[†] and Vladimir A. Baulin*[†,‡]

[†]Departament d'Enginyeria Quimica, Universitat Rovira i Virgili, 26 Avinguda dels Paisos Catalans, 43007 Tarragona, Spain
[‡]Institució Catalana de Recerca i Estudis Avançats (ICREA), 23 Passeig Lluis Companys, 08010 Barcelona, Spain

ABSTRACT: The stability of micelles self-assembled from block co-polymers can be altered by the degradation of the blocks. Slow degradation shifts the equilibrium size distribution of block co-polymer micelles and changes their properties. The quasi-equilibrium scaling theory shows that the degradation of hydrophobic blocks in the core of micelles destabilizes the micelles, reducing their size, while the degradation of hydrophilic blocks forming coronas of micelles favors larger micelles and may, at certain conditions, induce the formation of micelles from individual chains.

■ INTRODUCTION

Physicochemical properties of block co-polymers often determine their function in many useful applications ranging from biotechnology and drug delivery to painting and oil extraction.[1,2] The possibility to control ess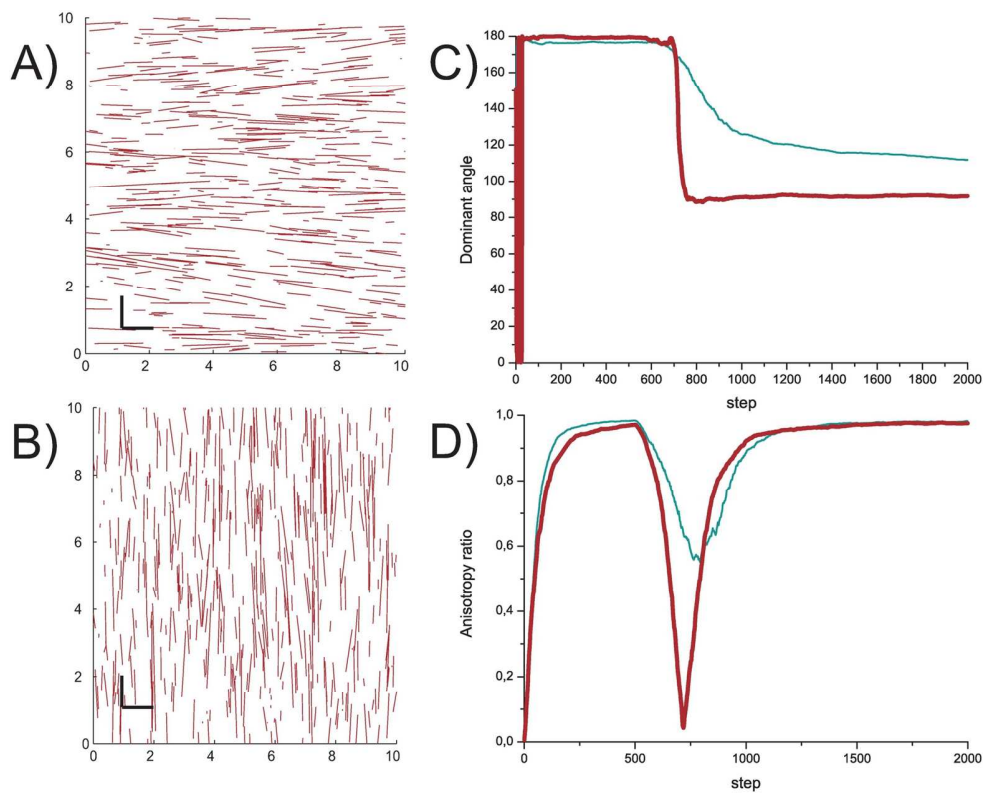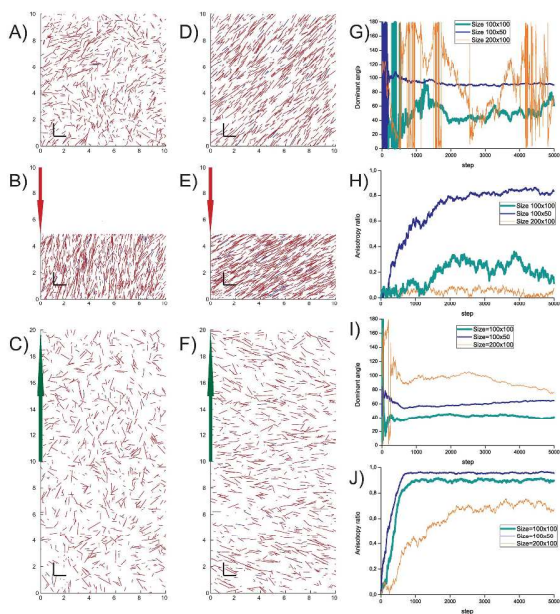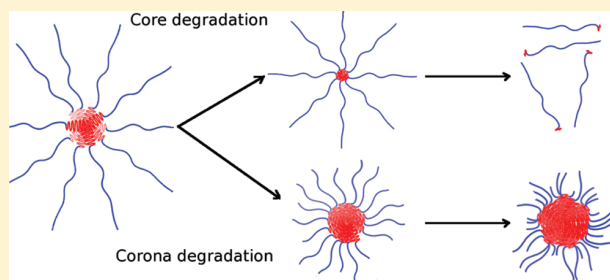ential properties of block co-polymers capable of adapting the behavior to changes in the environment is thus a challenging task. One of the main properties of amphiphilic diblock co-polymers in solution is their ability to self-assemble in micelles[3] composed of a hydrophobic core surrounded by a hydrophilic corona.[4] Such compact finite size aggregates can encapsulate hydrophobic agents in their cores.[5] In particular, this loading capacity of block co-polymers can be used for selective transport of hydrophobic nanoparticles and lipophilic active molecules to specific targets and through the cell membrane.[6]

However, the use of block co-polymer micelles for targeted drug delivery also implies the necessity to control the release of the transported particles from the cores of micelles, for example, by external stimuli. In turn, the release process is closely related to the thermodynamic stability of micelles. Micelles assembled from block co-polymers can be relatively stable.[7] This hinders the release of active components[8] and, thus, limits their use for biomedical applications.

Degradable polymers[9] provide for an additional degree of freedom, allowing for the control of the longevity and stability of block co-polymer micelles. Degradation of the polymer backbone may significantly change the thermodynamics of block co-polymer self-assembly and, thus, stability of the micelles. Tuning the rate of degradation would allow for the modulation of the thermodynamic stability of micelles to a large extent. In addition, tumor tissues have the tendency to selectively accumulate polymers. This effect is known as enhanced permeation and retention (EPR)[10] and is attributed to a larger size of the pores in blood vessels of tumor tissues. Polymers can interact with the cell membranes and reticuloendothelial system (RES),[11] which can potentially increase their cytotoxicity.[12] From this perspective, the degradation of polymers up to metabolites[13] may solve biocompatibility issues and excessive accumulation in tissues.

Usually, biomedical applications require long-circulating delivery vectors with constant release for days.[14] This implies that polymer degradation in such systems is much slower than the time required to reach the thermodynamic equilibrium. Kinetics of micelle formation from monomers can be rather fast. Characteristic times of exchange of oligomers between micelles and the bulk and the relaxation do not exceed milliseconds,[15] while for longer block co-polymers, the characteristic time is on the order of minutes.[16,17] Thus, in such systems, the self-assembly in micelles is a quasi-equilibrium process with a fixed length distribution of the blocks, which changes with time. Micelles of degradable block co-polymers can assemble and reassemble, changing their internal structure and shape[18,19] and, thus, changing the loading capacity of the cores. The balance between steric repulsion of hydrophilic blocks in the coronas of micelles and interaction of hydrophobic blocks forming part of the cores defines the finite size of micelles. Degradation of hydrophilic blocks[5,20] would then lead to destabilization of micelles, leading to fusion and formation of larger cores. In turn, degradation of hydrophobic blocks in the cores[21−27] may induce splitting the cores of micelles.

Using a scaling theory, we study the interplay between the degradation of one of the blocks of block co-polymers and equilibrium self-assembly and reassembly of block co-polymers into micelles in the case of both corona and core degradation. We present a scaling theory of block co-polymer self-assembly into micelles[28,29] and discuss the degradation kinetics of the polymer blocks. However, we note that scaling theories have limitations: (i) scaling theories, in principle, only apply to (infinitely) long chains; (ii) the theory does not include
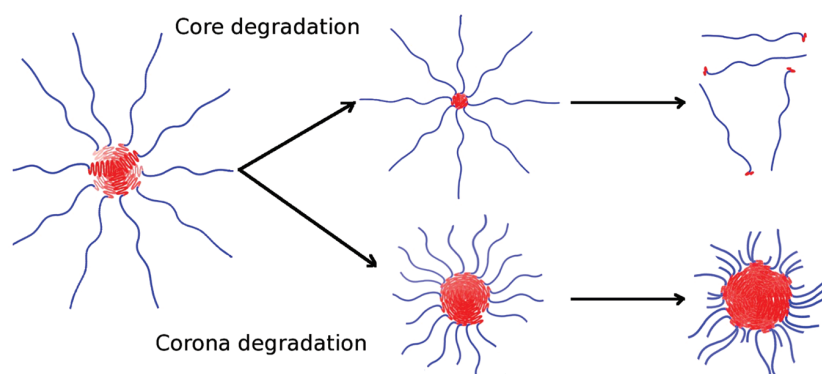
Figure 1. Quasi-equilibrium degradation of micelles. Core degradation induces the disassembly of micelles, while corona degradation induces growth of micelles.

kinetics; and (iii) it does not include morphological changes. We assume two types of degradation mechanisms: (i) Random chain scission mechanism[30] implies a stochastic process of a polymer chain division at a random position. This mechanism causes a gradual decrease in the number average molecular weight. Such random division of a chain is usually observed in hydrolytic degradation of polyesters[31,32] or certain polyamides.[33,34] (ii) End evaporation mechanism[35,36] occurs when the monomers are gradually detached from the ends of the polymer chain. This mechanism is typical for enzymatic degradation. The degradation of the blocks shifts the critical micellar concentration (cmc) and changes the size distributions and average sizes of the micelles (Figure 1). The degradation of the chains can induce or suppress the self-assembly process.

■ SELF-ASSEMBLY

Diblock co-polymers composed of soluble and insoluble blocks can spontaneously self-assemble into micelles.[1] The micellization is the entropy-driven process. The entropy of the mixture of individual chains in the solution is balanced by the tendency of insoluble blocks to reduce contacts with the solvent in the cores of micelles. Thus, the stability of the micelles is defined by the energy of insoluble blocks forming compact cores and the steric repulsion of soluble blocks in the coronas of micelles.[28,29] Characteristic equilibration time of block co-polymers exponentially depends upon the length of the insoluble block.[16,17] In the cases of long insoluble blocks and high interfacial tensions,[37] the relaxation time may be hours, and thus, non-equilibrium kinetics should be considered. However, we focus on situations when the hydrophobic block is relatively short or the interfacial tension is low. In this case, the relaxation time is small (milliseconds),[15] and thus, the kinetics of self-assembly is much faster than the degradation. If the degradation process is slow enough to allow for the equilibrium assembly of block co-polymers into micelles, the scaling model of equilibrium self-assembly can be applied. We assume that only one block, either insoluble or soluble, is degradable, so that the total number of block co-polymers does not change with time. In addition, we consider spherical micelles, while morphological transitions are not considered. We denote c_p as the number density of aggregates comprising p co-polymers,

where p is the aggregation number. The total free energy per unit volume of the solution of co-polymers at a given time is

$$\frac{F}{kT} = \sum_{p=1}^{\infty} c_p \left[\ln\left(\frac{c_p}{e}\Lambda^3\right) + \frac{F_p}{kT} \right] + \int_0^{\infty} c(n)\ln\left(\frac{c(n)}{e}\Lambda^3\right) dn \tag{1}$$

where the first term is the entropy and F_p is the free energy of a micelle comprising p co-polymers. Λ is the de Broglie wavelength. $p = 1$ corresponds to individual block co-polymer contributions, while the entropy of free fragments is taken into account in the last term. Degradation of blocks provokes the detachment of fragments of different lengths floating in the solution, and the last term takes into account the entropy of fragments, where $c(n)$ is their length distribution function. The total number of monomers in the self-assembly and degradation process is conserved. This is reflected in the conservation of mass condition

$$\sum_{p=1}^{\infty} p c_p = \phi \tag{2}$$

where φ is the total co-polymer concentration. Because we consider the degradation of one block, the total number of co-polymers in the solution is not changed with time and the degradation does not affect this condition. Minimization of the free energy (eq 1) subject to the constraint (eq 2) gives the quasi-equilibrium distribution of the co-polymers in the micelles.[38]

$$c_p = c_1^p \Lambda^{3(p-1)} \exp\left(-\frac{F_p - pF_1}{kT}\right) \tag{3}$$

This expression describes the distribution of micelles of degradable co-polymers at each time.

Explicit form of the free energy F_p is defined by the molecular structure of co-polymers forming a micelle and is the sum of the corona and the core contributions.

$$F_p = F_p^{corona} + F_p^{core} \tag{4}$$

The free energy of individual chains, $p = 1$, is also described by this expression, where the corona term transforms into the entropy contribution of a linear chain and the insoluble block gives the corresponding core contribution. The exact
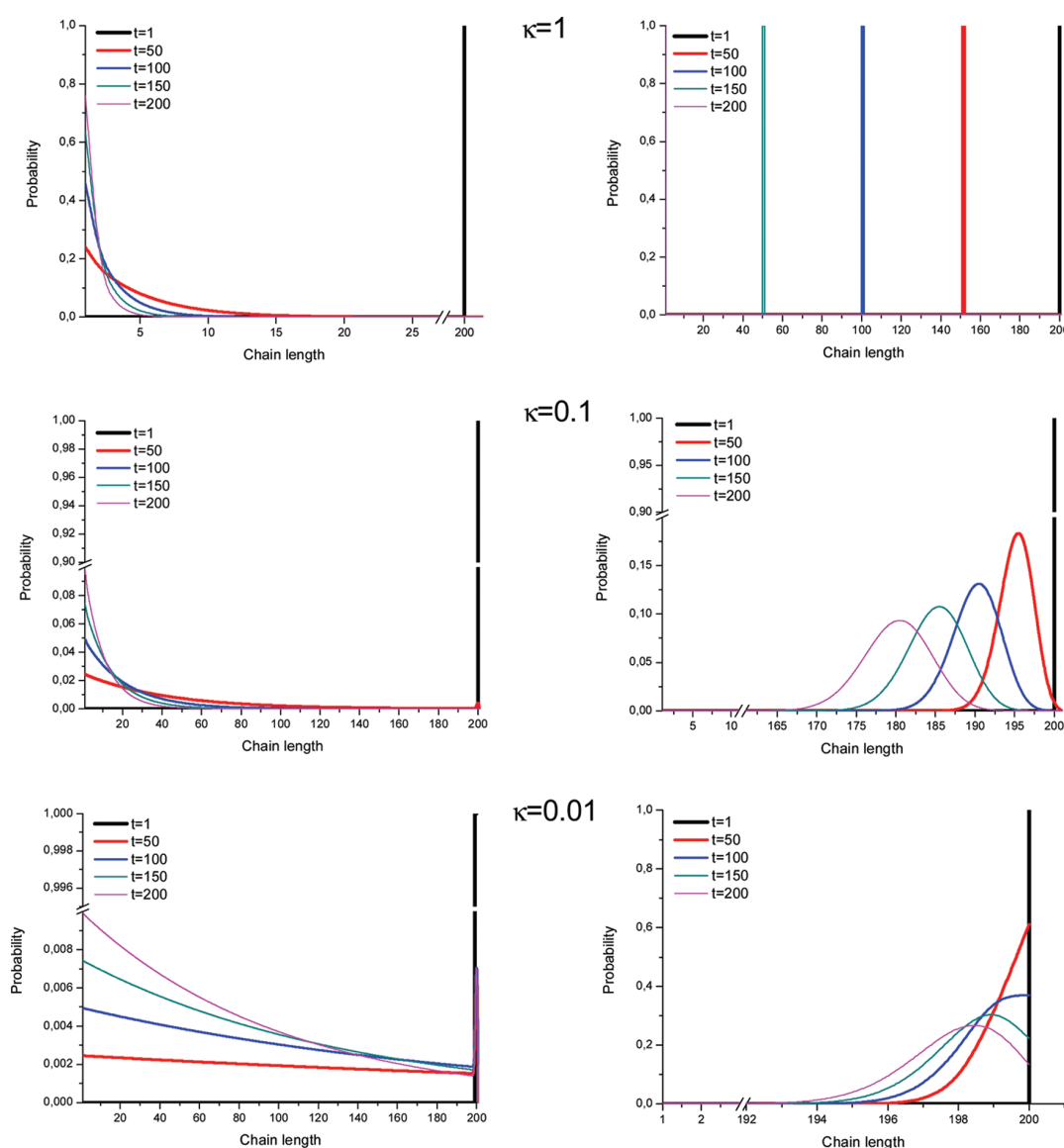
Figure 2. Length distributions in the random scission (left column) and end evaporation (right column) mechanisms for different degradation rates κ and initial length of 200.

expressions of F_p^{corona} and F_p^{core} depend upon the degradation mechanism and are functions of time.

In the following, we denote the chain length of the soluble block as N and the chain length of the insoluble block as N_c. We assume sufficiently long soluble chains, $N \gg 1$, and the monomers of both blocks being the same size a.

■ DEGRADATION KINETICS

We consider random chain scission and end evaporation mechanisms and degradation of soluble and insoluble blocks.

Random Chain Scission. The random scission mechanism implies a homogeneous distribution of splitting points along the chain. At a given time, a chain is divided into random parts. Thus, the distribution of fragments of different lengths $P(n,t)$ is given by[30]

$$\frac{1}{\kappa}\frac{\partial P(n,t)}{\partial t} = -nP(n,t) + \int_n^\infty \mathrm{d}y\, P(y,t) \tag{5}$$

The negative term refers to the loss of chains of length n, and the positive term describes the gain of chains of length n because of the degradation of longer chains (with lengths more than n) at a given time t. The coefficient κ takes into account the fraction of chains that degrade simultaneously at each time, practically defining the time scale. The initial distribution of chains at $t = 0$ is assumed to be monodisperse. This equation is solved numerically by considering the integral in the right-hand side $Q(n,t) = \int_n^\infty \mathrm{d}y P(y,t)$ as a numerical function. This function is calculated for a given time as a function of n, and then eq 5 is solved numerically. Typical length distribution functions are shown in the left column of Figure 2. Initial homogeneous distribution gradually disperses and shifts to small n.

Core Degradation. Insoluble blocks tend to avoid contacts with water and favor assembly into the core of the micelle. The degradation of insoluble blocks makes block co-polymers more soluble, and this would shift the equilibrium toward smaller micelles. Assuming that the core of a micelle is a dense and

homogeneous sphere formed by p co-polymers, the free energy of the core is given by[38]

$$F_p^{core} = kT(36\pi)^{1/3}\sigma N_c^{2/3}p^{2/3} + \frac{3\pi^2 p^{5/3}}{80N_c^{1/3}} \quad (6)$$

where σ is the surface tension of a sphere of radius $R_c = (3/(4\pi)pN_c)^{1/3}a$ and the second term describes the elastic contributions arising from the stretching of insoluble blocks in the core.[39] The "effective" surface tension of the core σ implicitly describes the fact that the insoluble chains tend to avoid contact with the solvent by forming a dense core. The lengths of the insoluble blocks N_c depend upon time, and for each time t, the length distribution is given by the equation of random scission degradation (eq 5).

Steric repulsion in the corona of the micelles, formed by soluble blocks, penalizes the formation of large micelles. Because the soluble block does not degrade, the corona of micelles is composed of chains of equal length N. The partition function of a monodisperse star Z_p yields the form[40,41]

$$Z_p \propto N^{\gamma_p - 1} \quad (7)$$

where N is the length of the arm.[41] γ_p values are the universal critical exponents of the star polymers.[42] The numerical values of γ_p are known exactly for a wide range of p[43] and, in the range $0 < p < 200$, can be interpolated by the power law expression $\gamma_p = 1 - 0.0893(p - 1.5)^{1.68}$. With this, the free energy of polydisperse corona is given by

$$F_p^{corona} = -kT \ln Z_p = -kT(\gamma_p - 1)\ln N \quad (8)$$

Equations 6 and 8 define the free energy of micelles of p co-polymers and the free energy of individual chains for $p = 1$. It allows for the calculation of the size distribution of micelles as a function of time (eq 3). The results are present in Figure 3a). The degradation of the core starts when the micelles are formed (concentration above cmc). The micelles gradually decrease in size and disassemble. The degradation rate κ is related to the time step in the degradation equation (eq 5). The chosen value $\kappa = 0.0003$ is low enough to ensure gradual changes in the size of the micelles. If the rate is higher, the micelles would disappear faster. In a real experimental situation, this parameter connects the time step with real time; e.g., $\kappa = 0.0003$ signifies that only 3 of 10 000 chains disassociate at one time step. In experiments, this parameter may vary in a wide range.

Corona Degradation. The situation is different when the soluble blocks can degrade while the insoluble blocks are stable. The cores of the micelles are formed by insoluble blocks, and the core contribution has the same form as in the previous case (eq 6); however, N_c remains constant. In turn, soluble blocks forming corona can now degrade with time, and the corona contribution changes. Coronas of micelles are formed by polydisperse arms with the length distribution $P(n,t)$ given by (eq 5). The partition function of a polydisperse star Z_p yields the form[40,41]

$$Z_p \propto n_1^{\gamma_p - \gamma_{p-1}} n_2^{\gamma_{p-1} - \gamma_{p-2}} ... n_{p-1}^{\gamma_2 - \gamma_1} n_p^{\gamma_1 - 1} \quad (9)$$

where $n_1 < n_2 < ... < n_{p-1} < n_p$ are the lengths of the corresponding arms, sorted in ascending order.[41] This partition
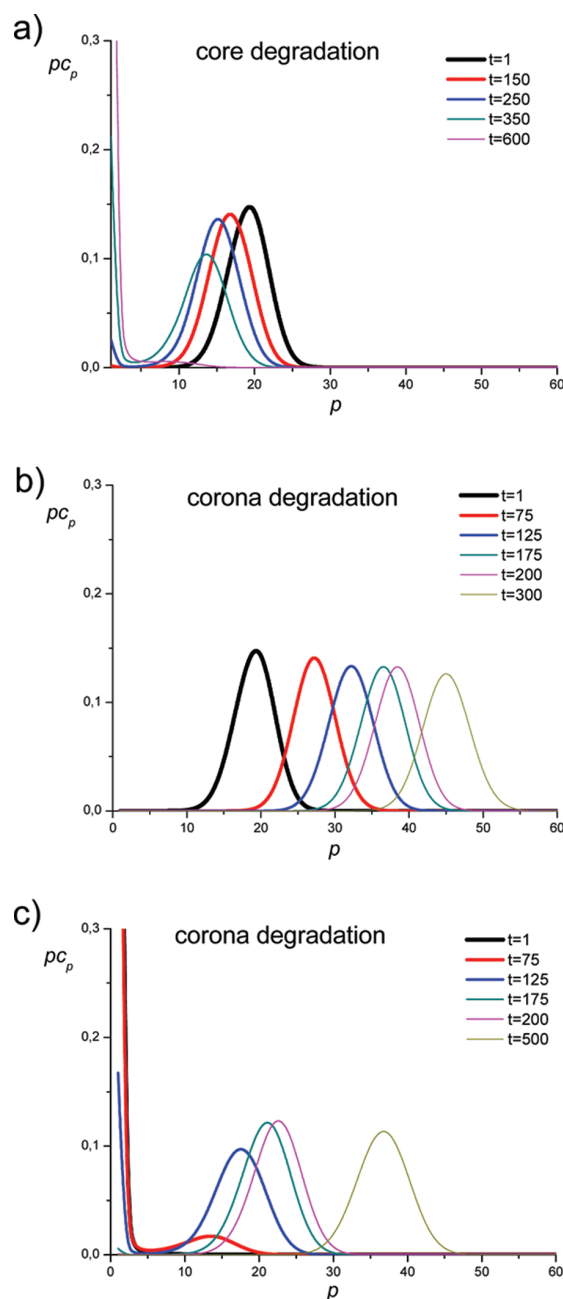
Figure 3. Time evolution of the normalized size distribution pc_p: (a) core degradation above cmc, with $\sigma = 0.81$ and $\kappa = 0.0003$; (b) corona degradation above cmc, with $\sigma = 0.81$ and $\kappa = 0.01$; and (c) corona degradation below cmc, with $\sigma = 0.75$ and $\kappa = 0.01$. The initial lengths of the blocks are $N = 200$ and $N_c = 20$, with co-polymer concentration $c_1 = 10^{-6}$.

function leads to the corresponding expression of the free energy of the corona.

$$F_p^{corona} = -kT[(\gamma_p - \gamma_{p-1})\ln n_1 + (\gamma_{p-1} - \gamma_{p-2})\ln n_2$$
$$+ ... + (\gamma_1 - 1)\ln n_p] \quad (10)$$

This expression defines, together with (eq 6), the free energy of the micelles and individual chains in the solution (eq 4). In fact, the scaling expression of the corona contribution of a micelle

with one arm, $F_{p=1}^{corona} = -kT(\gamma_1 - 1)\ln N$, corresponds exactly to the scaling expression of a soluble chain in a solution.[42]

The resulting size distribution of micelles (eq 3) is shown in panels b and c of Figure 3 for different times. The effect of corona degradation is opposite the case of core degradation. Figure 3b shows the corona degradation kinetics for 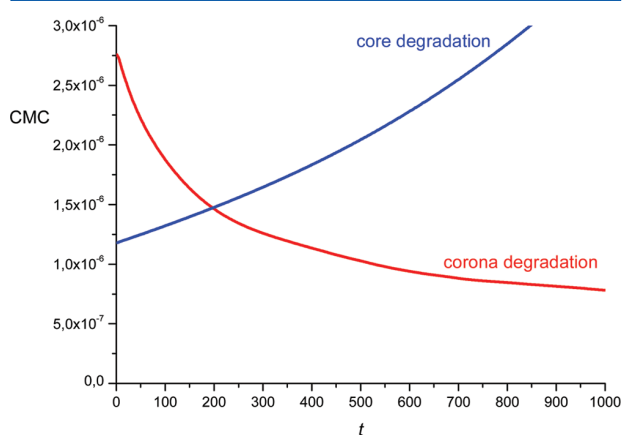the same initial conditions as in Figure 3a when the micelles are formed for conditions above cmc. Degradation of corona induces self-assembly of micelles from initially homogeneous solution of individual chains. Individual chains associate into micelles, and the distribution of micelles grows. Consequent degradation leads to the shrinkage of the corona; thus, larger micelles become more stable, and small micelles become unstable. The size distribution of the micelles becomes broader with time because of the increased polydispersity. Further degradation of hydrophilic blocks would lead to the growth of micelles, morphological changes[18] of the micelle shape, and consequent bulk phase separation.

Another important effect of corona degradation is the possibility to induce self-assembly of micelles from the solution below cmc (Figure 3c). The degradation induces the formation of micelles from initially homogeneous solution first for small aggregation numbers. Consequent degradation increases the number of micelles, the polydispersity, and the average size. Thus, the degradation influences the cmc, which is time-dependent (Figure 4). It decreases with time in the case of

Figure 5. Time evolution of the aggregation number of the maximum of the size distribution, p_{max}. Parameters are the same as in Figure 3.
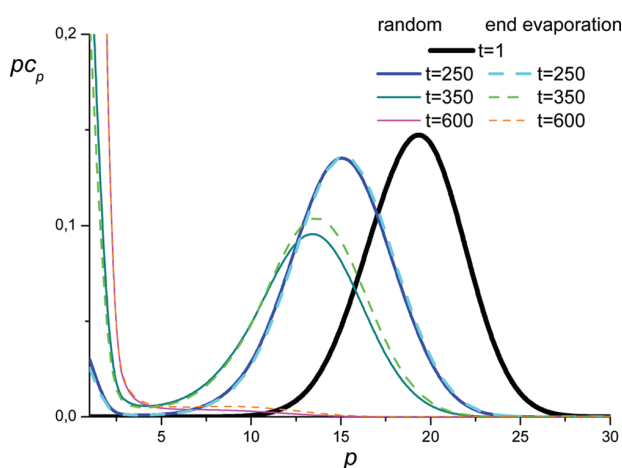
Figure 6. End evaporation kinetics of core degradation in comparison to random scission. Parameters are the same as in Figure 3a, except the degradation rate, $\kappa = 0.03$.

Figure 4. Time dependence of the cmc. Parameters are the same as in panels a and b of Figure 3.

corona degradation (red curve) and increases with time in the case of core degradation (blue curve).

The effect of degradation on the micellization process can be summarized in the plot showing the position of the maximum p_{max} of the size distribution c_p (Figure 5). In the case of core degradation (blue line), the maximum of the distribution moves to small numbers (see Figure 3a), until the micelles disappear completely (dashed line), while in the case of corona degradation (red curve), the size of the micelles increases (see Figure 3b), until the morphology changes or phase separation occurs. If the degradation starts below cmc, the self-assembly into micelles starts at a given time, which depends upon the rate of degradation κ.

End Evaporation. Random division of a chain is not the only degradation mechanism of polymer chains. Degradation in certain chemical reactions and enzymatic degradation may lead to the gradual decrease of the chains from the ends (chain-end-

activated degradation). The process of loosing the monomers from the end is described by the following process: $P(n, t + 1) - P(n,t) = \kappa(P(n + 1,t) - P(n,t))$, which can be written in the integral form similar to (eq 5) as

$$\frac{1}{\kappa}\frac{\partial P(n, t)}{\partial t} = -P(n, t)$$
$$+ \int_n^\infty \delta(y - n - 1)\mathrm{d}yP(y, t) \qquad (11)$$

where δ is the Dirac function. Using this equation instead of (eq 5), one can obtain the time dependence of the free energy of micelles for core and corona degradation. The right column of Figure 2 presents the kinetics end evaporation degradation. The starting and final chain-length distributions are very close for both types of degradations. That is why the micelle distributions shown for core degradation in Figure 6 also coincide. The difference is only seen for intermediate times. However, end evaporation degradation is much slower than random scission; thus, the rates of degradation differ in this example 100 times.

In conclusion, the scaling theory of quasi-equilibrium micellization coupled with the degradation of the blocks demonstrates that the degradation of hydrophilic blocks can induce self-assembly of co-polymers into micelles and increase the size of the micelles, while the degradation of the hydrophobic blocks destabilizes the micelles, reduces the equilibrium size of the micelles, and can lead to complete disassociation of the micelles. It is valid for the random scission mechanism assumed for degradation mechanics as well as for the enzymatic (chain-end) scission mechanism. These findings may suggest the ways of controlled self-assembly and destabilization of micelles by degradation of the blocks. Our model does not account for morphological transitions, and we plan to study them in the future with a more detailed microscopic theory.[44]

■ AUTHOR INFORMATION

Corresponding Author

*Telephone: +34-977-55-85-77. Fax: +34-977-55-96-21. E-mail: vladimir.baulin@urv.cat.

Notes

The authors declare no competing financial interest.

■ ACKNOWLEDGMENTS

■ REFERENCES

(1) Hamley, I. *Block Copolymers in Solution: Fundamentals and Applications*; John Wiley and Sons: New York, 2005.

(2) Riess, G.; Hurtrez, G.; Bahadur, P. *Block Copolymers*, 2nd ed.; Wiley: New York, 1985; Vol. 2.

(3) Alexandridis, P.; Holzwarth, J. F.; Hatton, T. A. *Macromolecules* **1994**, *27*, 2414−2425.

(4) Adams, M. L.; Lavasanifar, A.; Kwon, G. S. *J. Pharm. Sci.* **2003**, *92*, 1343−1355.

(5) Torchilin, V. P. *Pharm. Res.* **2007**, *24*, 1−16.

(6) Savic, R.; Luo, L.; Eisenberg, A.; Maysinger, D. *Science* **2003**, *300*, 615−618.

(7) Husseini, G. A.; Pitt, W. G.; Christensen, D. A.; Dickinson, D. J. *J. Controlled Release* **2009**, *138*, 45−48.

(8) Torchilin, V. *Eur. J. Pharm. Biopharm.* **2009**, *71*, 431−444.

(9) Scott, G. *Degradable Polymers, Principles and Applications*; Kluwer Academic Publishers: Dordrecht, The Netherlands, 2002.

(10) Matsumura, Y.; Maeda, H. *Cancer Res.* **1986**, *46*, 6387−6392.

(11) Pack, D. W.; Hoffman, A. S.; Pun, S.; Stayton, P. S. *Nat. Rev. Drug Discovery* **2005**, *4*, 581−593.

(12) Lynch, A. L.; Chen, R.; Dominowski, P. J.; Shalaev, E. Y.; YanceyJr., R. J.; Slater, N. K. H. *Biomaterials* **2010**, *31*, 6096−6103.

(13) Bastioli, C. *Handbook of Biodegradable Polymers*; Rapra Technology: Shawbury, U.K., 2005.

(14) Moghimi, S. M.; Hunter, A. C.; Murray, J. C. *Pharmacol. Rev.* **2001**, *53*, 283−318.

(15) Kaatze, U. *J. Phys. Chem. B* **2011**, *115*, 10470−10477.

(16) Lund, R.; Willner, L.; Stellbrink, J.; Lindner, P.; Richter, D. *Phys. Rev. Lett.* **2006**, *96*, No. 068302.

(17) Lund, R.; Willner, L.; Pipich, V.; Grillo, I.; Lindner, P.; Colmenero, J.; Richter, D. *Macromolecules* **2011**, *44*, 6145−6154.

(18) Geng, Y.; Discher, D. E. *J. Am. Chem. Soc.* **2005**, *127*, 12780−12781.

(19) Hu, Y.; Jiang, Z.; Chen, R.; Wu, W.; Jiang, X. *Biomacromolecules* **2010**, *11*, 481−488.

(20) Frazza, E. J.; Schmitt, E. E. *J. Biomed. Mater. Res.* **1971**, *5*, 43−58.

(21) Mahmud, A.; Xiong, X.-B.; Lavasanifar, A. *Eur. J. Pharm. Biopharm.* **2008**, *69*, 923−934.

(22) Pierri, E.; Avgoustakis, K. *J. Biomed. Mater. Res., Part A* **2005**, *75*, 639−647.

(23) Sun, H.; Guo, B.; Cheng, R.; Meng, F.; Liu, H.; Zhong, Z. *Biomaterials* **2009**, *30*, 6358−6366.

(24) Agrawal, S. K.; Sanabria-DeLong, N.; Coburn, J. M.; Tew, G. N.; Bhatia, S. R. *J. Controlled Release* **2006**, *112*, 64−71.

(25) Wang, Y.-C.; Tang, L.-Y.; Sun, T.-M.; Li, C.-H.; Xiong, M.-H.; Wang, J. *Biomacromolecules* **2008**, *9*, 388−395.

(26) Lee, J.; Cho, E. C.; Cho, K. *J. Controlled Release* **2004**, *94*, 323−335.

(27) Li, S.; Anjard, S.; Rashkov, I.; Vert, M. *Polymer* **1998**, *39*, 5421−5430.

(28) Sens, P.; Marques, C. M.; Joanny, J.-F. *Macromolecules* **1996**, *29*, 4880−4890.

(29) Baulin, V. A.; Lee, N.-K.; Johner, A.; Marques, C. M. *Macromolecules* **2006**, *39*, 871−876.

(30) Ben-Naim, E.; Krapivsky, P. *Phys. D* **1997**, *107*, 156−160.

(31) Li, S. *J. Biomed. Mater. Res.* **1999**, *48*, 342−353.

(32) Brown, D. W.; Lowry, R. E.; Smith, L. E. *Macromolecules* **1982**, *15*, 453−458.

(33) Garcia-Martin, M. G.; Hernandez, E. B.; Perez, R. R.; Galbis, J. A. *Polym. Degrad. Stab.* **2008**, *93*, 1370−1375.

(34) Ruiz-Donaire, P.; Bou, J. J.; Munoz-Guerra, S.; Rodriguez-Galan, A. *J. Appl. Polym. Sci.* **1995**, *58*, 41−54.

(35) Marques, C. M.; Turner, M. S.; Cates, M. E. *J. Chem. Phys.* **1993**, *99* (9), 7260−7266.

(36) Dubbeldam, J. L. A.; van der Schoot, P. *J. Chem. Phys.* **2005**, *123*, 144912.

(37) Zinn, T.; Willner, L.; Lund, R.; Pipichc, V.; Richter, D. *Soft Matter* **2012**, *8*, 623−626.

(38) Baulin, V. A.; Johner, A.; Avalos, J. B. *J. Chem. Phys.* **2010**, *133*, 174905.

(39) Zhulina, E. B.; Adam, M.; LaRue, I.; Sheiko, S. S.; Rubinstein, M. *Macromolecules* **2005**, *38*, 5330−5351.

(40) Johner, A.; Joanny, J. F.; Diez-Orrite, S.; Bonet-Avalos, J. *Europhys. Lett.* **2001**, *56*, 549−555.

(41) Baulin, V. A.; Johner, A.; Marques, C. M. *Macromolecules* **2005**, *38*, 1434−1441.

(42) Duplantier, B. *J. Stat. Phys.* **1989**, *54*, 581−680.

(43) Hsu, H.-P.; Nadler, W.; Grassberger, P. *Macromolecules* **2004**, *37*, 4658−4663.

(44) Pogodin, S.; Baulin, V. A. *Soft Matter* **2010**, *6*, 2216−2226.

FORM FOR THE ORAL PRESENTATION OF THE DOCTORAL THESIS AT
THE COMMISSION OF POSTGRADUATE AND DOCTORATE OF THE URV
BY THE REPRESENTATIVES OF THE DEPARTMENTS

(MODEL PER A LA PRESENTACIÓ ORAL DE LA TESIS DOCTORAL A LA COMISSIÓ DE POSTGRAU I DOCTORAT
DE LA URV PER PART DELS REPRESENTANTS DELS DEPARTAMENTS)

Agreed by the Commission of Doctorate of the URV held the 03/03/03
(Adaptada a la Comissió de Doctorat del DEQ/DEM el 09/05/08)

Thesis information
(Dades sobre la tesi)

First name, last name of the doctoral candidate (Nom i cognoms del doctorand/a)**:**

Alexander Muratov

Title of the thesis (Títol de la tesi)**:**

Modeling of Self-Organization of Microtubules in Plant Cells

First name, last name of the Supervisor(s) (Nom i cognoms del/s director/s/a/es)**:**

Dr. Vladimir Baulin

Responsible department for the thesis (Departament responsable de la tesi)**:**

Departament d'Enginyería Química

In order to support the report, some points to be addressed are listed below:
(Per tal que de fonamentar l'informe, relacionem un seguit de punts que podeu considerar)

- About contents (sobre continguts):
    - Justification, hypotheses and objectives (justificació, hipòtesis i objectius)
    - Methodology (metodologia)
    - Contributions and new findings (contribucions i coneixements nous)
    - Publications (books, articles, participation in congresses) or other products (resultats tangibles de la investigació: llibres, articles, comunicacions a congressos, …)
    - Research stages in other research groups (estades en altres grups de recerca)
    - Other merits like thesis collaborations, European doctorate, awards... (altres mèrits com tesi feta en col·laboració amb altres entitats, títol de doctorat europeu, premis…)

- About the format of the presentation (sobre els aspectes formals de la presentació)
    - Understandable for any member of the Commission, i.e. one representative with different backgrounds for each department (entenedora per a tots els membres de la Comissió, és a dir, un representant de cada departament i amb diferents perfils)
    - Short. The full description must be about one A4 or 3 minutes (curta; l'informe complet escrit hauria d'ocupar un full DIN A4 o 3 minuts de temps de presentació)
    - The "Contributions and new findings" section is limited to **150 words** (la secció de contribucions i nous coneixements està limitat a **150 paraules**)

- Justification, hypotheses and objectives (justificació, hipòtesis i objectius)

In plant cells microtubules are organized in parallel arrays adjacent to the cell's plasmatic membrane. These microtubules govern the deposition of cellulose microfibrils into cell wall, thus defining its anisotropy and causing directional growth. Microtubules reorgananize due to changes in the environment. We propose a model that can explan reorientation of microtubules due to external mechanical stress or due to the action of chemicals which can cause changes in microtubules' dynamics.

- Methodology (metodologia)

We are using two methods for our analysis: kinetic Monte-Carlo model and theoretical mathematic analysis.

- Contributions and new findings (contribucions i coneixements nous)

We have shown that the compression of initially disordered microtubule array may itself induce a global order,where microtubules are oriented along major stress-lines. We have also shown that external action of chemicals modifying microtubule dynamics cause ordering or even reordering of microtubules into arrays of different complexity. Since microtubules direct cellulose microfibrils assembly, what consequently indicates the direction of cell growth.

UNIVERSITAT ROVIRA I VIRGILI
MODELING OF SELF-ORGANIZATION OF MICROTUBULES IN PLANT CELLS
Alexander Muratov
Dipòsit Legal: T 966-2014

DOCTORAL PROGRAMME IN
CHEMICAL, ENVIRONMENTAL AND PROCESS ENGINEERING

DOCTORAL PROGRAMME IN
CHEMICAL, ENVIRONMENTAL AND PROCESS ENGINEERING

- Publications (books, articles, participation in congresses) or other products
(resultats tangibles de la investigació: llibres, articles, comunicacions a congressos, …)

Papers (articles)

Authors (autors)**:** Alexander Muratov and Vladimir A. Baulin
Title (títol)**:** Degradation versus Self-Assembly of Block Co'polymer Micelles
Journal (revista)**:** Langmuir
Volume (volum)**:** 28   **Pages** (pàgines)**:** 3071-3076   **Year** (any)**:** 2012
Impact index (índex d'impacte)**:4.187**
ISI category (àrea ISI)**:Physicsl Chemistry**   **AIF[1]** (AIF)**:** 4.014
Position in the category[2] (posició a l'àrea ISI)**:** 29/135

Authors (autors)**:** Alexander Muratov and Vladimir A. Baulin
Title (títol)**:** Gravitropism in plant cells and orientation of microtubules induced by cell elongation
Journal (revista)**:** Planta
Volume (volum)**:** N/A   **Pages** (pàgines)**:** N/A   **Year** (any)**:** 2014
Impact index (índex d'impacte)**:3.347**
ISI category (àrea ISI)**:Plant Sciences**   **AIF** (AIF)**:** 3.651
Position in the category (posició a l'àrea ISI)**:** 25/197

Congress contributions (contribucions a congressos)

Authors (autors)**:** A. Muratov and V. Baulin
Title (títol)**:** Self-organisation of microtubules in plant cell cortex under the influence of pressure
Congress (congrés)**:** 11th Greta Pifat-Mrzljak International School of Biophysics
Format (poster or oral) (format oral o pòster)**:** oral
Publication (publicació)**:**
Dates (dates)**:** 30.09.-09.10.2012   **Place** (lloc)**:** Primošten, Croatia

Authors (autors)**:** A. Muratov and V. Baulin
Title (títol)**:** Degradation versus Self-Assembly of Block Co-polymer Micelles
Congress (congrés)**:** 2nd Workshop on biomaterials and their interactions with biological and model membranes 2013
Format (poster or oral) (format oral o pòster)**:** poster
Publication (publicació)**:**
Dates (dates)**:** 24-26.02.2013   **Place** (lloc)**:** Salou, Spain

Authors (autors)**:** A. Muratov and V. Baulin
Title (títol)**:** XIII International Congress of the Spanish Biophysical Society
Congress (congrés)**:** 2nd Workshop on biomaterials and their interactions with biological and model membranes 2013
Format (poster or oral) (format oral o pòster)**:** oral
Publication (publicació)**:**
Dates (dates)**:** 19-21.06.2013   **Place** (lloc)**:** Valencia, Spain

---

[1] AIF: Aggregate Impact Factor (factor d'impacte agregat). See *Journal of Citation Reports*.
[2] Example: *Chemosphere* appears in the *Environmental Sciences* category and is 27/144 (27 out of 144)

Have you requested your thesis to be labelled with the mention "European Doctor"? Yes/Not (has tramitat la tesis amb la menció de "Doctor europeu? Si/No)**:** No

If not, why? (si no ho has fet, per què?)**:**
My work didn't include the stage abroad Spain

- Other merits like awards, prizes, recognitions, fellowships, etc. (altres mèrits com premis, reconeixements, beques, etc.)

Please, give as many details as possible in order to assess the merit (si us plau, proporciona tants detalls com puguis per tal de valorar el mèrit).

2011 - Mention on the 9th Doctoral Day among the participants in the Doctoral Programme of Chemical, Environmental and Process Engineering, 1st-year students, Universitat Rovira i Virgili.
2012 - EBSA (European Biophysical Societies' Association) grant for assistance the 11th Greta Pifat-Mrzljak International School of Biophysics.
2013 - Winner of the 10th Doctoral Day among the participants in the Doctoral Programme of Chemical, Environmental and Process Engineering, 3rd-year students, Universitat Rovira i Virgili.

- Comments (comentaris)

Please, comment any other relevant issue, if desired (si us plau, comenta qualsevol altre aspecte rellevant si així ho desitges).

Degradation versus Self-Assembly of Block Co-Polymer Micelles

Bibliography

[1] Bruce Alberts, Alexander Johnson, Julian Lewis, Martin Raff, Keith Roberts, and Peter Walter. *Molecular Biology of the Cell*. Garland Science, 4th edition, 2002.

[2] D. Chretien, Henrik Flyvbjerg, and Stephen D. Fuller. Limited flexibility of the inter-protofilament bonds in microtubules assembled from pure tubulin. *Eur Biophys J*, 27(5):490–500, 1998.

[3] I. M. Janosi, D. Chretien, and H. Flyvbjerg. Structural microtubule cap: stability, catastrophe, rescue, and third state. *Biophys J*, 83:1317–1330, 2002.

[4] Vincent VanBuren, David J. Odde, and Lynne Cassimeris. Estimates of lateral and longitudinal bond energies within the microtubule lattice. *Proc Natl Acad Sci U S A*, 99(9):6035–6040, 2002.

[5] S. R. Martin, M. J. Schilstra, and P. M. Bayley. Dynamic instability of microtubules: Monte carlo simulation and application to different types of microtubule lattice. *Biophys J*, 65(2):578–596, 1993.

[6] R A Walker, E T O'Brien, N K Pryer, M F Soboeiro, W A Voter, H P Erickson, and E D Salmon. Dynamic instability of individual microtubules analyzed by video light microscopy: rate constants and transition frequencies. *The Journal of cell biology*, 107(4):1437–1448, 1988.

[7] R F Gildersleeve, A R Cross, K E Cullen, A P Fagen, and R C Williams. Microtubules grow and shorten at intrinsically variable rates. *J Biol Chem*, 267(12):7995–8006, 1992.

[8] Sidney L. Shaw, Roheena Kamyar, and David W. Ehrhardt. Sustained microtubule treadmilling in arabidopsis cortical arrays. *Science*, 300(5626):1715–1718, 2003.

[9] E M Mandelkow, E Mandelkow, and R A Milligan. Microtubule dynamics and

UNIVERSITAT ROVIRA I VIRGILI
MODELING OF SELF-ORGANIZATION OF MICROTUBULES IN PLANT CELLS
Alexander Muratov
Dipòsit Legal: T 966-2014

Bibliography

microtubule caps: a time-resolved cryo-electron microscopy study. *The Journal of cell biology*, 114(5):977–991, 1991.

[10] T Mitchison and M Kirschner. Dynamic instability of microtubule growth. *Nature*, 312(5991):237–242, 1984.

[11] Marco Cosentino Lagomarsino, Catalin Tanase, Jan W. Vos, Anne Mie C. Emons, Bela M. Mulder, and Marileen Dogterom. Microtubule organization in three-dimensional confined geometries: Evaluating the role of elasticity through a combined in vitro and modeling approach. *Biophysical Journal*, 92(3):1046–1057, 2007.

[12] Richard Cyr. How and y plant microtubules branch. *Nature Cell Biology*, 7(10):927–929, 2005.

[13] C. W. Lloyd, R. Himmelspach, P. Nick, and C. Wymer. Cortical microtubules form a dynamic mechanism that helps regulate the direction of plant growth. *Gravitational and space biology bulletin: publication of the American Society for Gravitational and Space Biology*, 13:59–66, 2000.

[14] F D Sack. Plant gravity sensing. *International Review of Cytology*, 127:193–252, 1991.

[15] Olivier Hamant and Jan Traas. The mechanics behind plant development. *New Phytol*, 185(2):369–385, 2010.

[16] C L Wymer, S A Wymer, D J Cosgrove, and R J Cyr. Plant cell growth responds to external forces and the response requires intact microtubules. *Plant Physiol*, 110(2):425–430, 1996.

[17] P Nick, R Godbole, and Q Y Wang. Probing rice gravitropism with cytoskeletal drugs and cytoskeletal mutants. *Biol Bull*, 192(1):141–143, 1997.

[18] I. Brent Heath. A unified hypothesis for the role of membrane bound enzyme complexes and microtubules in plant cell wall synthesis. *Journal of Theoretical Biology*, 48(2):445–449, 1974.

[19] Kimura, Laosinchai, Itoh, Cui, Linder, and Brown. Immunogold labeling of rosette terminal cellulose-synthesizing complexes in the vascular plant vigna angularis. *The Plant cell*, 11(11):2075–2086, 1999.

[20] Anne Mie C. Emons, Herman Hofte, and Bela M. Mulder. Microtubules and cellulose microfibrils: how intimate is their relationship? *Trends in Plant Science*, 12(7):279–281, 2007.

Bibliography

[21] Alexander R Paredez, Christopher R Somerville, and David W Ehrhardt. Visualization of cellulose synthase demonstrates functional association with microtubules. *Science*, 312(5779):1491–1495, 2006.

[22] Alexander R Paredez, Staffan Persson, David W Ehrhardt, and Chris R Somerville. Genetic evidence that cellulose synthase activity influences microtubule cortical array organization. *Plant Physiol*, 147(4):1723–1734, 2008.

[23] M Yuan, P J Shaw, R M Warn, and C W Lloyd. Dynamic reorientation of cortical microtubules, from transverse to longitudinal, in living plant cells. *Proc Natl Acad Sci U S A*, 91(13):6050–6053, 1994.

[24] T I Baskin, J E Wilson, A Cork, and R E Williamson. Morphology and microtubule organization in arabidopsis roots exposed to oryzalin or taxol. *Plant Cell Physiol*, 35(6):935–942, 1994.

[25] Francis Corson, Olivier Hamant, Steffen Bohn, Jan Traas, Arezki Boudaoud, and Yves Couder. Turning a plant tissue into a living cell froth through isotropic growth. *Proc Natl Acad Sci U S A*, 106(21):8453–8458, 2009.

[26] Paul B. Green. Mechanism for plant cellular morphogenesis. *Science*, 138(3548):1404–1405, 1962.

[27] M C Ledbetter and K R Porter. A "microtubule" in plant cell fine structure. *J Cell Biol*, 19(1):239–250, 1963.

[28] O. Hamant, M. G. Heisler, H. Jonsson, P. Krupinski, M. Uyttewaal, P. Bokov, F. Corson, P. Sahlin, A. Boudaoud, E. M. Meyerowitz, Y. Couder, and J. Traas. Developmental patterning by mechanical signals in arabidopsis. *Science*, 322(5908):1650–1655, 2008.

[29] Olivier Hamant, Elliot M Meyerowitz, and Jan Traas. Is cell polarity under mechanical control in plants? *Plant Signal Behav*, 6(1):137–139, 2011.

[30] F. Baluska and K. H. Hasenstein. Root cytoskeleton: its role in perception of and response to gravity. *Planta*, 203:S69–S78, 1997.

[31] Y. Hashiguchi, M. Tasaka, and M. T. Morita. Mechanism of higher plant gravity sensing. *Am J Bot*, 100(1):91–100, 2012.

[32] J D Smith, P Todd, and L A Staehelin. Modulation of statolith mass and grouping in white clover (trifolium repens) growth in 1-g, microgravity and on the clinostat. *Plant J*, 12(6):1361–1373, 1997.

UNIVERSITAT ROVIRA I VIRGILI
MODELING OF SELF-ORGANIZATION OF MICROTUBULES IN PLANT CELLS
Alexander Muratov
Dipòsit Legal: T 966-2014

Bibliography

[33] S. Vitha, M. Yang, F. D. Sack, and J. Z. Kiss. Gravitropism in the starch excess mutant of arabidopsis thaliana. *Am J Bot*, 94(4):590–598, 2007.

[34] R Wayne, M P Staves, and A C Leopold. Gravity-dependent polarity of cytoplasmic streaming in nitellopsis. *Protoplasma*, 155:43–57, 1990.

[35] T L Yoder, H Q Zheng, P Todd, and L A Staehelin. Amyloplast sedimentation dynamics in maize columella cells support a new model for the gravity-sensing apparatus of roots. *Plant Physiol*, 125(2):1045–1060, 2001.

[36] Ingo Burgert and John W. C. Dunlop. Micromechanics of cell walls. In Przemyslaw Wojtaszek, editor, *Mechanical Integration of Plant Cells and Plants*, volume 9, pages 27–52. Springer Berlin Heidelberg, Berlin, Heidelberg, 2011.

[37] G. Leitz, B.-H. Kang, M. E.A. Schoenwaelder, and L. A. Staehelin. Statolith sedimentation kinetics and force transduction to the cortical endoplasmic reticulum in gravity-sensing arabidopsis columella cells. *Plant Cell*, 21(3):843–860, 2009.

[38] R. M. Perrin. Gravity signal transduction in primary roots. *Ann Bot*, 96(5):737–743, 2005.

[39] Elison B Blancaflor and Patrick H Masson. Plant gravitropism. unraveling the ups and downs of a complex process. *Plant Physiol*, 133(4):1677–1690, 2003.

[40] R Himmelspach and P Nick. Gravitropic microtubule reorientation can be uncoupled from growth. *Planta*, 212(2):184–189, 2001.

[41] Sherryl R. Bisgrove. The roles of microtubules in tropisms. *Plant Sci*, 175(6):747–755, 2008.

[42] T. Xu, N. Dai, J. Chen, S. Nagawa, M. Cao, H. Li, Z. Zhou, X. Chen, R. De Rycke, H. Rakusova, W. Wang, A. M. Jones, J. Friml, S. E. Patterson, A. B. Bleecker, and Z. Yang. Cell surface ABP1-TMK auxin-sensing complex activates ROP GTPase signaling. *Science*, 343(6174):1025–1028, 2014.

[43] D. A. Korasick, C. S. Westfall, S. G. Lee, M. H. Nanao, R. Dumas, G. Hagen, T. J. Guilfoyle, J. M. Jez, and L. C. Strader. Molecular basis for AUXIN RESPONSE FACTOR protein interaction and the control of auxin response repression. *Proceedings of the National Academy of Sciences*, 2014.

[44] Bodo Wiesler, Qi-Yan Wang, and Peter Nick. The stability of cortical microtubules depends on their orientation. *Plant J*, 32(6):1023–1032, 2002.

94

Bibliography

[45] Anna Akhmanova and Michel O. Steinmetz. Tracking the ends: a dynamic protein network controls the fate of microtubule tips. *Nature Reviews Molecular Cell Biology*, 9(4):309–322, 2008.

[46] K Fischer and P Schopfer. Physical strain-mediated microtubule reorientation in the epidermis of gravitropically or phototropically stimulated maize coleoptiles. *Plant J*, 15(1):119–123, 1998.

[47] Toshimitsu Ikushima and Teruo Shimmen. Mechano-sensitive orientation of cortical microtubules during gravitropism in azuki bean epicotyls. *J Plant Res*, 118(1):19–26, 2005.

[48] K Zandomeni and P Schopfer. Mechanosensory microtubule reorientation in the epidermis of maize coleoptiles subjected to bending stress. *Protoplasma*, 182(3-4):96–101, 1994.

[49] Olivier Hamant, Jan Traas, and Arezki Boudaoud. Regulation of shape and patterning in plant development. *Current Opinion in Genetics & Development*, 20(4):454–459, 2010.

[50] M. Sassi and T. Vernoux. Auxin and self-organization at the shoot apical meristem. *Journal of Experimental Botany*, 64(9):2579–2592, 2013.

[51] Marcus G. Heisler, Olivier Hamant, Pawel Krupinski, Magalie Uyttewaal, Carolyn Ohno, Henrik Jonsson, Jan Traas, and Elliot M. Meyerowitz. Alignment between PIN1 polarity and microtubule orientation in the shoot apical meristem reveals a tight coupling between morphogenesis and auxin transport. *PLoS Biol*, 8(10):e1000516, 2010.

[52] Magalie Uyttewaal, Agata Burian, Karen Alim, Benoît Landrein, Dorota Borowska-Wykret, Annick Dedieu, Alexis Peaucelle, Michal Ludynia, Jan Traas, Arezki Boudaoud, Dorota Kwiatkowska, and Olivier Hamant. Mechanical stress acts via katanin to amplify differences in growth rate between adjacent cells in arabidopsis. *Cell*, 149(2):439–451, 2012.

[53] L. Vineyard, A. Elliott, S. Dhingra, J. R. Lucas, and S. L. Shaw. Progressive transverse microtubule array organization in hormone-induced arabidopsis hypocotyl cells. *Plant Cell*, 25(2):662–676, 2013.

[54] J Tabony and D Job. Spatial structures in microtubular solutions requiring a sustained energy source. *Nature*, 346(6283):448–451, 1990.

UNIVERSITAT ROVIRA I VIRGILI
MODELING OF SELF-ORGANIZATION OF MICROTUBULES IN PLANT CELLS
Alexander Muratov
Dipòsit Legal: T 966-2014

Bibliography

[55] J Tabony and D Job. Gravitational symmetry breaking in microtubular dissipative structures. *Proc Natl Acad Sci U S A*, 89(15):6948–6952, 1992.

[56] J Tabony. Morphological bifurcations involving reaction-diffusion processes during microtubule formation. *Science*, 264(5156):245–248, 1994.

[57] J. Tabony. Self-organization in a simple biological system through chemically dissipative processes. *Nanobiology*, 4:117–137, 1996.

[58] J. Tabony, N. Glade, J. Demongeot, and C. Papaseit. Biological self-organization by way of microtubule reaction-diffusion processes. *Langmuir*, 18:7196–7207, 2002.

[59] Marileen Dogterom and Stanislas Leibler. Physical aspects of the growth and regulation of microtubule structures. *Phys Rev Lett*, 70(9):1347–1350, March 1993.

[60] Alexander Mogilner, Edith Geigant, and Karina Ladizhansky. An integrodifferential model for orientational distributions of f-actin in cells. *SIAM Journal on Applied Mathematics*, 59(3):787–809, 1998.

[61] R. Dixit and R. Cyr. Encounters between dynamic cortical microtubules promote ordering of the cortical array through angle-dependent modifications of microtubule behavior. *Plant Cell*, 16:3274–3284, 2004.

[62] K. Kruse, J. F. Joanny, F. Julicher, J. Prost, and K. Sekimoto. Generic theory of active polar gels: a paradigm for cytoskeletal dynamics. *The European Physical Journal E*, 16(1):5–16, 2005.

[63] Alexander Zumdieck, Marco Lagomarsino, Catalin Tanase, Karsten Kruse, Bela Mulder, Marileen Dogterom, and Frank JÃŒlicher. Continuum description of the cytoskeleton: Ring formation in the cell cortex. *Physical Review Letters*, 95(25):258103, 2005.

[64] Igor Aranson and Lev Tsimring. Theory of self-assembly of microtubules and motors. *Physical Review E*, 74(3):031915, 2006.

[65] Vladimir A. Baulin, Carlos M. Marques, and Fabrice Thalmann. Collision induced spatial organization of microtubules. *Biophys Chem*, 128(2-3):231–244, 2007.

[66] V. Ruhle, F. Ziebert, R. Peter, and W. Zimmermann. Instabilities in a two-dimensional polar-filament-motor system. *The European Physical Journal E*, 27(3):243–251, 2008.

Bibliography

[67] Xia-qing Shi and Yu-qiang Ma. Understanding phase behavior of plant cell cortex microtubule organization. *Proc Natl Acad Sci U S A*, 107(26):11709–11714, 2010.

[68] Simon H. Tindemans, Rhoda J. Hawkins, and Bela M. Mulder. Survival of the aligned: Ordering of the plant cortical microtubule array. *Phys Rev Lett*, 104(5):058103, 2010.

[69] Jun F. Allard, Geoffrey O. Wasteneys, and Eric N. Cytrynbaum. Mechanisms of self-organization of cortical microtubules in plants revealed by computational simulations. *Mol Biol Cell*, 21(2):278–286, 2010.

[70] E. C. Eren, R. Dixit, and N. Gautam. A three-dimensional computer simulation model reveals the mechanisms for self-organization of plant cortical microtubules into oblique arrays. *Mol Biol Cell*, 21:2674–2684, 2010.

[71] M. I. Molodtsov, E. L. Grishchuk, A. K. Efremov, J. R. McIntosh, and F. I. Ataullakhanov. Force production by depolymerizing microtubules: A theoretical study. *Proceedings of the National Academy of Sciences*, 102(12):4353–4358, 2005.

[72] Rhoda J. Hawkins, Simon H. Tindemans, and Bela M. Mulder. Model for the orientational ordering of the plant microtubule cortical array. *Phys Rev E Stat Nonlin Soft Matter Phys*, 82(1):011911, 2010.

[73] S. A. Baeurle. Multiscale modeling of polymer materials using field-theoretic methodologies: a survey about recent developments. *Journal of Mathematical Chemistry*, 46(2):363–426, 2008.

[74] H. T. Macgillivray, R. J. Dodd, B. V. McNally, J. F. Lightfoot, H. G. Corwin, and S. R. Heathcote. Monte-carlo simulations of galaxy systems: I: The local supercluster. *Astrophysics and Space Science*, 81(1-2):231–250, 1982.

[75] P. Kevin MacKeown. *Stochastic simulation in physics*. Springer, Singapore [u.a., 1997.

[76] Marco Werner, Jens-Uwe Sommer, and Vladimir A. Baulin. Homo-polymers with balanced hydrophobicity translocate through lipid bilayers and enhance local solvent permeability. *Soft Matter*, 8(46):11714, 2012.

[77] Sergey Pogodin, Marco Werner, Jens-Uwe Sommer, and Vladimir A. Baulin. Nanoparticle-induced permeability of lipid membranes. *ACS Nano*, 6:10555–10561, 2012.

97

UNIVERSITAT ROVIRA I VIRGILI
MODELING OF SELF-ORGANIZATION OF MICROTUBULES IN PLANT CELLS
Alexander Muratov
Dipòsit Legal: T 966-2014

Bibliography

[78] Artem Efremov, Ekaterina L Grishchuk, J Richard McIntosh, and Fazly I Ataullakhanov. In search of an optimal ring to couple microtubule depolymerization to processive chromosome motions. *Proceedings of the National Academy of Sciences of the United States of America*, 104(48):19017–19022, 2007.

[79] C Forastero, L I Zamora, D Guirado, and A M Lallena. A monte carlo tool to simulate breast cancer screening programmes. *Physics in Medicine and Biology*, 55(17):5213–5229, 2010.

[80] Lars Onsager. The effects of shape on the interaction of colloidal particles. *Ann N Y Acad Sci*, 51(4):627–659, 1949.

[81] Chris Ambrose, Jun F. Allard, Eric N. Cytrynbaum, and Geoffrey O. Wasteneys. A CLASP-modulated cell edge barrier mechanism drives cell-wide cortical microtubule organization in arabidopsis. *Nature Communications*, 2:430, 2011.

[82] Chris Ambrose, Yuan Ruan, John Gardiner, Laura M. Tamblyn, Amanda Catching, Viktor Kirik, Jan Marc, Robyn Overall, and Geoffrey Â O. Wasteneys. CLASP interacts with sorting nexin 1 to link microtubules and auxin transport via PIN2 recycling in arabidopsis thaliana. *Developmental Cell*, 24(6):649–659, 2013.

[83] Chunhua Zhang, Natasha V Raikhel, and Glenn R Hicks. Clasping microtubules and auxin transport. *Dev Cell*, 24(6):569–571, 2013.

[84] Klementina Kakar, Hongtao Zhang, Ben Scheres, and Pankaj Dhonukshe. CLASP-mediated cortical microtubule organization guides PIN polarization axis. *Nature*, 495(7442):529–533, 2013.